

THÈSE

Présentée a l'Université de Strasbourg
École Doctorale des Sciences Chimiques

pour obtenir le grade de
Docteur de l'Université de Strasbourg

par

DAVE VAN DITMARSCH

Selection of *Streptomyces griseus* aminopeptidases by droplet microfluidics

Soutenue publiquement le 18 décembre 2009

devant la commission d'examen :

Directeur de these : Prof. A.D. Griffiths

Université de Strasbourg, l'Institut de Science et d'Ingénierie Supramoléculaires, Laboratoire de Biologie Chimique, Strasbourg, France

Rapporteur : Prof. P. Soumillon

Université de Louvain-la-Neuve, Unité de Biochimie, Louvain-la-Neuve, Belgique

Rapporteur : Dr. E. Mastrobattista

Utrecht University, Faculty of Beta Sciences, Department of Pharmaceutics, Biopharmacy and Pharmaceutical Technology, Utrecht, Pays-Bas

Examineur : Dr. S. Ladame

Université de Strasbourg, l'Institut de Science et d'Ingénierie Supramoléculaires, Laboratoire de Chimie et de Reconnaissance de Biomolécules, Strasbourg, France

*“Develop success from failures.
Discouragement and failure are two of the surest stepping stones to success.”*

—
Dale Carnegie

ACKNOWLEDGMENTS

I would like to thank the jury members, Dr. Enrico Mastrobattista, Prof. Patrice Soumillion and Dr. Sylvain Ladame for taking time out of their schedules to take place in my PhD jury.

I owe the highest gratitude to my thesis supervisor: Prof. Andrew Griffiths. Thank you very much for providing me with the opportunity to do my PhD work in your laboratory. I have learned a great deal, both experimentally and personally, from being in your lab.

Special thanks go out to Dr. Oliver Miller. He was there for me from day one, with whatever question I might have. I cannot thank him enough for all the time and effort he has put into making me a better scientist. Hopefully Padawan's development was to satisfaction.

Thanks to Dr. Kerstin Blank, the SGAP model system was introduced in the lab. I won't soon forget all her scientific, but more even her non-scientific remarks.

Gabrielle Woronoff, Dr. Estelle Mayot et Dr. Abdeslam El Harrak, je vous remercie énormément pour toute votre aide vis-à-vis la synthèse de l'ACMS ainsi que pour la chimie en général. En particulier Gabrielle: j'espère ne pas avoir été trop invivable. Mais comme on dit : qui aime bien, châtie bien.

Je tiens à remercier également Julien Sylvestre, Dr. Jean Baudry et Prof. Jérôme Bibette d'avoir ouvert leur laboratoire ainsi que pour leur collaboration sur les émulsions 2D.

Merci à Dr. Valérie Taly Abécassis d'avoir organisé cette collaboration et d'avoir été mon superviseur non-officiel pour cet échange.

Lucia et Michaël, les autres gens dans “bureau 205”. Merci pour les discussions scientifiques, mais surtout pour les discussions non-scientifiques beaucoup plus fréquentes. Lucia, heureusement qu'il y avait au moins une personne dans le labo qui parle une langue encore plus moche que la mienne ! Michaël, je te souhaite surtout bon courage avec ‘Bob’ et la supervision du projet SGAP !

Thanks to the rest of the LBC, past and present members: Bachir, Shigeyoshi, Christoph, Jenifer, Linas, Yousr, Deniz, Christian, Victoire, Yannick, Ali, Sophie, Faith, Diana, Majdi, Antoine, François, Alexei, Agnes, Josh, Sylvie, Isabelle, Odile, Jean-Christophe, Thomas B, Thomas M, Felix, Lucas, Philippe, Matthieu, Florian.

I acknowledge a great deal to the Boehringer Ingelheim Fonds, the late Hermann Fröhlich and the late Monika Beutelspacher, Claudia Walther and all the other people working for BIF, for both financial and personal support.

Last but not least, I'd like to thank my friends here in Strasbourg. Even if I didn't see you quite as often as I wanted to the last couple of months, your support has been one of the things that has kept me going. Merci au Café Miro et à sa porte toujours ouverte, ainsi qu'à son Patron et à sa clientèle régulière de m'avoir soutenu; heureusement que l'endroit était tellement près du travail. Als allerlaatste ook nog veel dank aan mijn familie: ma, pa, Conny, Kenneth en oma. Zelfs al was het contact niet altijd zo frequent als gewenst, ik heb altijd in mijn achterhoofd gehouden dat jullie achter me stonden.

ABSTRACT

Streptomyces griseus aminopeptidase (SGAP; Enzyme Commission number 3.4.11.10) is a di-zinc protein that is stabilized by calcium ions, capable of catalyzing multiple reactions: it is (i) an aminopeptidase with a broad substrate specificity, (ii) a phosphodiesterase and (iii) a catechol oxidase. As such, it is considered to be an evolutionary intermediate, which means that it is a good model for answering outstanding questions in evolutionary biology. In the long run, fluorescence-activated droplet sorting (FADS)—a technique that combines the versatility of microtitre plate assays at higher throughput with the capacity to select for a specific activity like in fluorescence-activated cell sorting (FACS)—could be used to evolve this enzyme by directed evolution.

This project describes the development of a bacterial expression system for SGAP, a fluorescence-based SGAP peptidase assay and the use of this assay to perform a microfluidic activity-based selection of SGAP. The enrichment factor achieved in the model sort was 28.9, close to the theoretical maximum.

A wide distribution of fluorescence signals was observed in droplets containing single bacterial cells expressing SGAP, which could be attributable to differences in the expression level of SGAP. In an effort to ameliorate this effect, SGAP was fused to mCherry—a red fluorescent protein—was constructed and some preliminary experiments were performed with this construct. Both N-terminal and C-terminal fusion proteins were found to retain SGAP peptidase activity and exhibited mCherry fluorescence, the two variables correlating with an R^2 of 0.9991 in the case of the N-terminal fusion (mCherry::SGAP)

and with an R^2 of 0.9997 in the case of the C-terminal fusion (SGAP::mCherry). It did not prove possible to detect the mCherry fluorescence in droplets due to the limited sensitivity of the optical setup.

Next, since many of the unanswered questions in enzyme evolution require the simultaneous selection or counterselection of a second activity, 7-aminocoumarin-4-methanesulfonic acid (ACMS) was synthesized, which, after grafting an amino acid to this molecule, could function as a second fluorogenic peptidase substrate. ACMS is more hydrophilic than the commonly-used 7-amino-4-methylcoumarin (AMC) and was shown not to leak from droplets.

Finally, as a side-project, work done on 2D emulsions using *in vitro* transcription and translation of *lacZ* demonstrated that the surfactant/oil mixture used in 2D emulsions was biocompatible. Additionally, it proved possible to detect *lacZ* at very low concentrations, permitting genomic or metagenomic analyses to be performed.

RÉSUMÉ DÉTAILLÉ

Introduction

L'évolution dirigée est un format d'évolution en laboratoire mimant de façon accélérée l'évolution naturelle et qui permet la sélection d'un caractère particulier par le biais des cycles itératifs de mutation et de sélection. Pour ce faire, l'information génétique, ou génotype, (ADN par exemple) et le phénotype (par exemple, l'activité enzymatique) doivent rester associés. Dans la nature, ce lien est assuré par la cellule, qui confine l'information génétique ainsi que ses produits d'expression. Au laboratoire, le génotype et le phénotype peuvent être couplés par une variété de techniques, notamment "phage display", "ribosome display", ou compartimentation *in vitro* (CIV). Cette dernière technique implique la création d'une émulsion dans laquelle les molécules d'ADN ou d'ARN sont compartimentées dans les gouttelettes aqueuses, qui sont dispersées dans une phase d'huile non miscible additionnée d'un tensioactif pour stabiliser l'émulsion. Cette individualisation des gènes permet leur maintien avec leurs produits dans la même gouttelette établissant ainsi un lien entre le génotype et le phénotype. Les gènes peuvent être exprimés dans des gouttelettes par le biais de deux voies: (i) de la transcription et de la traduction *in vitro* (TTIV), ou (ii) de l'expression *in vivo* où le produit est obtenu par sécrétion ou lyse des cellules. La CIV a été utilisée avec succès pour sélectionner une grande variété d'enzymes protéiques et de ribozymes à partir de grandes banques de gènes.

La CIV présente toutefois deux inconvénients majeurs : le degré élevé de polydispersité observé dans les émulsions produites par agitation ou l'homogénéisation et la difficulté de modifier le contenu des gouttelettes après qu'elles aient été générées. Récemment, ces inconvénients ont toutefois pu être contournés par le couplage de la CIV et de technologie microfluidique. Ceci permet de réduire la polydispersité ($< 3\%$) et confère un parfait contrôle du devenir des gouttelettes. En effet, ces gouttelettes peuvent être mélangées rapidement, fusionnées, divisées, incubées et triées en fonction de leur fluorescence.

L'exploitation du potentiel du couplage CIV/microfluidique (CIVm) en vue de l'évolution dirigée de protéines a constitué un des principaux objectifs de cette thèse. La protéine modèle utilisée est l'aminopeptidase de *Streptomyces griseus* (SGAP ; EC3.4.11.10). La SGAP est une protéine monomérique, possédant deux ions de zinc dans son site actif. Elle clive plusieurs acides aminés N-terminaux de peptides et de protéines, de préférence des résidus grands et hydrophobes tels que la leucine et la phénylalanine. Il a été démontré que la spécificité du clivage de ces acides aminés peut être modulée par la concentration de CaCl_2 , bien que le mécanisme par lequel se produit cet effet ne soit pas clairement compris à ce jour.

La SGAP est multi-spécifique, puisqu'elle peut également hydrolyser des liaisons phosphomonoester et phosphodiester (figure 0.1). D'autre part, la SGAP présente une flexibilité réactionnelle puisqu'elle est également capable de catalyser l'oxydation de catéchol lorsque les ions de zinc dans le site actif sont remplacés par des ions de cuivre.

Étant donné ses flexibilités réactionnelle et de spécificité de substrat, la SGAP peut être considérée comme un intermédiaire évolutif, ce qui en fait un outil intéressant pour la caractérisation des voies d'évolution des enzymes, plus particulièrement pour l'étude de l'évolution et l'émergence de nouvelles spécificités de substrats ou de nouvelles activités. En effet, si une nouvelle activité doit apparaître, il est possible de modifier la palette de réactivités existante plutôt que d'évoluer une activité complètement *de novo*.

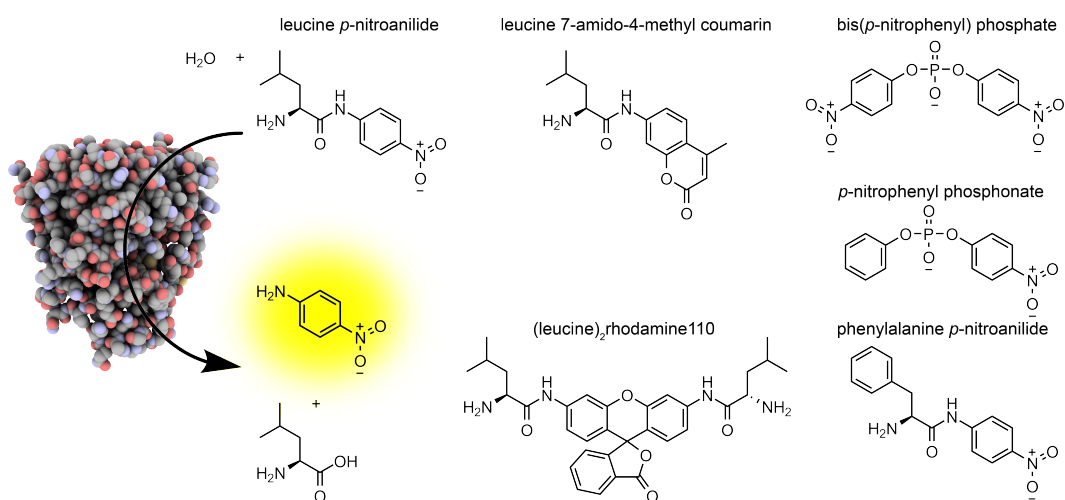


Fig. 0.1: La SGAP et certains de ses substrats. La leucine *p*-nitroanilide (Leu-*p*NA)) et la phénylalanine *p*-nitroanilide sont des substrats chromogènes couramment utilisés pour mesurer l'activité peptidase. La leucine 7-amido-4-méthylcoumarin et la bis-(L-leucinyl)-rhodamine 110 (leucine₂rhodamine110) sont des substrats fluorogènes également utilisés pour mesurer l'activité peptidase. Enfin, le bis-(*p*-nitrophényl) phosphate et le *p*-nitrophényl phosphonate sont des substrats chromogènes qui peuvent être utilisés pour analyser l'activité phosphoesterase de la SGAP. Sur la gauche la réaction standard chromogène est montrée, dans laquelle la SGAP hydrolyse la Leu-*p*NA) en la L-leucine et du *p*NA, qui peut être détecté par une augmentation de l' A_{405} .

Étant donné que la SGAP contient un pont disulfure (Cys245-Cys250), l'expression de cette protéine en CIV peut se faire suivant deux stratégies : l'utilisation d'un kit TTIV oxydant ou l'expression dans l'espace périplasmique bactérien. A cause des raisons techniques (tensioactifs fluorés compatibles avec la TTIV non disponibles), ce projet a été initié avec la stratégie d'expression *in vivo*.

Objectifs

Comme dit plus haut, un premier objectif de cette thèse a concerné la mise en place de système d'évolution dirigée par CIVm. Un second objectif de cette thèse a visé à estimer la possibilité d'évoluer "l'évolutivité". L'évolutivité est définie comme "la capacité d'une entité (par exemple une enzyme) d'acquérir une autre fonction par le biais de la mutation". Nous nous sommes attachés à voir s'il était possible de rendre la SGAP plus "évolutive" en réalisant une série d'évolutions dirigées successives de la SGAP pour une première activité, puis pour une seconde activité, puis pour la première...

Toutefois, avant d'effectuer l'évolution dirigée de la SGAP par CIVm il était nécessaire de déterminer si les gènes pouvaient être sélectionnés en fonction de l'activité du variant de la SGAP qu'ils codaient. Une telle "sélection modèle" impliquerait le mélange de cellules exprimant la SGAP de type sauvage avec des cellules exprimant un mutant inactif (E131A) de la SGAP et enrichir sélectivement la variante de type sauvage.

Le second objectif de cette thèse était donc de préparer le système de sélection de la SGAP en vue d'expériences ultérieures d'évolution dirigée. Un système d'expression bactérien modèle reproductible a été obtenu en clonant le gène codant pour la SGAP dans un vecteur d'expression approprié (un dérivé du plasmide pAK). En parallèle, un nouveau test basé sur de la fluorescence pour l'activité de la SGAP a été développé : la CIVm est actuellement uniquement compatible avec les tests basés sur la fluorescence de

sorte que les tests chromogènes conventionnellement utilisés pour mesurer l'activité de la SGAP n'étaient pas adaptés. Le test a été optimisé pour son utilisation en gouttelettes et, enfin, a permis la caractérisation des cellules uniques en microgouttelettes sur la base de l'activité de la SGAP.

Résultats

La mise au point du système d'analyse par fluorescence de l'activité de la SGAP impliquait le clonage du gène codant pour la SGAP dans un système d'expression approprié, l'optimisation des conditions d'induction, la synthèse d'un nouveau substrat fluorogénique basé sur la rhodamine110 et l'optimisation de l'analyse proprement dite.

L'optimisation de l'outil microfluidique comportait les étapes suivantes : (i) la détermination de la compatibilité des différents mélanges d'huile/tensioactif avec l'activité SGAP, (ii) la mesure de la fuite du fluorophore (le produit de la réaction) entre les gouttes, et (iii) la mise au point des conditions d'encapsulation de bactéries permettant l'obtention d'enrichissement efficaces au cours des sélections.

Initialement, il a été constaté que la SGAP était active dans les gouttelettes microfluidiques, mais le niveau d'activité était très faible et localisé dans les cellules. Pour s'assurer que l'ensemble des gouttelettes devienne fluorescent, il était nécessaire de lyser les cellules pour en libérer le contenu. Différents agents lytiques ont été testés et optimisés dans des microplaques. À la suite de ces expériences, un antibiotique très puissant (polymyxin B) a été choisi en raison de sa rapidité d'action et le fait qu'il n'inhibe pas l'activité aminopeptidase de la SGAP.

L'ajout de l'agent lytique aux gouttelettes a permis d'observer que la réaction est déjà terminée après environ 20 minutes. Toutefois, une large distribution des activités a été observée entre les gouttelettes, probablement suite à des fluctuations du niveau

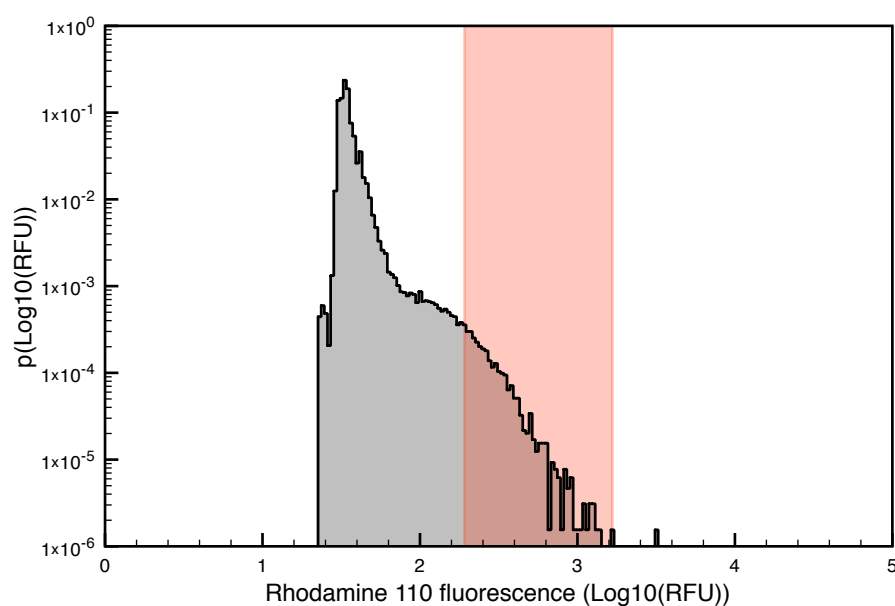
d'expression entre les différentes bactéries. Afin de permettre la normalisation du signal de l'analyse pour l'expression de protéine, la protéine SGAP a été fusionnée avec mCherry, une protéine fluorescente dans les longueurs d'ondes rouge ($\lambda_{ex} = 587$ nm ; $\lambda_{em} = 610$ nm) qui pourrait être co-détectée avec l'activité SGAP au sein de la même gouttelette dans le dispositif microfluidique.

En vue de l'évolution dirigée de SGAP vers d'autres substrats aminopeptidase, il a également été nécessaire de préparer d'autres substrats marqués par des différents fluorophores. Ces derniers permettront la mesure de l'activité aminopeptidase contre plusieurs substrats en même temps, permettant à la fois de réaliser la sélection et la contre-sélection nécessaire à l'étude sur l'évolutivité. L'aminocoumarine a été choisie comme deuxième fluorophore car son spectre d'émission n'interfère pas avec la détection de rhodamine 110 ou de mCherry. Toutefois, une fuite très rapide entre les gouttes a été observée, sans doute en fonction de son hydrophobicité. Cette fuite a été réduite par l'ajout d'un groupe caractéristique acide sulfonique. En outre, le fluorophore a été fonctionnalisé pour permettre le greffage d'acides aminés et, par conséquent, la synthèse de nouveaux substrats aminopeptidase.

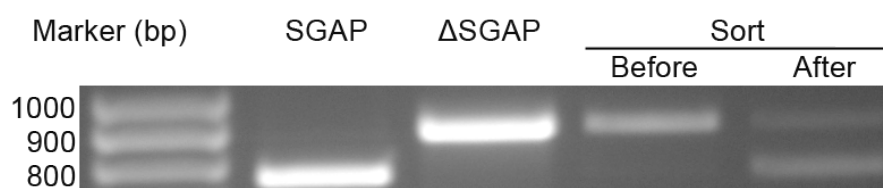
Finalement il a été montré qu'un enrichissement sélectif en bactéries exprimant la SGAP sauvage (active) peut être obtenu à partir d'un mélange de cette souche et de bactéries exprimant la Δ SGAP (inactive). Cette sélection modèle réalisée en gouttelettes microfluidiques (figure 0.2) a ainsi pu être réalisée avec un facteur d'enrichissement observé (28,9) proche du facteur théorique (110,5).

Conclusions

Nous avons démontré que le système d'expression périplasmique dans des cellules *E. coli* peut être utilisé de façon reproductible dans des analyses basées sur la fluorescence en



(a) Histogramme de la sélection modèle



(b) Gel d'agarose après la sélection modèle

Fig. 0.2: Les résultats d'une sélection modèle utilisant la SGAP et la Δ SGAP en système microfluidique. Une suspension à 0,026 unités de $DO_{600\text{ nm}}$ *E. coli* K12 TB1 contenant soit le plasmide pKB4-SGAP-his, soit le plasmide pKB4- Δ SGAP-his (dans un rapport respectivement de 1 sur 10) a été encapsulée dans du tampon PBS (1 \times) additionné de 2 mg ml $^{-1}$ de polymyxine B, 1 g l $^{-1}$ de BSA, 120 μ M de bis-(L-leucinyl)-rhodamine 110, 100 μ M de ZnCl $_2$, 1 mM de CaCl $_2$ et 50 μ M de résorufine. Des gouttelettes de 12 pl ont été produites et incubées hors puce dans un capillaire en verre maintenu à 4 $^{\circ}$ C dans un système Peltier de refroidissement. Les gouttelettes ont été réinjectées (15 l h $^{-1}$) dans un dispositif d'analyse et espacée avec de l'huile HFE 7500 (500 l h $^{-1}$). 2000 gouttelettes ont été sélectionnées et récupérées dans 70 μ l de phase aqueuse (tampon Pfu 1 \times). Le contenu de la moitié de ces gouttelettes a ensuite été amplifié par PCR, puis digéré par l'enzyme Sall (marqueur de restriction du gène sauvage) et les produits analysés par électrophorèse en gel d'agarose. (a) Profil d'activité de la population. Les intensités de fluorescence (RFU) ont été calculées à partir des signaux des photomultiplicateurs en utilisant la relation Intensité (RFU) = Signal (V)/Gain 7,2 . $p(\log_{10}(\text{RFU})) = \frac{\text{nombre de gouttelettes à } x \log_{10}(\text{RFU})}{\text{nombre totale de gouttelettes}}$, ce qui indique la probabilité pour une gouttelette d'être à $x \log_{10}(\text{RFU})$. La fenêtre de tri utilisée (les 0,3 % des gouttelettes les plus actives) est ombrée en rouge. (b) Analyse des digestions Sall sur gel d'agarose. L'apparition d'une bande à 800 bp après tri (piste Sort/after) démontre l'enrichissement en variant SGAP sauvage.

microplaques.

En outre, une formulation huile fluorée/tensioactif fluoré compatible avec l'activité aminopeptidase de la SGAP a été identifiée. L'activité aminopeptidase dans des gouttelettes microfluidiques a été démontrée après environ 20 minutes d'incubation, temps suffisamment court pour rendre la fuite de rhodamine 110 (le produit final de la réaction aminopeptidase) des gouttelettes négligeable.

La compartimentation des bactéries en gouttelettes microfluidiques nécessite la lyse des cellules afin de permettre détection de la fluorescence générée par l'activité SGAP. Pour ce faire, un antibiotique bactériolytique très puissant a été utilisé et s'est montré être un outil efficace et reproductible.

Cependant, une large distribution des signaux de fluorescence a été observée, ce qui nécessite une normalisation. Pour cela, la protéine sera exprimée en fusion avec mCherry, ce qui permettra de normaliser l'activité de la SGAP par son niveau d'expression.

Enfin, pour faciliter la détection utilisant de multiples fluorophores, l'acide 4-méthanesulfonique 7-aminocoumarine (ACMS) a été synthétisée. Le groupe caractéristique acide sulfonique de cette aminocoumarine rend la molécule très hydrophile, de manière efficace à la prévention de fuite des microgouttelettes. En outre, il y a un groupement amine, ce qui permettra la fonctionnalisation avec des acides aminés et ce qui, par conséquent, fait de l'ACMS une molécule intéressante pour la synthèse de nouveaux substrats aminopeptidase.

Finalement, une sélection modèle a pu être réalisée avec succès, démontrant la possibilité d'enrichir spécifiquement la SGAP sauvage à partir d'un mélange actif/inactif.

ABBREVIATIONS

δ	chemical shift in $^1\text{H-NMR}$
ΔSGAP	frameshift mutation of SGAP, leading to an early stop codon
ϵ	ratio of positive versus negative in microfluidics
ϵ_0	ratio of positive versus negative at the onset of a sorting experiment
ϵ_1	ratio of positive versus negative after a sorting experiment
η_{exp}	experimental enrichment factor
η_m	theoretical enrichment factor
λ	number of bacteria per droplet
λ_{em}	emission wavelength (of a given fluorophore)
λ_{ex}	excitation wavelength (of a given fluorophore)
λ_n	wavelength at n nm
$^1\text{H-NMR}$	proton nuclear magnetic resonance
A_n	absorbance at n nm
ACMS	7-aminocoumarin-4-methanesulfonic acid
AMC	7-amino-4-methylcoumarin
Amp ⁺	denotes media supplemented with 100 $\mu\text{g ml}^{-1}$ ampicillin
APAP	<i>Aeromonas proteolytica</i> aminopeptidase
bp	basepair
BSA	bovine serum albumin
CAD	computer-aided design
Cam ⁺	denotes media supplemented with 30 $\mu\text{g ml}^{-1}$ chloramphenicol
ddH ₂ O	double distilled water
DMF	dimethylformamide
DMSO	dimethylsulfoxide
DNA	deoxyribonucleic acid
dNTPs	deoxynucleoside triphosphate mixture
E131A	glutamic acid to alanine mutation at amino acid 131
EC	Enzyme Commission
EDTA	ethylenediaminetetraacetic acid
eq	equivalent(s)
FACS	fluorescence-activated cell sorter
FADS	fluorescence-activated droplet sorting
FDG	fluorescein-di- β -D-galactopyranoside
GFP	<i>Aequorea victoria</i> green fluorescent protein

GOLD	Genomes On Line Database
HEPES	N-2-hydroxyethylpiperazine-N'-2-ethanesulfonic acid
IVC	<i>in vitro</i> compartmentalization
IVTT	<i>in vitro</i> transcription and translation
kbp	kilobases
k_{cat}	catalytic constant
K_M	Michaelis constant
L2R	bis-(L-leucinyl)-rhodamine 110
LB	lysogeny broth
Mb	megabases
mCherry::SGAP	fusion protein with mCherry fused to the N-terminus of SGAP
MeSH	medical subject heading
MQW	MilliQ water
NFW	DNase- and RNase-free water
NMR	nuclear magnetic resonance
OD_n	optical density at n nm
ODU_n	optical density units at n nm
PBS	phosphate-buffered saline
PCR	polymerase chain reaction
PDB	RCSB protein data bank
PMT	photomultiplier tube
Q_{aq}	total flowrate for the aqueous phase in microfluidics
Q_{em}	total flowrate for reinjected emulsion in microfluidics
Q_{oil}	flowrate for the surfactant-free oil phase in microfluidics
Q_{surf}	flowrate for the oil phase containing surfactant in microfluidics
RBS	ribosomal binding site
rcf	relative centrifugal force
RFU	relative fluorescence units
rpm	rotations per minute
SB	super broth
SGAP	<i>Streptomyces griseus</i> aminopeptidase
SGAP::mCherry	fusion protein with mCherry fused to the C-terminus of SGAP
Str ⁺	denotes media supplemented with 10 $\mu\text{g ml}^{-1}$ streptomycin
TAE	Tris-acetate EDTA buffer
TB1 cells	<i>Escherichia coli</i> K12 TB1 cells
Tet ⁺	denotes media supplemented with 0.1 $\mu\text{g ml}^{-1}$ tetracycline
v/v	volume per volume
w/o/w	water-in-oil-in-water
w/v	weight per volume
w/w	weight per weight
wt	wildtype

CONTENTS

<i>Acknowledgments</i>	iii
<i>Abstract</i>	v
<i>Résumé détaillé</i>	vii
<i>Abbreviations</i>	xv
<i>List of figures</i>	xxi
1. <i>Introduction</i>	1
1.1 Microfluidics	1
1.2 <i>Streptomyces griseus</i> aminopeptidase	3
1.2.1 Identification	5
1.2.2 Structure	6
1.2.3 Function	10
1.3 Goals of the project	20
2. <i>Materials and methods</i>	27
2.1 Materials	27
2.2 Bacterial strains	27
2.3 Preparation of buffers, media and reagents	28
2.3.1 Lysogeny broth media	28
2.3.2 Super broth media	28
2.3.3 LB agar plates	28
2.3.4 K_2HPO_4	28
2.3.5 Ampicillin	29
2.3.6 Chloramphenicol	29
2.3.7 Streptomycin	29
2.3.8 Tetracyclin	29
2.3.9 L-arabinose	30
2.3.10 N-2-hydroxyethylpiperazine-N'-2-ethanesulfonic acid	30
2.3.11 Phosphate-buffered saline	30
2.3.12 $CaCl_2$ stock solutions	30
2.3.13 $ZnCl_2$ stock solutions	31

2.3.14	Polymyxin B	31
2.3.15	Bovine serum albumin	31
2.3.16	Bis-(L-leucinyl)-rhodamine 110	31
2.3.17	Assay Mixture	32
2.3.18	EA surfactant in HFE 7500 oil	32
2.4	Standard procedures	32
2.4.1	Streaked plates	33
2.4.2	Overnight cultures	33
2.4.3	Induction cultures	33
2.4.4	Preparation of induced cells for microplate assays and microfluidic experiments	33
2.4.5	Measurement of optical density	34
2.4.6	Making competent cells	34
2.4.7	Transformation protocols	35
2.4.8	Agarose gels	36
2.4.9	Preparation of plasmid DNA	37
2.4.10	Polymerase chain reaction	39
2.4.11	Site-directed mutagenesis	39
2.4.12	Fluorescence-based measurements	39
2.4.13	DNA sequencing	41
2.4.14	Production of microfluidic devices	41
2.4.15	Ligation	41
2.5	Primers	41
2.5.1	Sequencing primers	41
2.5.2	Cloning primers	42
2.5.3	Site-directed mutagenesis primers	42
3.	<i>Development of a fluorescence-based assay for SGAP aminopeptidase activity</i>	44
3.1	Introduction	44
3.2	Materials and methods	47
3.2.1	Plasmid preparation	47
3.2.2	Making inactive mutants	48
3.2.3	Fluorescence-based assays with bacteria	49
3.2.4	K_M measurement	51
3.3	Results and discussion	52
3.4	Conclusions	63
4.	<i>Microfluidics with SGAP</i>	64
4.1	Introduction	64
4.2	Materials and methods	65
4.2.1	Testing the exchange of free rhodamine 110 between droplets	65
4.2.2	Occupancy	66
4.2.3	Screening	66
4.2.4	Sorting	68

4.3	Results and discussion	69
4.4	Conclusions	77
5.	<i>Normalization for expression level of SGAP — fusion protein with mCherry</i> . .	79
5.1	Introduction	79
5.2	Materials and methods	81
5.2.1	Cloning	81
5.2.2	Correlating mCherry fluorescence to SGAP activity	83
5.2.3	Comparison of SGAP peptidase activity between mCherry::SGAP and SGAP::mCherry	85
5.3	Results and discussion	85
5.4	Conclusions	88
6.	<i>Synthesis of 7-aminocoumarin-4-methanesulfonic acid</i>	91
6.1	Introduction	91
6.2	Materials and methods	93
6.2.1	Protection of 3-aminophenol	95
6.2.2	Pechmann condensation with protected 3-aminophenol	95
6.2.3	Sulfonation of protected 7-aminocoumarin	96
6.2.4	Deprotection of protected 7-aminocoumarin	96
6.2.5	Measurement of excitation and emission spectrum	97
6.2.6	Testing the exchange of free 7-aminocoumarin-4-methanesulfonic acid between droplets	97
6.3	Results and discussion	97
6.4	Conclusions	100
7.	<i>Flat and crystallizable emulsions</i>	102
7.1	Introduction	102
7.2	Materials and methods	104
7.2.1	<i>In vitro</i> transcription and translation	104
7.2.2	Emulsification and plating of emulsion	106
7.2.3	Analysis of flat emulsion	107
7.3	Results and discussion	107
7.4	Conclusions	113
8.	<i>General discussion</i>	114
8.1	Overall summary	114
8.2	Overall conclusions	116
8.3	Future work	119
9.	<i>Supplementary information</i>	121
9.1	Computer-aided design (CAD) files of microfluidic devices	121
9.2	ACMS synthesis	123

9.3	DNA and amino acid sequence of wildtype <i>Streptomyces griseus</i> aminopeptidase	128
9.4	Additional figures	130
	<i>Bibliography</i>	137

LIST OF FIGURES

0.1	La SGAP et certains de ses substrats	ix
0.2	Les résultats d’une sélection modèle utilisant la SGAP et la Δ SGAP en système microfluidique	xiii
1.1	Possible schemes for FADS	4
1.2	Structure of SGAP at 1.58 Å resolution.	7
1.3	Superposition of APAP onto SGAP	8
1.4	Hypothetical secondary calcium binding pocket in SGAP	9
1.5	Proposed catalytic mechanism of SGAP	15
1.6	SGAP-E131A in relation to the catalytic site	16
1.7	Proposed reaction mechanism for BNPP hydrolysis by SGAP	19
1.8	Catechol oxidase activity	21
3.1	Proposed fluorescence-based assay for peptidase activity of SGAP	45
3.2	Approach to making a frameshift mutation of SGAP	50
3.3	SGAP peptidase activity as a function of <i>E. coli</i> K12 TB1 cell density	53
3.4	SGAP peptidase activity as a function of Zn^{2+} and Ca^{2+} concentrations	55
3.5	The effects of different methods of cell lysis on SGAP peptidase activity in a cell suspension	57
3.6	The chemical structure of polymyxin B	58
3.7	Effect of substrate concentration on SGAP peptidase activity	60
3.8	The effect of ice-incubation and reheating on SGAP peptidase activity	62
4.1	The exchange rate of rhodamine 110 in microfluidic droplets	70
4.2	Determination of droplet occupancy and initial mean number of cells per droplet (λ)	72
4.3	The effect of different lytic agents on bacterial lysis and the SGAP peptidase assay in microfluidics	74
4.4	Results from a FADS-based model selection of SGAP from a mixture of SGAP and Δ SGAP	75
5.1	Structural visualization of fusion sites and mCherry	80
5.2	Excitation and emission spectra rhodamine 110 and mCherry	82
5.3	Plasmids used in the cloning of mCherry::SGAP and SGAP::mCherry	84
5.4	Correlation between mCherry fluorescence and SGAP reaction velocity	87

5.5	Quantitative comparison of SGAP peptidase activity between the fusion proteins mCherry::SGAP and SGAP::mCherry	89
6.1	Determination of the exchange rate of 7-amino-4-methylcoumarin between droplets	92
6.2	Synthesis strategy 7-aminocoumarin-4-methanesulfonic acid	94
6.3	Excitation and emission spectra of ACMS	99
6.4	Leakage of ACMS from microfluidic droplets	101
7.1	pIVEX2.2EM-LacZ plasmid	105
7.2	Analysis data for 2D emulsions	110
7.3	Photograph of a 2D emulsion containing $\Delta lacZ$	112
9.1	CAD designs of the devices used in this project	122
9.2	ACMS synthesis: $^1\text{H-NMR}$ data for protection of 3-aminophenol	124
9.3	ACMS synthesis: $^1\text{H-NMR}$ data for Pechmann condensation	125
9.4	ACMS synthesis: $^1\text{H-NMR}$ data for sulfonation of aminocoumarin	126
9.5	$^1\text{H-NMR}$ spectrum of 7-aminocoumarin-4-methanesulfonic acid	127
9.6	DNA and amino acid sequence SGAP	129
9.7	Graphical representation of an assay system for measuring two SGAP peptidase activities simultaneously using two fluorophores	131
9.8	Assessment of the detection limit for SGAP versus ΔSGAP	132
9.9	Optimization PCR of mCherry fragment	133
9.10	Theoretical graph indicating the possible scenarios when selecting for a secondary activity for SGAP with and without counterselection	134
9.11	Hypothetical graph indicating what would happen when fluorescence signals in microfluidics can be normalized based on expression level	135
9.12	Cloning of arabinose induction cassette into pKB3-CalB-his	136

1. INTRODUCTION

In this chapter, the reasons for using droplet-based microfluidics will be explained (section 1.1), followed by a discussion of the model enzyme: *Streptomyces griseus* aminopeptidase (SGAP; section 1.2). More specifically, the identification (section 1.2.1), structure (section 1.2.2) and function (section 1.2.3) of SGAP will be addressed. Finally, the goals of this PhD project will be highlighted, together with the reasons why SGAP is interesting for this project (section 1.3).

1.1 Microfluidics

Microtitre-plates are currently the most flexible and most widely-used screening platform, owing to the compartmentalization of the assays in the separate wells. However, reducing assay volumes to below 1–2 μl is problematic [1] and maximum is approximately 1 sample s^{-1} , even if sophisticated (and expensive) robotic handling is employed. Ultra high-throughput, on the other hand, can be obtained through the use of fluorescence-activated cell sorting (FACS), in which cells are analyzed and sorted at a rate of up to 7×10^4 cells s^{-1} [2]. Because cell fluorescence is detected in a continuous aqueous stream during FACS [3], the fluorescent marker(s) must remain either inside or on the surface of the cells to be sorted. So it is not possible to detect secreted enzymes using fluorogenic substrates. Additionally, in the case of intracellular enzymes, diffusion of the substrate and/or product across the cell membrane presents many challenges. Conventional FACS machines typically require a starting population of more than 10^4 cells [3] and are very

expensive. Moreover, FACS machines generate aerosols, which have serious implications concerning biosafety when working with biohazardous samples [4].

The aforementioned issues with FACS can potentially be circumvented by using microfluidic systems. When using these systems, it is possible to handle small numbers of cells, while working in inexpensive, sterile, aerosol-free, disposable devices [2, 5]. Continuous flow devices that sort cells by dielectrophoretic actuation, electrokinetic actuation, hydrodynamic flow-switching and optical forces are among the devices that have already been demonstrated to work (listed by Perroud *et al.* [6]). Still, compared to conventional FACS, flexibility is limited due to the absence of assay compartmentalization.

In order to increase the versatility of conventional FACS, assays can be confined in emulsion droplets by a technique called *in vitro* compartmentalization (IVC) [7]. As a result of compartmentalization, the reactions are separated as in microtitre plates, which consequently allows selection for enzymatic activity [8, 9]. However, there are three factors that limit the useability of IVC/FACS: (i) double (water-in-oil-in-water or w/o/w) emulsion structures must be generated since a standard FACS can only analyze aqueous streams (costly and laborious modifications need to be made to a FACS machine so that it can use an oil-based sheath fluid); (ii) the high degree of polydispersity in these w/o/w emulsions seriously limits quantitative analysis; and (iii) it is difficult to modify the contents of the droplets after they have been created [10]. To overcome these limitations, droplet-based microfluidic systems can be used, because these systems allow precise control over droplets. For example highly monodisperse droplets can be generated [11], fused [12–14], split [12, 15, 16] and separated or sorted by charging them and steering them with an electric field [17] or by exploiting dielectrophoresis [18], electrocoalescence [19], localized heating [20], or Rayleigh-Plateau instabilities [21]. Until the very recent demonstration of fluorescence-activated droplet sorting (FADS) [22] it has not been possible to sort droplets based on their fluorescence. During FADS the

assays are compartmentalized, as in microtitre-plates, but the assays are analyzed and sorted rapidly (at a rate of $\sim 10^3$ samples s^{-1}), which is analogous to FACS, essentially combining the best of both techniques.

FADS, in principle, can be performed in two different setups, which are depicted in figure 1.1. The first setup represents the procedure if it was performed on an integrated chip and the second represents the procedure if it was performed by incubating the emulsion off-chip and reinjecting the emulsion in another chip. A general review [23] was recently published providing an overview of the basics of many different droplet-based microfluidics modules. Glass capillaries [24] were used as off-chip reservoirs for the incubation of the SGAP peptidase assay. On-chip incubation in delay lines has been described as well [25].

In short, droplet microfluidics and FADS were chosen for this project to have the best of two different types of analysis: microtitre plates, with their inherent separation of reactions and versatility, and FACS for the throughput and the capacity to isolate specific samples of interest. In the following section the model protein will be discussed before discussing the goals of the project and the role of the model protein in achieving these goals.

1.2 *Streptomyces griseus* aminopeptidase

After showing that microfluidics can form a bridge between the separated reactions of microtitre wells and the throughput of FACS, the model system will be discussed. The initial identification of SGAP, followed by its structure and function will be explained.

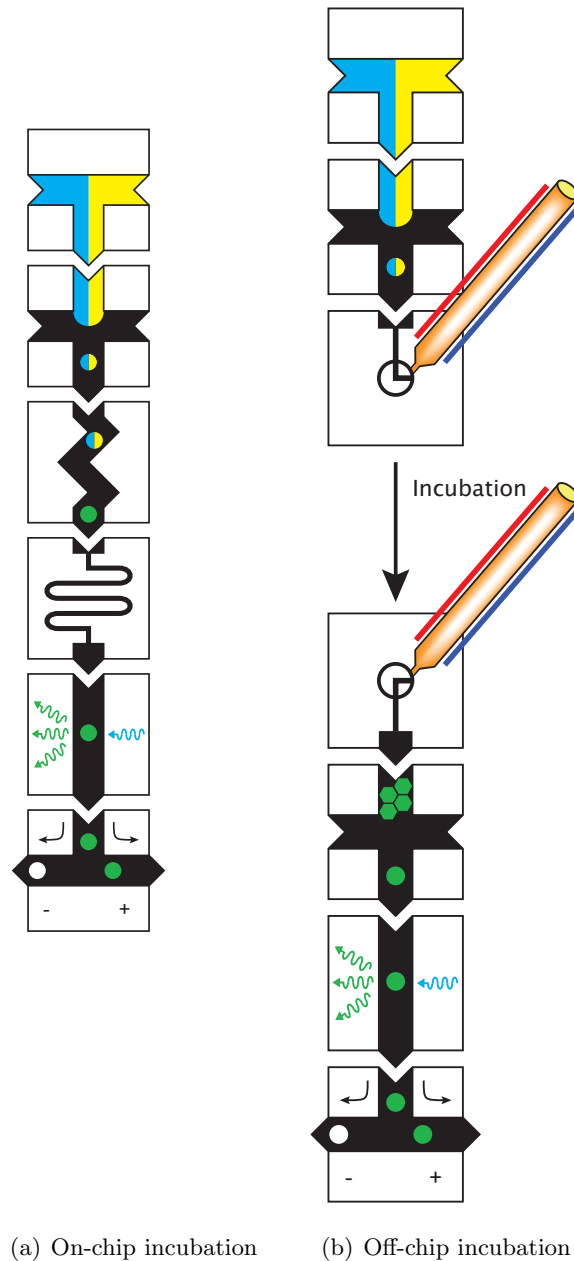


Fig. 1.1: Possible schemes for FADS. (a) The left scheme shows an integrated device for on-chip incubation in which a co-flow would lead to droplet formation (first two units). The droplets would then be mixed (third unit), incubated in a delay line (fourth unit) before fluorescence detection (fifth unit) and selection (sixth unit). (b) The second option is depicted on the right-hand side, with an off-chip incubation. An emulsion would be made by a co-flow and then incubated in a glass capillary off-chip. After a period of incubation, the droplets would be reinjected, fluorescence measured and selected.

1.2.1 Identification

Vosbeck and colleagues were the first to specifically report purification protocols and preliminary tests on what they called aminopeptidase-1 and aminopeptidase-2 from Pronase (EC 3.4.24.-) [26–28]. The MeSH term Pronase is defined as: “A proteolytic enzyme obtained from *Streptomyces griseus*,” and falls into the tree structure of hydrolases (D08.811.277). Because of very few differences in amino acid composition, however, it was soon argued that aminopeptidase-1 and aminopeptidase-2 were in fact products of the same gene [27]. Early experiments demonstrated that this extracellular aminopeptidase is small, monomeric, heat-stable, and highly active exhibiting highest activity in slightly alkaline conditions (pH around 8.0). Additionally, SGAP was found to contain zinc and calcium under native conditions, to be calcium-activated and calcium-stabilized, to prefer large, hydrophobic residues as the last or second-to-last amino acid, easy to immobilize and purified readily [26–30].

Further characterization of *Streptomyces griseus* aminopeptidase (SGAP; EC 3.4.11.10) started more than a decade after the first purifications and characterizations, confirming that SGAP was indeed a small zinc metalloprotein—284 amino acids with a putative molecular weight of 29.7 kDa—that was activated and stabilized by calcium as well as reversibly inactivated by chelating and free amino acids [30–34].

Nowadays, SGAP is counted as part of the M28 evolutionary family (clan MH) of metallopeptidases [35]. According to the MEROPS peptidase database, this family contains carboxypeptidases and aminopeptidases that have co-catalytic zinc ions from organisms ranging from humans to Archaea. In addition, a recent paper showed that analogous L-leucine aminopeptidases are common in *Streptomyces* spp. [36].

Similar leucine aminopeptidases, such as *Aeromonas proteolytica* aminopeptidase, porcine liver aminopeptidase and bovine lens aminopeptidase were also shown to contain zinc

ions, which is common in nature for aminopeptidases [37–42]. Furthermore, there are indications of variable activities of aminopeptidases with different cofactors or cofactor compositions [38–40, 43–45]. Interestingly, calcium stabilizes SGAP and modulates activity by decreasing affinity for and hydrolysis of an N-terminal lysine while increasing affinity for and hydrolysis of an N-terminal leucine as well as affinity for transition-state analogue-based inhibitors, such as bestatin [31, 32, 34, 46–48].

1.2.2 Structure

Structural studies on SGAP were performed largely after the basic characterization of SGAP had been completed. These crystallographic studies showed that the basic structure of SGAP consists of eight β -sheets and nine α -helices (Figure 1.2) [49–51]. Further structural details from the crystallographic studies include the dizinc binding pocket and the primary calcium binding pocket (Figure 1.2 (c) and (d)). The two zinc ions are around 3.6 Å apart from each other and the calcium binding pocket is ~ 25 Å away from the zinc ions [50, 52].

It was mentioned earlier that peptidases with high similarities to SGAP also contain zinc ions. The similarities between different aminopeptidases, however, go beyond being metalloproteins. Sequence similarity between SGAP and *Aeromonas proteolytica* aminopeptidase (APAP) is only $\sim 30\%$. Nonetheless, they have similar tertiary structures (see Figure 1.3), metal centers and putative reaction mechanisms [33].

It was long thought that the calcium binding site depicted in Figure 1.2 (d) affected overall structure of the protein or had some long-distance effect causing these shifts in affinity and hydrolysis [34, 49, 53]. However, Arima and colleagues argued for the existence of a second putative calcium binding pocket in SGAP (Figure 1.4), based on residues that are important in calcium stabilization and activation [52]. So far, no structural studies have been published to support this hypothesis.

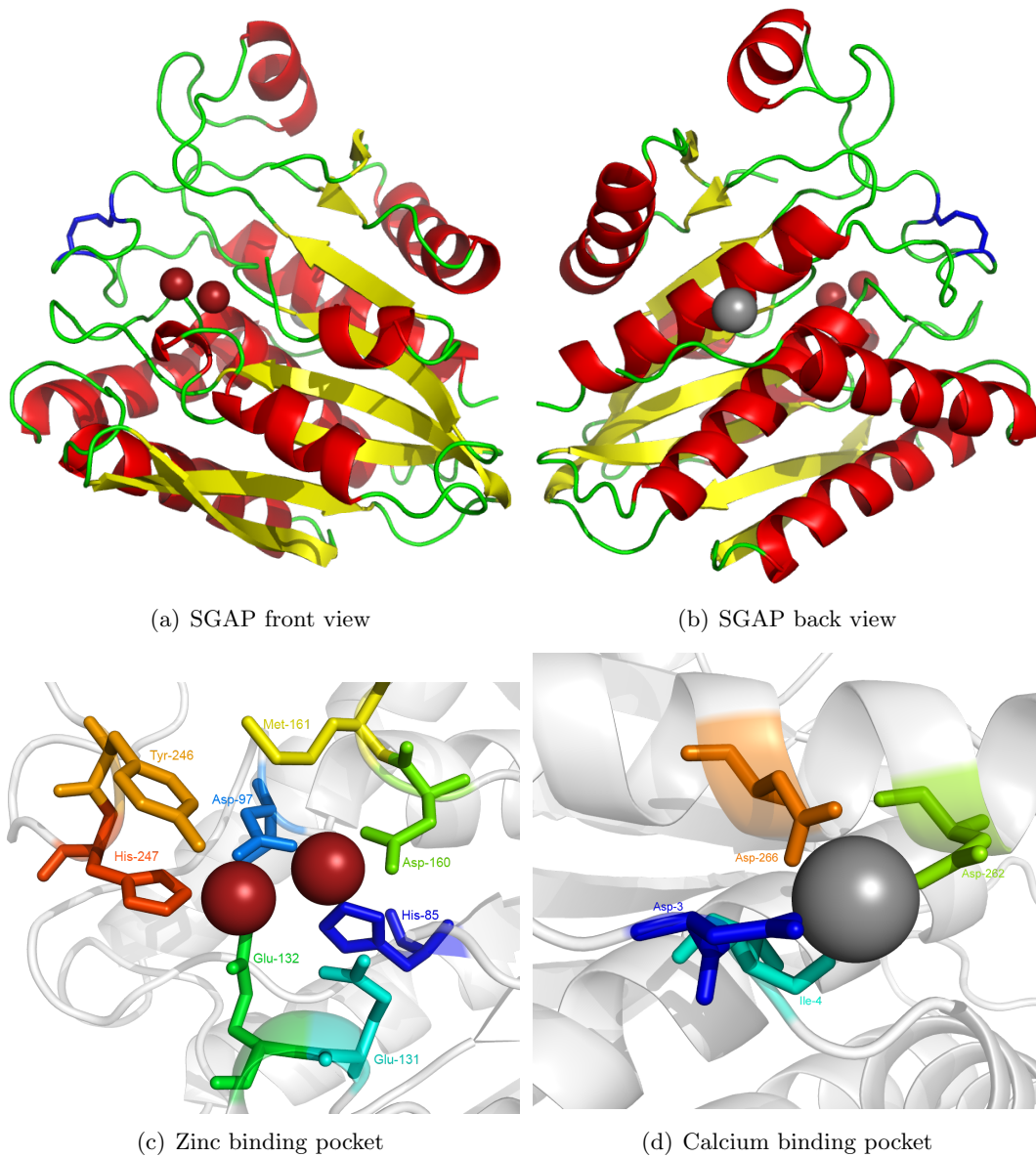


Fig. 1.2: Structure of SGAP at 1.58 Å resolution. α -helices are indicated in red, β -sheets are indicated in yellow and the Cys245-Cys250 disulfide bridge is blue (a, b). The two zinc ions are represented by dark red spheres and the calcium ion is depicted as a dark gray sphere in all views. (a) and (b) are the front and back view of the protein, respectively, turned over 180° on the y-axis of the protein. Detailed structures for the binding pockets of the zinc ions and calcium ion are shown in (c) and (d), respectively. For the detailed binding pockets, the interacting residues are colored and named individually and the underlying structure of the protein is visible as the translucent white cartoon. Visualized using PDB file 1CP7 [50].

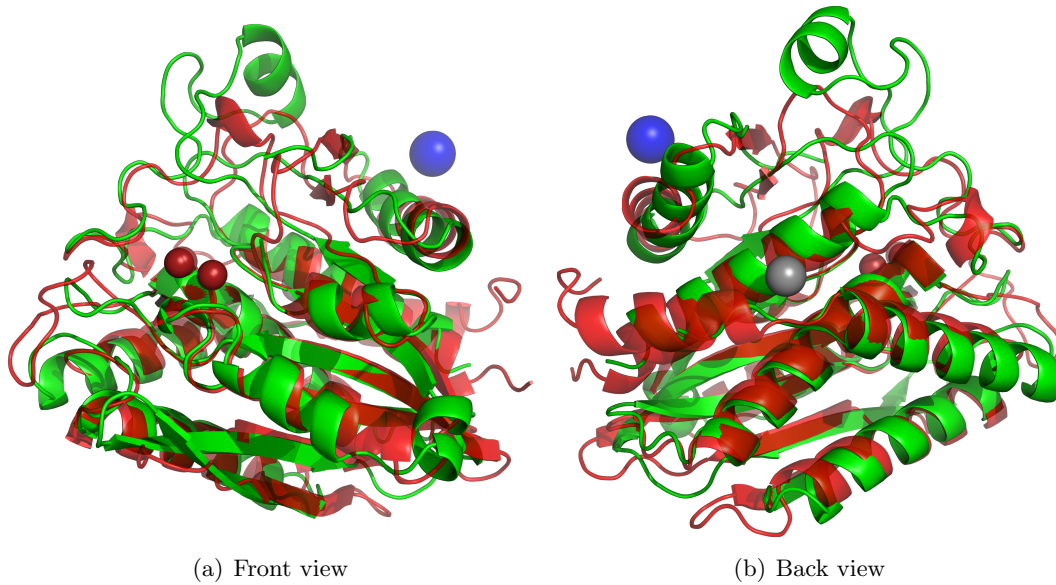


Fig. 1.3: Superposition of APAP (0.95 Å resolution; PDB file 1RTQ [54]) onto SGAP (1.58 Å resolution; PDB file 1CP7 [50]) based on the complete enzymes. The structures were aligned using the UCSF Chimera package from the Resource for Biocomputing, Visualization, and Informatics at the University of California, San Francisco (supported by NIH P41 RR-01081) [55]. SGAP is depicted in solid green, with its zinc ions in dark red spheres and the bound calcium ion as a dark gray sphere. APAP is made slightly translucent and depicted in red with the bound zinc ions as dark red spheres and the bound sodium as a blue sphere. (b) The back view is turned over 180° on the y-axis with respect to (a) the front view .

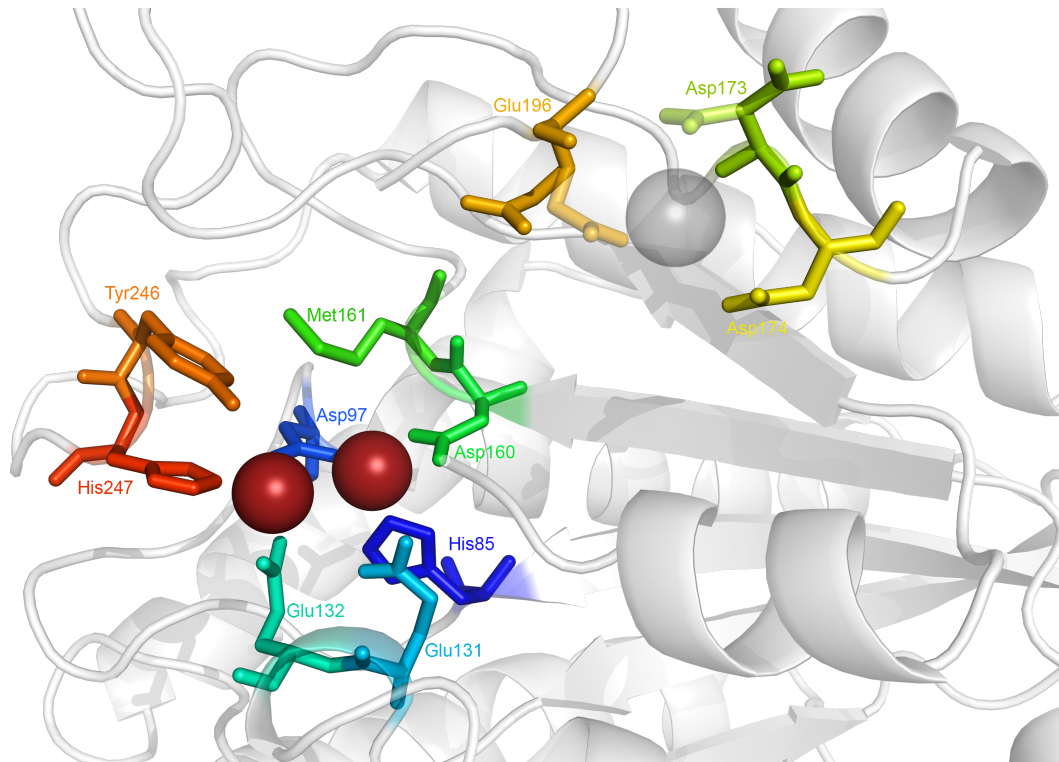


Fig. 1.4: Hypothetical secondary calcium binding pocket in SGAP [52]. The binding site of zinc is drawn to show the location of the secondary calcium site in the protein. The solid colors represent native conformations. Calcium binding (translucent gray sphere) probably changes the conformation of Glu-196 and Asp-173, as seen by the transparency of those residues. The underlying structure of the protein is visible as the translucent white cartoon. Visualized using PDB file 1CP7 [50].

1.2.3 Function

The way SGAP functions has been studied ever since the discovery of the protein. It has been demonstrated that SGAP preferentially hydrolyzes N-terminal leucine, methionine and phenylalanine residues [32]. The length of the peptide is important for the hydrolytic activity of SGAP and the penultimate residue also contributes to catalytic efficiency (see Table 1.1) [56]. When the penultimate residue is proline, SGAP is not active [32].

Two aspects that are very similar in reaction mechanisms of aminopeptidases are, firstly, that acidic residues (specifically Glu-131 in SGAP) mediate a bifurcated interaction between the metal ions and, secondly, that one of the metals assists activation of water into a nucleophilic hydroxide ion [42, 53]. The reaction mechanism of SGAP will be explained later on in this section.

Recently, it was demonstrated that SGAP is a promiscuous enzyme, because SGAP also hydrolyzes phosphoester bonds and oxidizes catechols [57–61]. What enzyme promiscuity is exactly and which type of promiscuity holds true for SGAP, will be discussed in this section. Its two known different promiscuous activities will be discussed in this section as well.

Promiscuous activity

The old views of protein catalysis were “lock and key” and induced-fit [62, 63]. Now a new view is emerging [64]. In this view, rather than having only one ideal conformation, an enzyme can exist in different states that have similar free energy levels. From the existence of proteins that are natively unstructured, but become structured when a ligand is present [65–67], it becomes clear that proteins can probably exist in multiple conformations. Hypothetically, multiple conformations could mean that one enzyme has multiple functions [68]. Proteins with multiple activities are, apparently, quite abundant

Tab. 1.1: Kinetic parameters of SGAP for several substrates in the presence of calcium [56]. Leu = L-leucine, pNA = *p*-nitroanilide, Phe = L-phenylalanine, Ser = L-serine, Tyr = L-tyrosine. pNA is the leaving group that is generally used for chromogenic assays, which is detected at A₄₀₅.

Substrate	k_{cat} (s ⁻¹)	K_m (mM)	k_{cat}/K_m (mM ⁻¹ s ⁻¹)
Leu-pNA	441 ± 21.2	0.55 ± 0.05	802
Leu-Phe	457 ± 40.4	1.49 ± 0.22	309
Leu-Ser	485 ± 40.4	2.05 ± 0.21	237
Leu-Tyr	114 ± 4.35	0.55 ± 0.06	209
Phe-pNA	21.8 ± 1.2	0.47 ± 0.05	46.4
Phe-Phe	212 ± 10.7	0.28 ± 0.05	785
Phe-Phe-Phe	463 ± 13.4	0.36 ± 0.01	1290

[68, 69].

Besides the evidence that supports the new view of protein dynamics, it has been hypothesized from the 1950s onwards that gene duplication is important in molecular evolution [70] and has since become a more widely accepted idea [71, 72] with more and more supporting data being published.

The theoretical role of gene duplication in evolution was first postulated by Jensen [72]. The idea is that enzymes must have possessed a minor secondary activity that gave them a selective advantage over other enzymes in evolution. As a theoretical example, the native function of SGAP is cutting N-terminal amino acids. Another known function is oxidation of catechols. If this catechol oxidation is sufficiently high with respect to the catechol oxidase activity of other enzymes or the metal-activated oxidation of catechols, then SGAP has a selective advantage to evolve into a catechol oxidase over proteins that do not possess this function. In time, doubling of the gene for SGAP could lead to the divergent evolution of SGAP, with one gene variant remaining largely the same in order to continue its aminopeptidase role and another gene variant evolving into a catechol oxidase. The causative agent of such divergent evolution of proteins could be, for example, changing environmental conditions.

This entire idea might explain why in nature common binding sites or mechanistic features are so prevalent [73–83]. In general then, it is not strange that different sequences can fold into similar configurations and thus catalyze similar reactions or that one configuration can catalyze multiple reactions. Promiscuity, which is hypothesized to be present since the beginning of evolution, could then be thought of as a method of generating complexity in nature without needing to develop new genes from scratch [69].

The existence of the so-called protein superfamilies, for which there is no clear definition [83], only supports the role of divergence in evolution (e.g. [74–76, 78–84] and many more in [68]). When looking at APAP and SGAP (Figure 1.3), the structures are very

similar, even though there is only 30% overlap in sequence. These two enzymes fall into the classic definition of a superfamily (sharing less than 50% sequence similarity, yet having a common function [85]).

However, promiscuity and evolution only go together if a certain secondary function in a protein becomes advantageous within only a few mutations [86]. Interestingly, promiscuity almost never leads to decreased performance in the original reaction [87]. Stepwise in evolution, it is then logical to assume that enzymes go from being a specialist to being a generalist and then back to being a specialist [86].

Within the broad space covered by the term ‘multiple activities’, there are some specific types of promiscuous activity that are slightly ambiguous in their definitions [69, 84]:

- **Moonlighting** is when a protein has an additional function that is not based on its original active site. Often this is structural or regulatory, rather than functional.
- **Multi-specificity** is when a protein has a comparable function, but for a distinctly different ligand. This may or may not be based on different residues than those involved in the original function.
- **Cross-reactivity** is when a protein has overlapping functions for ligands resembling the original ligand. They can also be substrate analogues.
- **Promiscuity** (or poly-reactivity) is when a protein has multiple functions at a single active site. The mechanism of action is often different between the functions. In poly-reactivity, the residues that are used in catalyzing a reaction can be the same as with the other reactions or be different.

SGAP, as will become clear in the following subsections, is an enzyme that exhibits promiscuity, cross-reactivity and multi-specificity. Since SGAP has a broad substrate specificity, it can be considered to be cross-reactive. In addition, SGAP can hydrolyze

phosphomonoesters and phosphodiesteres. These reactions are hydrolytic in nature, but the substrates are distinctly different from peptides, which means that SGAP is multi-specific. Finally SGAP can oxidize catechols, which is a fundamentally different reaction type than hydrolysis. Consequently, SGAP is also promiscuous or poly-reactive. Why these characteristics make SGAP a good model enzyme to investigate evolution will be explained in section 1.3.

Aminopeptidase activity

Since hydrolyzing N-terminal amino acids is the primary function of SGAP, the catalytic mechanism for the aminopeptidase activity is largely understood [42, 49–51, 88, 89] and is depicted in a simplified way in Figure 1.5. The canonical catalytic mechanism is briefly described here.

Tyr-246 stabilizes the binding of the amino acid that will be cut, possibly by polarization of the carbonyl carbon of the N-terminal amino acid. Glu-131, Asp-160 and Arg-202 then interact with the N-terminal amine group. Glu-131 works as a general base that takes up one electron from the water molecule that interacts with both zinc ions. The zinc ions, together with Tyr-246, stabilize the tetrahedral intermediate formed by the oxygen in the peptide in this step. The hydroxide nucleophile attacks the carbonyl carbon of the targeted peptide bond. A *gem*-diolate intermediate is then formed, which is a diolate that has both hydroxy moieties on the same carbon. Subsequently the electron that was taken up by Glu-131 is transferred to the amine group of the bond that will be cut. This will lead to breaking down of the *gem*-diolate intermediate and the release of the amino acid.

The importance of Glu-131 for catalytic activity is demonstrated by the significant decrease of activity (four to five orders of magnitude) when mutating this residue to alanine or aspartic acid [88, 89] (for structural details of the active site, see figure 1.6).

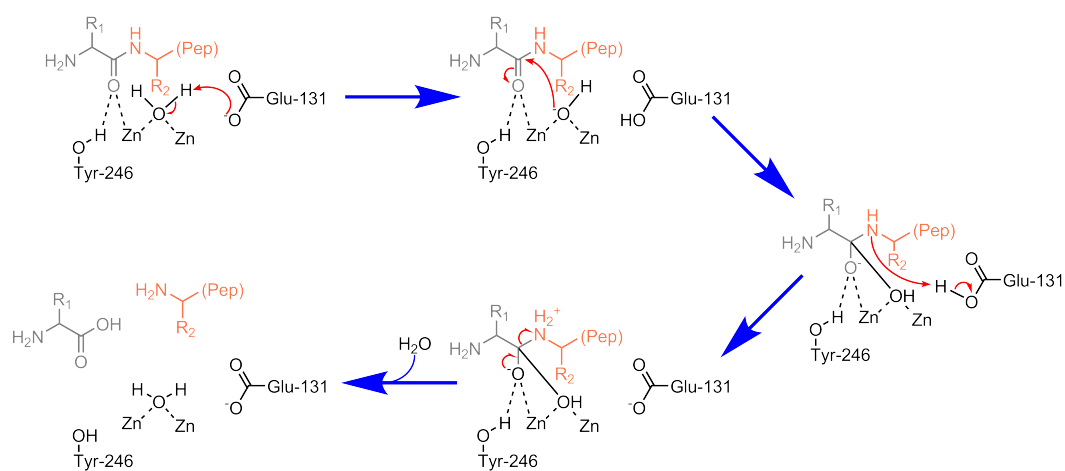


Fig. 1.5: Proposed catalytic mechanism of SGAP. The mechanism is more elaborately described in the text. The ultimate residue that will be cleaved off the peptide (Pep) is colored gray. The penultimate residue is colored in orange and electron-transfers have been indicated by red arrows. Adapted from Hershcovitz *et al.* [89].

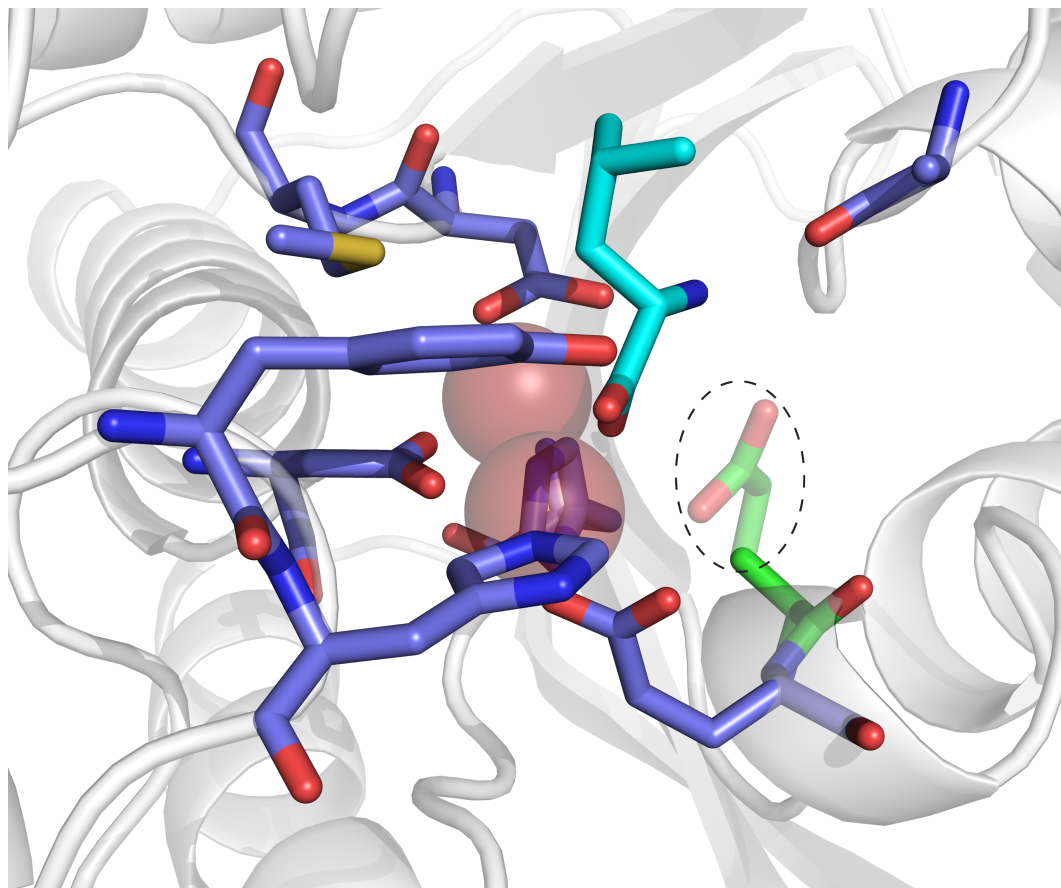


Fig. 1.6: SGAP-E131A in relation to the catalytic site at a resolution of 1.70 Å. The two zinc ions are represented by the translucent dark red spheres. All stick residues are colored with atomic colors (red for oxygen, blue for nitrogen, yellow for sulfur). The residues that are important for binding or catalytic activity have a lavender color for the carbons. The bound L-leucine has cyan-colored carbons. The mutation E131A is seen in the bottom right corner and has green as an atomic carbon color. The solid green is the alanine and the translucent part of the residue, outlined by the dashed ellipse, is where the glutamic acid is located in the wildtype. The underlying structure of the protein is visible as the translucent white cartoon. Visualized using PDB file 1F2O [51].

Glu-196 is probably important in defining the specificity of SGAP. Assuming that the second calcium binding site exists, the Glu-196 residue would be forced into a different conformation by the addition of calcium [52, 90] (Figure 1.4). Two separate papers by Arima *et al.* suggest that a second calcium binding site exists. In one paper [52] they found that Asp-173, Asp-174 and Glu-196 are important for the stability of SGAP. In addition, these residues increase the catalytic activity of SGAP when calcium is added. However, when mutating Glu-196 into an alanine, SGAP peptidase activity for lysine is almost completely abolished. In the second paper [90] they showed that Glu-196 is important in the substrate binding site. Furthermore, they showed that mutating Glu-196 into many other amino acids means that calcium-activation is lost. They again showed a greater effect on SGAP peptidase activity for lysine than on SGAP peptidase activity for leucine when mutating Glu-196. Taking these two results together leads to the conclusion that Glu-196 is involved in the possible binding of a second calcium ion and simultaneously affects substrate specificity of SGAP. Structural data supporting this hypothesis is not yet available.

Phosphodiesterase activity

Several publications have reported phosphodiesterase hydrolyzing activity of di-zinc substituted SGAP [57, 58, 60, 61]. Many of the enzymes exhibiting phosphomonoesterase, phosphodiesterase (cyclic as well as non-cyclic) or phosphotriesterase activity are based on active sites containing zinc ions [91–94], analogous to the active site of SGAP.

The first time that SGAP was demonstrated to hydrolyze phosphodiesteres was in 1999 [57]. The specific hydrolysis of bis(*p*-nitrophenyl) phosphate (BNPP) is $33.7 \text{ nmol min}^{-1} \text{ mg}^{-1}$ ($k_{cat}/K_M = 100 \text{ M}^{-1} \text{ s}^{-1}$). In comparison, several phosphatases or phosphodiesterases hydrolyse BNPP with specific activities of 0.3–2450 $\text{nmol min}^{-1} \text{ mg}^{-1}$ [95, 96]. Compared to autohydrolysis of BNPP, SGAP speeds up breakdown 10^{10} -fold and com-

pared to synthetic metal-containing models by 10^6 -fold [57, 60]. In 2000, it was shown that BNPP-hydrolysis by SGAP was not incidental, since hydrolysis of *p*-nitrophenyl phenylphosphonate (NPPP), which contains a P–C bond, is also quite effective and comparable to some phosphatases and phosphodiesterases [58]. SGAP seems to possess catalytic specificity toward some phosphate-based substrates [60]. The observations that phosphomonoester and phosphotriester hydrolysis by SGAP are beyond the spectrophotometric detection limit indicates that SGAP is specifically a phosphodiesterase [58].

The postulated mechanism is similar to peptide hydrolysis (see figure 1.7), since BNPP hydrolysis is also inhibited by, for example, bestatin—an inhibitor of peptide hydrolysis [57]. Furthermore, BNPP and Leu-*p*NA competitively bind to SGAP [57]. The hypothesis is that the P–O[−] unit emulates the carbonyl group of a peptide [57, 60]. Then, a hydroxide ion attacks the phosphate, leading to the release of one of the *p*NA units of BNPP. It is hypothesized that the water molecule involved in the phosphodiesterase activity is close to Tyr246 [60]. Nonetheless, it has been suggested that Glu-131 is also involved in some way in this reaction [58, 60], although its exact function is unknown. Although analogy to the *gem*-diolate is expected, phosphodiester hydrolysis has been hypothesized to pass via an “in-line” S_N2 type attack in bulk and in phosphodiesterase enzymes [97, 98]. The exact reaction mechanism in SGAP remains to be determined.

Catechol oxidase activity

Only one short communication from 2005 has mentioned the catechol oxidase activity of SGAP [59]. A general catechol oxidase reaction is depicted in Figure 1.8, along with the two substrates that were used in the paper. SGAP substituted with copper (CuCu-SGAP) approaches the catechol oxidase activity of the respective enzyme from

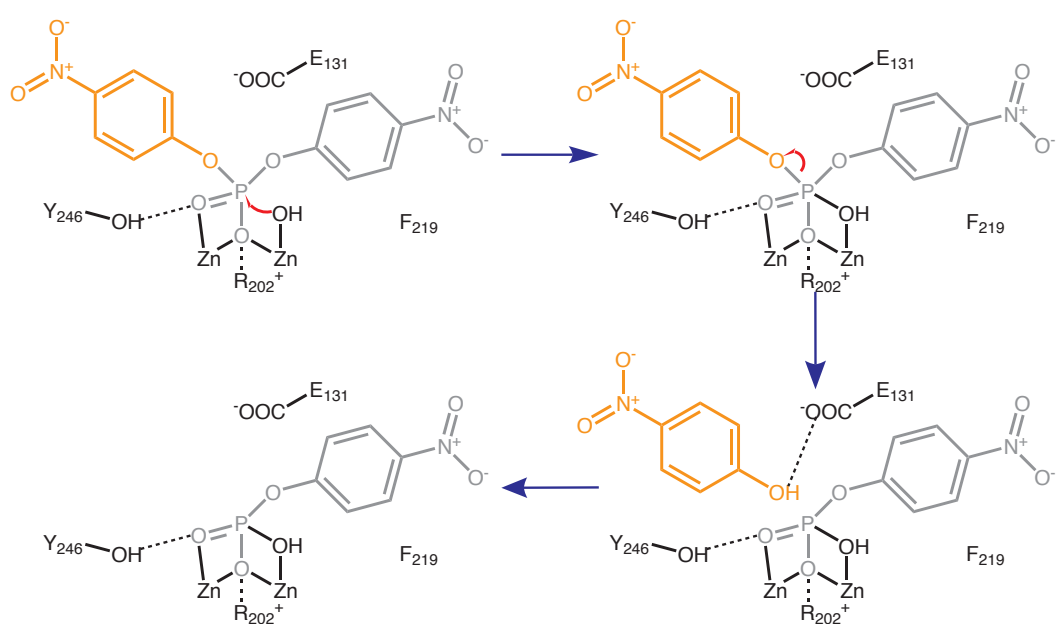


Fig. 1.7: Proposed reaction mechanism for BNPP hydrolysis by SGAP [61].

gypsywort [99] (Table 1.2) and is more active than metal complex-based catechol oxidase activity. Interestingly, bestatin is once again a potent inhibitor of this activity with a similar K_i to amino acid hydrolysis (8.8 μM versus 11.0 μM , respectively). Therefore, catechol probably binds to the protein in a similar fashion to amino acids. Furthermore, it has been demonstrated that one single substrate molecule binds per protein molecule [59].

In the chromogenic assay described in the paper demonstrating catechol oxidase activity in SGAP, 3,5-di-*tert*-butylcatechol (DTC; Figure 1.8) was used. A biologically important catechol, dopamine, is also slowly oxidized by SGAP with a k_{cat}/K_m of 0.162 $\text{mM}^{-1} \text{s}^{-1}$. Even though oxidation and hydrolysis are very different reactions, there is some structural analogy between catechol and L-leucine (Figure 1.8). This structural analogy is the hypothetical basis for the activity of the protein on both substances.

When H_2O_2 is added to the reaction, the k_{cat}/K_m nearly doubles, mostly due to an increase in k_{cat} . The hypothesis following this observation is then that H_2O_2 helps the formation of a $\text{Cu}^{2+}_{2-\mu-\eta^2:\eta^2}$ -peroxo intermediate [59, 100], allowing the reaction to run more easily. In a $\mu-\eta^2:\eta^2$ state, an O_2^{2-} -molecule is situated between the two copper atoms [100].

1.3 Goals of the project

In the previous sections, it was discussed that FADS could bridge the versatility of microtitre plate assays and the throughput of FACS. Next, the proposed model enzyme, SGAP, was introduced, together with the principles of promiscuous activity. These principles were then applied to SGAP for its palette of reactions, where the broad substrate specificity for the peptidase activity could be interpreted as cross-reactivity, the phosphoesterase activity could be interpreted as multi-specificity and the catechol oxidase

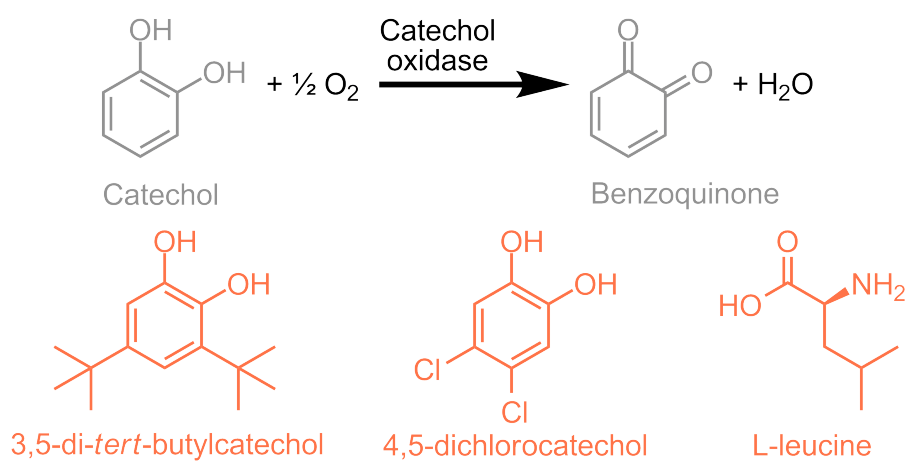


Fig. 1.8: Catechol oxidase activity. The upper part of the image is the general reaction catalyzed by a catechol oxidase enzyme. In this reaction catechol is oxidized to benzoquinone and water is released in the process. Generally, this reaction is visualized by measuring A_{420} , which is the peak absorbance for benzoquinone or benzoquinone analogues. The lower part of the figure shows two analogues that were used in the measurements by da Silva and colleagues [59], as well as L-leucine in a theoretically comparable orientation as the catechols. 3,5-di-tert-butylcatechol is the substrate used in standard chromogenic assays and 4,5-dichlorocatechol was used as a slow substrate to titrate binding stoichiometry of catechol and SGAP.

Tab. 1.2: Kinetic parameters of SGAP versus *Lycopus europaeus* catechol oxidase and synthetic metal complexes for 3,5-di-*tert*-butylcatechol [59, 99].

Enzyme	k_{cat} (s ⁻¹)	K_m (mM)	k_{cat}/K_m (mM ⁻¹ s ⁻¹)
SGAP	1.45	0.44	3.3
<i>Lycopus europaeus</i> catechol oxidase	5.0	160	32
Synthetic metal complexes [59]			0.0010–0.45

activity could be interpreted as promiscuity. In this section it will be explained why these properties make SGAP a good candidate for directed evolution by microfluidics/IVC, which is the long-term aim of this project.

There are not many proteins known to possess such diverse activities as SGAP. Still, there may be some overall structural overlap between structures that are involved in the reactions (see for example Figure 1.8). Catalytic promiscuity and evolution have been coupled many times before in literature. How they are coupled and what then makes a promiscuous enzyme such an interesting model for directed evolution, will also be explained in this section.

As a general rule, enzymes that pass through several cycles of directed evolution often become less active, but accept more substrates (becoming a so-called ‘generalist’) before specializing again to a new function [101]. But if the protein of interest does not possess an inherent cross-reactivity, it will be difficult to evolve this activity.

It was explained in section 1.2.3 that structurally similar binding sites are very common in nature and that it is suspected that gene duplication plays an important role in evolution. Furthermore, similar protein structures can perform very disparate functions. In contrast, various different types of conformation have been implicated in similar functions. SGAP is cross-reactive, multi-specific and promiscuous in the form in which it is found in nature, which probably makes it an evolutionary intermediate [84]. Consequently, it is an ideal model system for various sorts of experiments in directed evolution.

The long-term aims of this project are to address several outstanding questions in evolution biology through directed evolution via droplet microfluidics. There are several fundamental questions that can be addressed using SGAP. Examples of such questions are:

-
- *How does genetic drift function?* To answer this question it would be interesting to have a duplicated gene in the system and select for two activities at the same time. It would then become apparent whether the two parental genes each evolve in a different direction and thus become specialists or whether there would be a different outcome.
 - *What is the influence of negative selection on the evolution of a protein?* SGAP, with its multiple inherent activities, allows selection for multiple activities. So far, an enzyme has not been selected with and without counterselection for the native activity in the laboratory. It is, therefore, unknown whether the sequence and function would differ between an evolved protein that is theoretically allowed to retain its original function, and one that is specifically chosen to lose the original function (see supplementary figure 9.10).
 - *What would be the influence on evolution if a ‘generalist’ is specifically selected?* This question is the contrary of the previous question (see supplementary figure 9.10). If two reactions are used in a selection, it is also possible to specifically select a protein that possesses both activities. It would be interesting to see whether this protein is more adept at evolving a third activity.
 - *Can evolvability be evolved?* Evolvability, or the potential of an entity to evolve [102, 103], is a contentious issue in evolution biology [104, 105]. In particular, it seems hard to test and thus definitively assess whether evolvability can be evolved or selected. SGAP is an interesting candidate to empirically test this hypothesis, again because of the palette of reactions that it already catalyzes. The idea would then be to go back and forth between two activities in the scope of directed evolution. Completely hypothetically, four rounds of selection could be performed for phosphodiesterase activity, followed by four rounds of selection for aminopeptidase function. Repeating this cycle several times would ‘train’ the protein. Finally, the

‘trained’ protein could be compared to the parental protein to see whether it evolves towards the catechol oxidase function more rapidly or not, thereby supplying an answer to this question.

The microfluidics setups currently available preclude the use of absorbance-based assays, which is in direct contrast to all the SGAP activity assays performed so far. These assays were based on the cleavage of L-leucinyl-*para*-nitroaniline (Leu-*p*NA). After hydrolysis, the freed *p*NA is detected by an increase in absorbance at 405 nm (A_{405}). The primary goal of this project was to devise a strategy to enable the use of SGAP in microfluidics and demonstrate that a model selection can be performed based on SGAP activity. To this end, bis-(L-leucinyl)-rhodamine 110 was chosen as a fluorogenic substrate. Hydrolysis of this compound liberates rhodamine 110, which can be monitored by way of fluorescence ($\lambda_{ex} = 488$ nm and $\lambda_{em} = 525$ nm).

At the outset of the project, there was not a suitable fluorinated oil/surfactant combination to allow *in vitro* transcription and translation or the amplification of single genes in droplets, which is necessary for IVTT. Therefore, a bacterial expression system was chosen, in which recombinant SGAP would need to be expressed in the periplasm, because it has a Cys245-Cys250 disulfide bond.

The principal goal of this project was to prepare and validate this new and untested system for selections in microfluidics, in the aim of allowing directed evolution to be performed later on. To this end the assay needed to be developed in microplate (chapter 3) before being verified in microfluidics. Finally performing a model selection would be performed to validate activity-based selection of SGAP (chapter 4).

A second goal of this project concerned a general observation that the distribution of the fluorescence signal from reactions is often very broad in the droplets, certainly in systems where individual cells are analyzed. A source of this variation is from cell-to-cell variations in expression levels [106]. An internal normalization standard should

allow the distribution to be tightened considerably (see supplementary figure 9.11). To this end, a fusion protein was made with a fluorescent marker. mCherry [107], a red fluorescent protein, was chosen for the fusion, since most peptidase substrates are based on rhodamine 110 (green fluorescence) or coumarin (blue fluorescence). The experiments pertaining to this are explained mostly in chapter 5, but some of the microfluidics results are mentioned in chapter 4.

In addition, since many of the possible long-term questions depend on detection of and selection for multiple activities, a new substrate needed to be synthesized. At the outset of the project there were no fluorescence-based assays known for catechol oxidation or phosphodiesterase activity. Consequently, a secondary substrate was sought for the SGAP aminopeptidase activity. Generally, if the substrate is not based on rhodamine 110 for a peptidase assay, it is based on 7-aminocoumarin. However, these substrates leak from the droplets (L. Granieri, personal communication). It was, therefore, necessary to try to synthesize a 7-aminocoumarin that would not exhibit this behavior. This synthesis and the preliminary results for this molecule in microfluidics are discussed in chapter 6.

Finally, in collaboration with the Bibette laboratory (ESPCI, Paris), 2D emulsions, or flat and crystallizable emulsions, were developed to detect rare activities in large gene libraries as a side-project. The biological validation of this technique is described in chapter 7.

2. MATERIALS AND METHODS

The protocols described in this chapter are standard practices and not experimental. Experimental techniques are described in Chapters 3-7.

2.1 Materials

Unless explicitly stated, materials came from Sigma and were of molecular biology grade. MilliQ water (MQW; Millipore SAS, Molsheim, France) was purified to 18.2 M Ω cm resistivity. When running experiments in which nucleases or RNases could have been harmful, DNase-free and RNase-free water (NFW) was used.

2.2 Bacterial strains

For cloning in all vectors except pKB4, XL10 Gold cells (Stratagene Corp., Agilent Technologies, Massy, France) were used. XL10 Gold cells have a Tet^R $\Delta(mcrA)183$ $\Delta(mcrCB-hsdSMR-mrr)173$ *endA1 supE44 thi-1 recA1 gyrA96 relA1 lac* Hte [F' *proAB lacI^qZ* Δ M15 Tn10 (Tet^R) Amy Cam^R] genotype.

All other cloning experiments, as well as protein expression experiments, were performed in *Escherichia coli* K12 TB1 cells (New England Biolabs, Ozyme, St. Quentin Yvelines, France), with the genotype F⁻ *ara* $\Delta(lac-proAB)$ [ϕ 80*dlac* $\Delta(lacZ)$ M15] *rpsL(Str^R) thi hsdR*.

2.3 Preparation of buffers, media and reagents

Unless otherwise specified, all solutions were kept at room temperature.

2.3.1 Lysogeny broth media

Lysogeny broth (LB) was made by dissolving the appropriate amount of powder in water, followed by autoclaving the media for 5 minutes at 121°C.

2.3.2 Super broth media

Super broth (SB) was made by dissolving 20 g l⁻¹ tryptone, 10 g l⁻¹ yeast extract and 5 g l⁻¹ sodium chloride in MQW. The medium was then autoclaved for 5 minutes at 121°C.

2.3.3 LB agar plates

LB agar plates were made by dissolving 4 grams of LB agar powder in 100 ml of MQW. The agar was subsequently sterilized by microwave [108]. LB agar was supplemented with antibiotics when the agar was below 60°C. The plates were left to dry for approximately one hour and then put at 4°C. Before use, the plates were incubated in a 37°C oven upside down for one hour to dry completely.

2.3.4 K₂HPO₄

For stock solutions of 1.5 M K₂HPO₄ (molecular weight: 174.18 g mol⁻¹), 65.32 grams of powder were weighed out and dissolved to a final volume of 250 ml using MQW. The solution was then separately autoclaved at 121°C for 5 minutes. The final concentration of K₂HPO₄ in media was always 50 mM (a 30-fold dilution from the stock solution).

2.3.5 *Ampicillin*

An ampicillin stock solution of 100 mg ml⁻¹ was prepared in MQW, aliquotted and stored at -20°C. The final working concentration of ampicillin was 100 µg ml⁻¹, a 1 000-fold dilution of the stock solution. Media supplemented with ampicillin are denoted Amp⁺.

2.3.6 *Chloramphenicol*

A chloramphenicol (Roth Sochiel E.U.R.L., Lauterbourg, France) stock solution of 30 mg ml⁻¹ was prepared in pure ethanol. The stock solution was stored at -20°C. The final working concentration of chloramphenicol was 30 µg ml⁻¹, a 1 000-fold dilution of the stock solution. Media supplemented with chloramphenicol are denoted Cam⁺.

2.3.7 *Streptomycin*

A streptomycin stock solution of 100 mg ml⁻¹ was prepared in MQW, aliquotted and stored at -20°C. The final working concentration of streptomycin was 10 µg ml⁻¹, a 10 000-fold dilution of the stock solution. Media supplemented with streptomycin are denoted Str⁺.

2.3.8 *Tetracyclin*

A tetracyclin stock solution of 1 mg ml⁻¹ was prepared in pure ethanol, aliquotted and stored at -20°C. The final working concentration of tetracyclin was 0.1 µg ml⁻¹, a 10 000-fold dilution of the stock solution. Media supplemented with tetracyclin are denoted Tet⁺.

2.3.9 L-arabinose

A 20% (w/w) stock solution of L-arabinose (Roth Sochiel E.U.R.L., Lauterbourg, France) was prepared in MQW. The stock solution was filtered through a 0.22 μm filter, aliquotted and stored at -20°C until use. The final concentration used in inductions was 0.02% (w/w), a 1 000-fold dilution of the stock solution.

2.3.10 N-2-hydroxyethylpiperazine-N'-2-ethanesulfonic acid

Initially, a 0.5 M solution of N-2-hydroxyethylpiperazine-N'-2-ethanesulfonic acid (HEPES; molecular weight: 238.31 g mol^{-1} ; Roth Sochiel E.U.R.L., Lauterbourg, France) was made by dissolving 59.58 grams of powder in 200 ml MQW. The pH was adjusted to 8.5 using 1 M or 5 M NaOH. The solution was then adjusted to 250 ml and filtered through a 0.22 μm filter. For use, 4 ml of concentrated HEPES solution was diluted to 50 ml in MQW (to a final concentration of 40 mM) and the pH was verified after dilution. The diluted solution was kept at 4°C .

2.3.11 Phosphate-buffered saline

A purchased 10 \times phosphate-buffered saline (PBS) solution was filtered through a 0.22 μm filter and served as a stock solution. For use, the stock solution was diluted tenfold (to 1 \times) in MQW and the pH was verified to be 7.4 after dilution. The diluted solution was kept at 4°C until use.

2.3.12 CaCl_2 stock solutions

Working solutions were made in MQW at 250 mM and 50 mM concentrations. The solutions were filtered through a 0.22 μm filter. Unless otherwise specified, the working

concentration of CaCl_2 was 1 mM.

2.3.13 ZnCl_2 stock solutions

Working solutions were made in MQW at final concentrations of 50 mM and 10 mM. The solutions were filtered through a 0.22 μm filter. Unless otherwise specified, the working concentration of ZnCl_2 was 100 μM .

2.3.14 Polymyxin B

As soon as the polymyxin B arrived, a 50 mg ml^{-1} stock solution in MQW was made. The solution was filtered through a 0.22 μm filter and split into aliquots of ≤ 1 ml. The aliquots were immediately transferred to -20°C . The aliquot that was used was kept at 4°C , but for no more than 2 weeks. The final concentration of polymyxin B in solutions was 2 mg ml^{-1} .

2.3.15 Bovine serum albumin

Protease-free bovine serum albumin (BSA; Roth Sochiel E.U.R.L., Lauterbourg, France) was dissolved to a final concentration of 10 g l^{-1} in either 40 mM HEPES, pH 8.5 or 10 mM PBS, pH 7.4, depending on the experiment. The solution was filtered through a 0.22 μm filter and kept at 4°C until use. The working concentration of BSA was always 1 g l^{-1} .

2.3.16 Bis-(L-leucinyl)-rhodamine 110

Bis-(L-leucinyl)-rhodamine 110 (L2R; Promega, Charbonniere, France) was dissolved to a concentration of 100 mM in DMSO. Final concentrations in assays were either 10 μM

or 120 μM , unless otherwise stated. It is worth noting that the final concentration of DMSO in the reactions was always 5% (v/v), regardless of the substrate concentration that was used.

2.3.17 *Assay Mixture*

Unless otherwise specified, the Assay Mixture for standard fluorescence-based assays used in experiments throughout this project contained 100 μM ZnCl_2 , 1 mM CaCl_2 , 2 mg ml^{-1} polymyxin B, 1 g l^{-1} protease-free BSA, 120 μM L2R and 5% (v/v) DMSO. When necessary, the assay mixture was supplemented with 50 μM resorufin or 0.1 μM rhodamine 110 for microfluidics. The assay mixtures were made in 40 mM HEPES, pH 8.5 or 1 \times PBS, pH 7.4.

2.3.18 *EA surfactant in HFE 7500 oil*

EA surfactant (RainDance Technologies, Lexington, MA, USA), a PEG-PFPE amphiphilic block copolymer [109], was diluted to 2% (w/w) in HFE 7500 fluorinated oil (3M, St. Paul, MN, USA) by heating to 50°C for approximately 5–10 minutes in a water bath.

2.4 *Standard procedures*

When refrigeration was required during the centrifugation of small samples (≤ 2 ml) a Hettich Mikro 22 R microcentrifuge was used. Otherwise, an Eppendorf table-top microcentrifuge (Eppendorf SARL, Le Pecq, France) was used. Samples in 15 ml or 50 ml conical centrifugation tubes were centrifuged in an Eppendorf 5810R Centrifuge (Eppendorf SARL, Le Pecq, France).

2.4.1 Streaked plates

A culture was streaked out on an LB agar plate (Str⁺ or Tet⁺, if appropriate) directly from a glycerol stock at -80°C using a metal 1 µl inoculation loop. The plate was put in an incubator at 37°C for 14h and then stored at 4°C.

2.4.2 Overnight cultures

A single colony was picked from a plate with a metal 1 µl inoculation loop and used to inoculate 5 ml of liquid media in a 50 ml conical tube. The tube was incubated at 37°C for 14h with 230 rpm agitation. Liquid cultures were stored for, at most, 5 days at 4°C.

2.4.3 Induction cultures

5 ml of SB/Cam⁺ containing K₂HPO₄ in a 50 ml conical tube was inoculated with a 1% seed of an overnight culture of *E. coli* K12 TB1 cells carrying the appropriate plasmid. The dilution culture was incubated at 37°C with 230 rpm agitation until reaching 1–2 Optical Density Units at 600 nm (ODU₆₀₀). Then the cultures were diluted to 0.2 ODU₆₀₀ into induction media, with a final volume of 5 ml. The induction media consisted of SB/Cam⁺ supplemented with K₂HPO₄ and L-arabinose. Induction cultures were incubated for 24h at 18°C with 230 rpm agitation.

2.4.4 Preparation of induced cells for microplate assays and microfluidic experiments

1 ml of induced cells was washed twice by spinning down at 3 000 rcf, 4°C for 5 minutes and re-suspending in ice-cold buffer (either 40 mM HEPES or 1× PBS). After the second washing step the optical density of the cells was measured. The cells were diluted to

the appropriate OD₆₀₀ just before use. Unless specifically noted otherwise the bacterial suspensions were used at 0.50 ODU₆₀₀ for fluorescence-based analyses and 0.052 ODU₆₀₀ for microfluidic experiments.

2.4.5 *Measurement of optical density*

The OD₆₀₀-measurements were performed in a Uvikon 922 Spectrophotometer (Kontron Instruments) using 1 cm path-length disposable cuvettes. Cultures at a density of ≥ 1 ODU₆₀₀ were diluted tenfold to allow precise measurements.

2.4.6 *Making competent cells*

Chemically competent cells

XL10 Gold cells were streaked out on an LB/Tet⁺ plate. The following day, an overnight culture in LB/Tet⁺ was started. The day after, a culture of 250 ml of LB media was inoculated with a 1% (v/v) seed of the overnight culture and left to grow until 0.4–0.6 ODU₆₀₀. Subsequently, the culture was aliquotted into four 50 ml centrifugation tubes and pelleted by centrifugation (3 000 ref, 15 minutes, 4°C). From then on, the entire protocol was performed on ice. The pellets were re-suspended in 5 ml of ice-cold 50 mM CaCl₂ each. The samples were pooled into 2 aliquots that were adjusted to 20 ml each and left on ice for 20 minutes before centrifuging again. 450 µl ice-cold, sterile glycerol was added to each sample. The volume was adjusted to 3 ml with ice-cold 50 mM CaCl₂ before re-suspension. Once re-suspended, the cells were incubated on ice for 2.5 hours before aliquotting and storing at -80°C.

Electrocompetent cells

The MQW and 10% (v/v) solution of glycerol in MQW were filtered through a 0.22 μm filter prior to use. *E. coli* K12 TB1 cells were streaked out on an LB/Str⁺ plate. The following day an overnight culture was started in SB/Str⁺ containing K₂HPO₄. The day after, 250 ml of SB containing K₂HPO₄ was inoculated with a 1% (v/v) seed of the overnight culture. When the culture reached 0.5–0.7 ODU₆₀₀ it was aliquotted into 4 \times 50 ml and put on ice for 30 minutes. From then on, the entire protocol was performed on ice. The cells were pelleted by centrifugation (3 000 rcf, 15 minutes, 4°C). Each pellet was then re-suspended in 50 ml of ice-cold MQW and spun down again. The pellets were re-suspended in 10 ml of ice-cold MQW and pooled. The cells were incubated for another 30 minutes on ice and subsequently centrifuged. The pellet was re-suspended in 40 ml of 10% (v/v) glycerol, spun down, and re-suspended in 1.6 ml of 10% (v/v) glycerol before aliquotting and storing at -80°C.

2.4.7 Transformation protocols

Transformation by heat-shock

For each transformation, a 1.5 ml microcentrifuge tube was incubated on ice for 2 minutes. 1 μl of DNA (at a concentration of 0.1 ng μl^{-1}) was added to the microcentrifuge tube. The chemically-competent cells were always thawed on ice. Once the cells were thawed completely, 50 μl of cells or 10 μl of cells (when using commercial XL10 Gold cells) were added to the DNA and mixed gently. The mixture was left on ice for 30 minutes before heat-shocking in a water bath at 42°C for 30 seconds. After heat-shock, the mixture was put back on ice for an additional 2 minutes, before being made up to 500 μl with LB. The mixture was incubated in an Eppendorf Thermomixer (Eppendorf SARL, Le Pecq, France) at 37°C with 800 rpm mixing for 1 hour. Finally, 100 μl of cells

were plated on an LB agar plate containing the appropriate antibiotic. The plates were incubated at 37°C for 14 hours and then stored at 4°C for ≤ 4 weeks.

Transformation by electroporation

For each transformation, a 2 mm path-length electroporation cuvette (BTX, Harvard Apparatus SARL, Les Ulis, France) was chilled on ice and *E. coli* K12 TB1 cells were thawed on ice. 1 μ l of DNA or ligation mixture was added to the cuvette and 50 μ l of TB1 cells were added. Electroporation was performed using a Bio-Rad Genepulser Xcell (Bio-Rad, Marnes-la-Coquette, France) set at 2500 kV, 200 Ω resistance and 25 μ F capacitance. The cells were made up to 500 μ l with LB and transferred to a 1.5 ml microcentrifuge tube. They were then incubated for 60 minutes at 37°C, 800 rpm in an Eppendorf Thermomixer. Next, 100 μ l of cells were plated on an LB agar plate containing the appropriate antibiotic. The plates were incubated at 37°C for 14 hours and then stored at 4°C for ≤ 4 weeks.

2.4.8 Agarose gels

Agarose gels were made with 1.0% (w/v) agarose in Tris-acetate EDTA (TAE-buffer) to separate fragments larger than 1 kilobase (kbp). To separate fragments between 100 basepairs (bp) and 1 kbp, 1.5% (w/v) agarose gels were made. All gels contained 0.5 μ g ml⁻¹ ethidium bromide and a 1.5 mm thick GT Mini Comb (Bio-Rad, Marnes-la-Coquette, France) was used to form the wells.

Electrophoresis

Gels were electrophoresed using a Bio-Rad PowerPac Basic (Bio-Rad, Marnes-la-Coquette, France) at 80 V during 45 minutes for fragments larger than 1 kbp and at 60

V for 70 minutes for fragments between 100 bp and 1 kbp. For purification purposes, a setting of 60 V for 60 minutes was used.

Purification from gel

After electrophoresing the gel, the desired bands were excised and purified using a Wizard SV Gel and PCR Clean-Up System (Promega, Charbonniere, France) following the manufacturer's instructions.

Quantification

Quantification of band intensities on agarose gels was performed using a Kodak Gel Logic 200 Imaging System and Kodak Molecular Imaging Software version 4.0.5f7 (Carestream Health, New Haven, CT, USA).

2.4.9 Preparation of plasmid DNA

Mini prep

An overnight culture was grown in 5 ml of medium in a 50 ml conical tube. 1.5 ml of the culture were spun down at 6800 rpm in a tabletop centrifuge for 2 minutes. Next, a GeneJET Plasmid Miniprep kit (Fermentas GmbH, St. Leon-Rot, Germany) was used to purify the plasmid following the manufacturer's instructions. Purified plasmid was eluted with 50 μ l of EB buffer and then stored at -20°C .

Midi prep

50 ml of liquid media were inoculated with a 0.2% (v/v) seed of an overnight culture and then divided equally between three 50 ml conical tubes. The tubes were incubated at

37°C for 14h with 230 rpm agitation. The DNA was purified with a QIAGEN Plasmid Midi kit (QIAGEN S.A., Courtabœuf, France) following the manufacturer's instructions, until the addition of isopropanol to the purified DNA. After addition of the isopropanol, the solutions were aliquotted into four 2 ml microcentrifuge tubes. The DNA was spun down at 21 910 rcf for 30 minutes at 4°C. The supernatant was removed and each pellet was re-suspended in 500 µl of 70% (v/v) ethanol. The tubes were spun again for 10 minutes at 21 910 rcf, 4°C. After removing the supernatant, the pellets were dried by leaving the tubes open for approximately 30 minutes. Each pellet was re-suspended in 100 µl of NFW and the samples were pooled back together. Purified DNA was stored at -20°C.

Ethanol-precipitation

The solution of DNA was supplemented with 1 µl of 20 mg ml⁻¹ glycogen (Fermentas GmbH, St. Leon-Rot, Germany) before adding a $\frac{1}{10}$ volume of 3 M NaOAc, pH 5.3 and 3 volumes of 95% ethanol. The solution was mixed briefly. After incubating, the solution was cooled to -20°C for 1 hour and then centrifuged at 21 910 rcf for 30 minutes at 4°C. The supernatant was removed and the pellet was re-suspended in 100 µl of 70% (v/v) ethanol. The tube was centrifuged again at 21 910 rcf for 10 minutes at 4°C. After removing the supernatant, the pellet was dried by leaving the tube open on the bench for approximately 30 minutes. The pellet was then re-suspended in 30 µl of NFW and stored at -20°C.

Quantification

DNA concentrations were routinely quantified using a Nanodrop ND-1000 Spectrophotometer and ND-1000 V3.6.0 software (Thermo Fisher Scientific, Courtabœuf, France).

2.4.10 *Polymerase chain reaction*

The polymerase chain reaction (PCR) was routinely performed using a Bio-Rad DNA Engine Tetrad thermal cycler (Bio-Rad, Marnes-la-Coquette, France). Samples were prepared in a Captair Bio PCR hood (Erlab D.F.S. S.A.S., Val de Reuil, France). Pfu Turbo or Native Pfu (both from Stratagene Corp, Agilent Technologies, Massy, France) were used as the DNA polymerase. PCR mixtures consisted of 0.5 μM primers, 0.05 U μl^{-1} polymerase, 0.2 mM dNTPs and $1\times$ PCR buffer, containing the appropriate DNA template or bacteria.

Normal PCR reactions were performed in a final volume of 50 μl , whereas colony PCR reactions were performed in a final volume of 20 μl . The different PCR programs are described in table 2.1.

For colony PCR, single colonies were picked from appropriate plates using a 1 μl metal inoculation loop that was sterilized in a flame between samples.

2.4.11 *Site-directed mutagenesis*

Site-directed mutagenesis was performed using the QuikChange II Site-Directed Mutagenesis Kit (Stratagene Corp., Agilent Technologies, Massy, France) according to the manufacturer's instructions. The PCR program is described in table 2.1.

2.4.12 *Fluorescence-based measurements*

Fluorescence measurements were performed in a Molecular Devices SpectraMax M5 Spectrofluorometer with SoftMax V5.2 software (Molecular Devices, St. Grégoire, France). Typically, 20 readings were taken per measurement per well with a low photomultiplier tube (PMT) sensitivity. If possible, the temperature in the machine was

Tab. 2.1: The different programs of thermal cycling used in PCRs.

Step	Normal PCR	Colony PCR	QuikChange
	Heat lid to 100°C	Heat lid to 100°C	Heat lid to 100°C
1	95°C, 3 minutes	95°C, 10 minutes	95°C, 30 seconds
2	95°C, 30 seconds	95°C, 30 seconds	95°C, 30 seconds
3	57°C, 30 seconds	57°C, 30 seconds	55°C, 60 seconds
4	72°C, 2 minutes	72°C, 2 minutes	68°C, 12 minutes
5	Return to 2, 24 times	Return to 2, 24 times	Return to 2, 15 times
6	72°C, 10 minutes	72°C, 10 minutes	Store at 4°C
7	Store at 4°C	Store at 4°C	

maintained at 25°C. Assays performed in 96-well plates were at a final volume of 200 µl per well, and 40 µl per well in 384-well plates. In all cases, half of the final volume was a bacterial suspension or protein solution and the other half consisted of the other reaction components.

2.4.13 *DNA sequencing*

DNA was sequenced by Eurofins MWG Operon (Ebersberg, Germany). Sequenced DNA was clipped to exclude regions of low accuracy and aligned using the Vector NTI 10.0 alignment tool (Invitrogen, Paisley, Scotland). Sequencing data was checked by eye when any deviations from the expected sequence were observed.

2.4.14 *Production of microfluidic devices*

Microfluidic devices were manufactured from PDMS as described by Baret *et al.* [22].

2.4.15 *Ligation*

Ligations were routinely performed using 40 U of T4 DNA ligase (New England Biolabs, Ozyme, St. Quentin Yvelines, France), 1× ligation buffer and 100 fmol of DNA in a final volume of 10 µl. A 1:1 molar ratio of insert to vector backbone was used. Ligations were incubated at 16°C in an Eppendorf Thermomixer for 14h.

2.5 *Primers*

2.5.1 *Sequencing primers*

Table 2.2 lists the two primers that were used for sequencing: AraForw (forward primer) and SrHind3 (reverse primer).

2.5.2 *Cloning primers*

Table 2.2 lists the primers that were used for cloning.

2.5.3 *Site-directed mutagenesis primers*

Table 2.2 lists primers that were used for QuikChange site-directed mutagenesis. 090406_NAct_fw and 090406_NAct_bw were used to negate an inactivating mutation that occurred in the cloning procedure of mCherry::SGAP.

Tab. 2.2: Sequences of primers used for sequencing, cloning and site-directed mutagenesis. For the PCR primers the different features on the primers have been denoted by color coding. Most of these features, except for the BglII restriction site in KB87 and the EcoRI restriction site in KB88, were features that were newly introduced into the amplicon after PCR reactions.

Name	Sequence (5' → 3')	Features
<i>Sequencing primers</i>		
AraForw	AGT CCA CAT TGA TTA TTT GCA CGG	
SrHind3	TGA CGC AGT AGC GGT AAA CG	
<i>Cloning primers</i>		
KB87	ACG CTA GGA AGA TCT AGC GCC GGA CAT CCC GC	BglII
KB88	CAG GTC AGG AAT TCG GTT GGT GGT TCG CCG G	EcoRI
090113_pKB4_C_FW	ATC GAT CGA TGA ATT CAC GTA CGA GCT CAG TGG TTT ACG TAG TCG TGC TAT GGT GAG CAA GGG CGA GGA GGA TAA CAT GG	random, EcoRI, SacI, SGLRSRA
090107_pKB4_C_BW	CGA TCG ATC GAT CGA TGA ATT CCT TGT ACA GCT CGT CCA TGC CGC CG	random, EcoRI
090107_pKB4_N_FW	CGA TCG ATC GAT CGA TAG ATC TCA TGG TGA GCA AGG GCG AGG AGG ATA ACA TGG	random, BglII
090113_pKB4_N_BW	GAT CGA TCG ATC GAT AGA TCT ACA CGT ACG AGC TCA GAC GAC TAC GTA AAC CAC TCT TGT ACA GCT CGT CCA TGC CGC CG	random, BglII, SacI, SGLRSRA
sgap_forw_BglII	ACG CTA AGG AAG ATC TAG CGC CGG ACA TCC CGC	BglII
sgap_rev_EcoRI	CAG GTC AGG AAT TCG GTT GGT GGT TCG CCG G	EcoRI
<i>Site-directed mutagenesis primers</i>		
sgap-E131A-fw	CGG TTC GCC TGG TGG GGC GCC GCG GAG CTG GGC CTG ATC GGC T	
sgap-E131A-bw	AGC CGA TCA GGC CCA GCT CCG CGG CGC CCC ACC AGG CGA ACC G	
090406_NAct_fw	CAA GAG TGG TTT ACG TAG TCG TGC TGA GCT CGT ACG TGT AG	
090406_NAct_bw	CTA CAC GTA CGA GCT CAG CAC GAC TAC GTA AAC CAC TCT TG	

3. DEVELOPMENT OF A FLUORESCENCE-BASED ASSAY FOR SGAP AMINOPEPTIDASE ACTIVITY

3.1 Introduction

In section 1.3 it was explained that SGAP is a good model system to test several outstanding questions in evolution biology. The long-term aim is to answer these questions through directed evolution in microdroplets following the FADS technique [22]. However, at the outset of this project there were no fluorescence-based assays available for any of the activities of SGAP. As the only detection method currently available in droplet microfluidics is fluorescence, a fluorogenic substrate for SGAP activity was needed.

There are fluorogenic substrates available for phosphodiesterase activity, of which umbelliferone-based substrates are the most well-known [110]. Bis-(4-methylumbelliferyl)-phosphate has been used in various assays to detect phosphodiesterase activity since then, but SGAP is unable to hydrolyze this substrate (K. Blank, personal communication).

The proposed assay for SGAP peptidase activity is shown in figure (see figure 3.1). The fluorescence-based assay relies on the hydrolysis of bis-(L-leucinyI)-rhodamine 110 (L2R), which is detected by the liberation of rhodamine 110 ($\lambda_{ex} = 488$ nm and $\lambda_{em} = 525$ nm). Ideally, in order to determine enzyme kinetics better, a mono-substituted fluorogenic substrate would be used, but there was no mono-substituted fluorogenic substrate available for SGAP at the outset of the project.

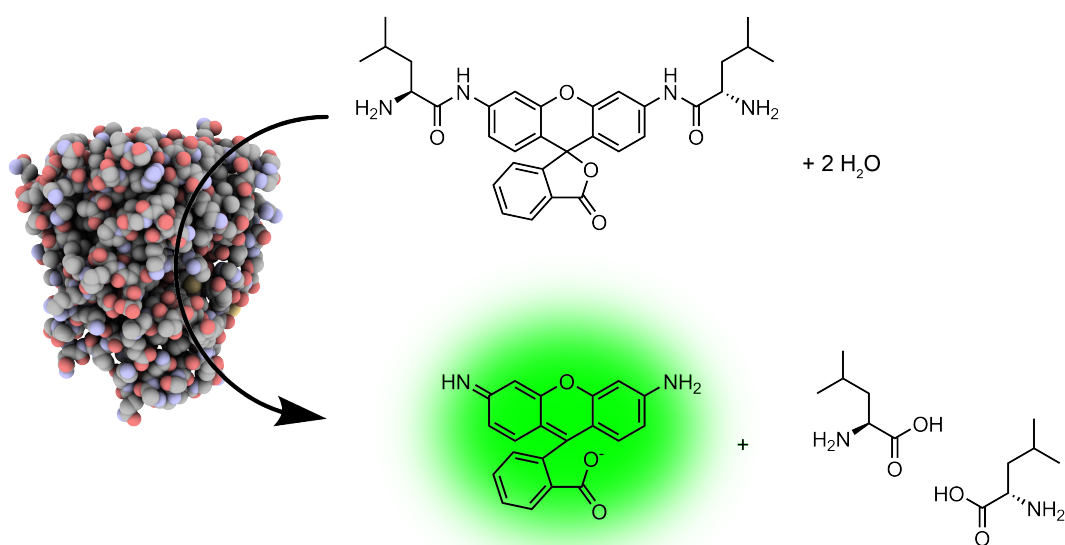


Fig. 3.1: Proposed fluorescence-based assay for peptidase activity of SGAP. In this reaction the fluorogenic substrate bis-(L-leucyl)-rhodamine 110 (L2R; top right) is hydrolyzed by SGAP into two L-leucine groups and a fluorescent rhodamine 110 leaving group (λ_{ex} = 488 nm, λ_{em} = 525 nm; bottom right).

A problem with the preexisting assays is that most use purified SGAP. A system was, therefore, needed for measuring aminopeptidase activity in crude bacterial lysates or *in vitro* transcription and translation (IVTT).

At the beginning of the project there were no biocompatible surfactants with which IVTT was feasible. In addition there was no system available for amplifying single genes in microfluidic droplets, which is necessary for IVTT. Therefore, an *in vivo* approach was chosen.

One feasible *in vivo* system for SGAP is to have it expressed periplasmically in bacteria, since in the periplasm are the conditions sufficiently oxidative to form and maintain disulfide bonds. Periplasmic expression of SGAP has not been reported in the literature before, which means that this system will need to be validated from the very first steps, including induction conditions.

In addition it is important that an assay is as simple as possible with a minimal number of steps in order to be feasible with microfluidic droplets (see figure 1.1). The simplest approach would consist of encapsulating bacterial cells already expressing SGAP with an assay mixture that will lyse or permeabilize the cells quickly while guaranteeing high peptidase activity of SGAP.

The cells must be lysed quickly after encapsulation because previous experiments have shown that L2R does not penetrate cells.

In this chapter the development of a fluorogenic assay for SGAP peptidase activity, which is compatible with droplet microfluidics, is described. The first thing that was checked was whether the fluorogenic assay itself was functional. Next, the concentrations of the cofactors (zinc and chloride) were verified before testing different lytic agents and determining the K_M of SGAP for L2R. Finally it was checked whether the assay could be incubated on ice without losing activity, since an ice incubation was necessary to

incubate microfluidic droplets for given amounts of time.

3.2 Materials and methods

The general methods have been described previously (see Chapter 2). Whenever deviations were made from the standard procedures, or when specific protocols were used, they are described more elaborately in this section.

3.2.1 Plasmid preparation

The basic plasmid for all manipulations (pKB4) has been described elsewhere [25]. Briefly, pKB4 is based on the plasmid pAK400 ([111]), which contains the strong ribosomal binding site (RBS) T7G10 and a *pelB* signal peptide for periplasmic expression. With slight modifications, this plasmid has been used for the expression of the enzyme *Candida antarctica* lipase B (CalB) in the periplasm of *E. coli* (pKB3-CalB-His [112]). The plasmid pKB3-CalB-His contains an N-terminal FLAG tag (flanked by an upstream *NcoI* and a downstream *BglIII* site) and a C-terminal His tag (flanked by an upstream *EcoRI* and a downstream *HindIII* site; see supplementary figure 9.12). In contrast to pKB3-CalB-His, which possesses a *lac* promoter, the derivative used for SGAP expression contains the arabinose inducible promoter of the pBAD series of plasmids (Invitrogen). To obtain this new plasmid the *lac* promoter region has been replaced with a DNA fragment coding for the *araC* repressor and the *araBAD* promoter (see supplementary figure 9.12). The gene for SGAP was amplified from the plasmid pET9d-SGAP ([88]) using the primers *sgap_forw_BglIII* and *sgap_rev_EcoRI*. The PCR fragment was purified, cut with *BglIII* and *EcoRI* and cloned into the pKB3-CalB-His derivative, yielding the new plasmid pKB4-SGAP-his. This new plasmid was verified by sequencing (section 2.4.13).

3.2.2 Making inactive mutants

Missense mutation

A missense mutation (glutamate to alanine at amino acid 131 or E131A) was made by QuikChange. The primers (sgap-E131A-fw and sgap-E131A-bw) are described in table 2.2. After the QuikChange, the plasmids were transformed by electroporation into TB1 cells (section 2.4.7). Ten colonies were grown as overnight cultures (section 2.4.2), induced (section 2.4.3) and checked in a standard fluorescence-based assay (section 2.4.12) with HEPES Assay Mixture (section 2.3.17). The plasmids from clones lacking significant SGAP activity were purified by Midi prep (section 2.4.9) and subsequently verified by sequencing (section 2.4.13).

Frameshift mutation

A frameshift mutation leading to a premature stop codon (Δ SGAP) was made as indicated in figure 3.2. 2 μ g of plasmid were restricted using 20 U of SalI in 1 \times NEBuffer 3, supplemented with 100 μ g ml⁻¹ BSA, in a final volume of 50 μ l for 1 hour at 37°C. Next, the DNA was ethanol-precipitated (section 2.4.9) before filling in the overhang. To this end 2 U of T4 DNA polymerase were added to 1 μ g of purified and restricted DNA, 500 μ M dNTPs and 1 \times NEBuffer 2, supplemented with 100 μ g ml⁻¹ BSA, in a final volume of 50 μ l. The reaction was incubated at 12°C for 15 minutes before inactivation by adding EDTA to a final concentration of 10 mM and incubating at 75°C for 20 minutes. The DNA was ethanol-precipitated (section 2.4.9), ligated (section 2.4.15), and transformed by electroporation into TB1 cells (section 2.4.7). Ten colonies were grown as overnight cultures (section 2.4.2), induced (section 2.4.3), and checked for the absence of SGAP activity (section 2.4.12), using HEPES Assay Mixture (section 2.3.17). The plasmids from interesting clones were purified by Midi prep (section 2.4.9) and

subsequently verified by sequencing (section 2.4.13).

3.2.3 Fluorescence-based assays with bacteria

Dilution series

An overnight culture (section 2.4.2) of *E. coli* K12 TB1 pKB4-SGAP-his cells was prepared and induced according to the standard protocol (section 2.4.3). The cells were washed as usual (section 2.4.4), except that the suspension was adjusted to a final OD₆₀₀ of 2.00 ODU. A serial dilution was then made of this suspension, diluting to 1.00 ODU₆₀₀, 0.50 ODU₆₀₀, 0.10 ODU₆₀₀, 0.050 ODU₆₀₀ and 0.025 ODU₆₀₀. Using the different suspensions a standard fluorescence-based assay (section 2.4.12) was performed using PBS Assay Mixture (section 2.3.17) containing 2 mg ml⁻¹ polymyxin B.

Lytic agents

An overnight culture of *E. coli* K12 TB1 pKB4-mCherry-SGAP cells was prepared (section 2.4.2) and induced (section 2.4.3). The cells were washed (section 2.4.4) and PBS Assay Mixture was prepared without polymyxin B (section 2.3.17). PBS was used as the no lysis control. PBS Assay Mixtures containing different lytic agents were supplemented to final concentrations of 2 mg ml⁻¹ polymyxin B, 1 × PopCulture (Novagen, EMD chemicals, San Diego, CA, USA), 1 × BugBuster (Novagen, EMD chemicals, San Diego, CA, USA), 1 × BugBuster Primary Amine Free (Novagen, EMD chemicals, San Diego, CA, USA), 10% (v/v) ethanol, 10% (v/v) chloroform or 10% (v/v) isopropyl alcohol. The densities of the bacterial samples were verified by measuring mCherry fluorescence ($\lambda_{ex} = 587$ nm and $\lambda_{em} = 610$ nm). The bacterial suspension was at 0.025 ODU₆₀₀ in the analysis.

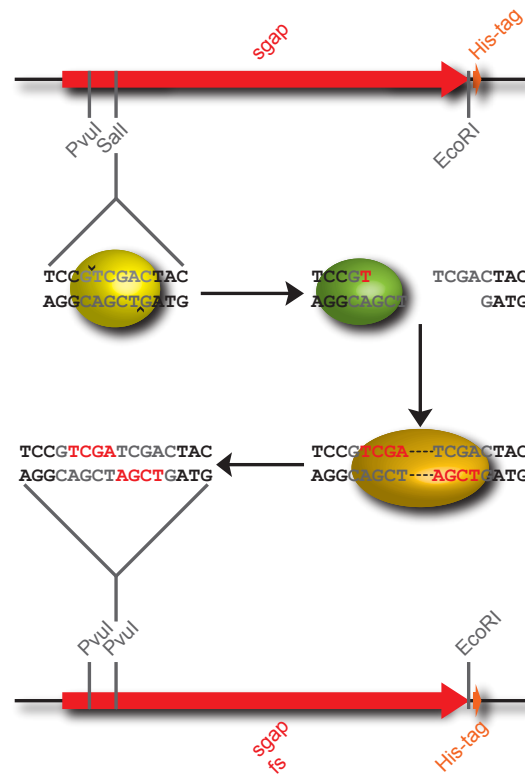


Fig. 3.2: Approach to making a frameshift mutation of SGAP. This frameshift leads to the introduction of a stop codon early in the encoding sequence. SGAP wildtype is restricted using SalI (a single-cutting restriction enzyme for the entire plasmid of pKB4-SGAP-his) indicated in yellow, with the recognition sequence in grey and the adjacent three basepairs in black. Within the grey recognition sequence the restriction site is indicated by the black arrowheads. The restricted plasmid is blunt-ended by using T4 DNA polymerase (indicated in green). The blunt-ended plasmid (with the inserted sequence indicated in red) is then re-ligated using T4 DNA ligase (orange protein; section 2.4.15). The re-ligated plasmid is 4 nucleotides longer and the SalI site has disappeared, while introducing a PvuI restriction site.

Cofactor optimization

An overnight culture of *E. coli* K12 TB1 pKB4-SGAP-his cells was prepared (section 2.4.2) and induced (section 2.4.3). Subsequently, the cells were washed (section 2.4.4) and standard PBS Assay Mixture was prepared (section 2.3.17), but without CaCl₂ or ZnCl₂. From the stock solutions of CaCl₂ appropriate dilutions were prepared to yield final concentrations of 5 mM, 4 mM, 3 mM, 2 mM and 1 mM. The stock solutions of ZnCl₂ were used to prepare dilutions with final concentrations of 500 μM, 400 μM, 300 μM, 200 μM and 100 μM. PBS was used to supplement the samples without CaCl₂ and/or ZnCl₂. A 2D grid of ZnCl₂ and CaCl₂ concentrations was prepared in the wells of a 384-well plate and the washed cells were added in order to optimize the cofactor concentrations.

Ice incubation assay

An overnight *E. coli* K12 TB1 pKB4-mCherry-SGAP-his culture was prepared (section 2.4.2), induced (section 2.4.3) and washed (section 2.4.4). PBS Assay Mixture was prepared (section 2.3.17) and added in a 1:1 volume ratio to the cells. A fluorescence measurement (section 2.4.12) over 10 minutes was started immediately and the mix was incubated on ice. Ten minute-measurements were performed every 20 minutes from the ice-incubated sample. mCherry fluorescence was measured as well ($\lambda_{ex} = 587$ nm and $\lambda_{em} = 610$ nm) to ensure that there were no big differences in the quantities of cells between samples.

3.2.4 K_M measurement

Purified SGAP was purchased and diluted in 1× PBS. The final quantity of protein was 50 U per sample. PBS Assay Mixture was prepared without polymyxin B and L2R

(section 2.3.17). L2R was serially diluted such that final concentrations in the assay were between 500 μM and 50 μM with 50 μM steps between the concentrations. Each sample, including the sample without L2R, contained 5% (v/v) DMSO. The fluorescence assay was performed following the standard protocol (section 2.4.12).

3.3 Results and discussion

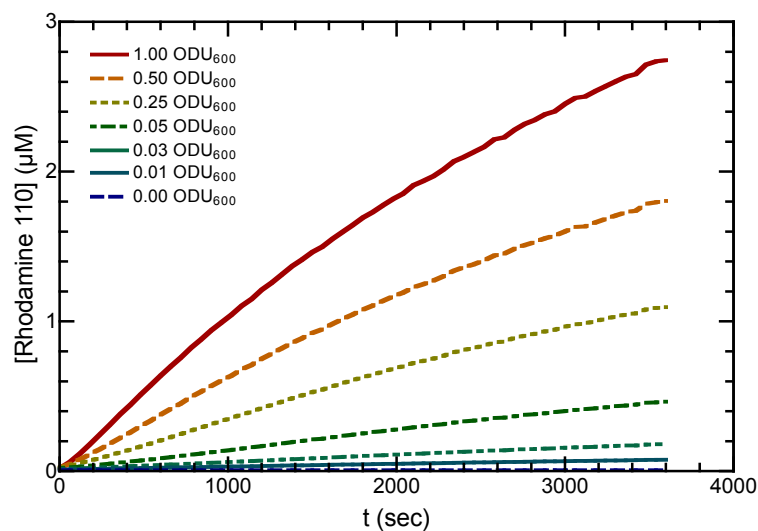
The directed evolution of SGAP by droplet-based microfluidics necessitated a new expression strategy and a fluorescence-based assay for SGAP peptidase activity.

The bacterial strain (*Escherichia coli* K12 TB1) and the expression vector (pKB4) have previously been used to express β -lactamase in the periplasm [25]. In this case, β -lactamase was subsequently purified from the periplasm. Protein purification is not feasible in droplets, so the assay for SGAP peptidase activity needed to be compatible with crude lysates.

SGAP was expressed using the system described by Frenz *et al.* [25]: cells were grown in SB/Cam⁺, supplemented with 50 mM K₂HPO₄, and induced with L-arabinose. It was found that induction worked best when cells were diluted into induction media containing 0.02% (w/v) L-arabinose to 0.2 ODU₆₀₀ and then incubating the cells for between 14-24 hours at 18°C with 230 rpm agitation (data not shown).

The fluorescence-based assay for SGAP peptidase was initially developed in microplate. The assay is described in figure 3.3.

Different suspensions of TB1 cells were prepared with OD₆₀₀s between 0 and 1 ODU. It was found that initial rate of reaction was proportional to OD₆₀₀ with a R² value of 0.988. A slight increase of rhodamine 110 fluorescence was observed in the absence of enzyme, leading to an apparent SGAP peptidase activity in the absence of enzyme. This background activity could be attributable to autohydrolysis or endogenous peptidases of the *E. coli*



(a) Dilution series

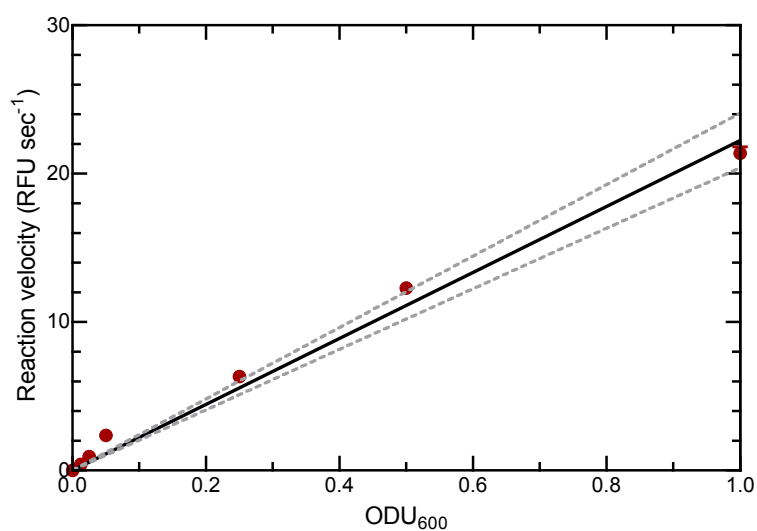
(b) ODU₆₀₀ versus reaction velocity

Fig. 3.3: SGAP peptidase activity as a function of *E. coli* K12 TB1 cell density. (a) Reaction profiles for different densities of washed *E. coli* K12 TB1 pKB4-SGAP-his in PBS Assay Mixture (section 2.3.17). Fluorescence of free rhodamine 110 was measured over one hour at 20 second intervals ($\lambda_{ex} = 488$ nm and $\lambda_{em} = 525$ nm) at 25°C. Signals were averaged between three wells for each sample. (b) Initial reaction velocities of the above data plotted against cell density. A linear correlation between the density of bacteria and the reaction velocity was observed. The black line represents this correlation, with $R^2 = 0.988$. The grey dashed lines indicate the 95%-confidence interval of the fit.

K12 TB1 cells.

SGAP, as described in the introduction, is a di-zinc enzyme that loses activity in the absence of zinc ions and exhibits enhanced activity upon the addition of calcium ions in the presence of zinc ions. Final concentrations of 100 μM ZnCl_2 and 1 mM CaCl_2 were chosen for the previous experiment (K. Blank, personal communication). However, with a completed assay system it was decided to optimize the cofactor concentrations (figure 3.4).

This was done by measuring initial peptidase activity of SGAP in conditions where both CaCl_2 and ZnCl_2 concentrations were varied (0-5 mM and 0-500 μM , respectively). Three samples were prepared for each combination of concentrations and initial reaction velocities were averaged between these samples.

The plots that resulted from this experiment (figure 3.4) show that the ZnCl_2 concentration is more important than the CaCl_2 concentration. Without ZnCl_2 the reaction velocity decreases to around 1 RFU sec^{-1} , whereas with 500 μM ZnCl_2 , the velocity increases to nearly 10 RFU sec^{-1} . CaCl_2 concentration did not appear to affect the reaction velocity as much. This remains more or less stable. For example, when looking at 100 μM ZnCl_2 , the reaction velocity was always around 5 RFU sec^{-1} , whether the CaCl_2 concentration was 5 mM or 0 mM.

The conditions with the highest measured activity were with 0.25 mM CaCl_2 and 500 μM ZnCl_2 . The reaction velocity was then 9.12 RFU sec^{-1} . The conditions that were used beforehand (1 mM CaCl_2 + 100 μM ZnCl_2) show a reaction velocity of 5.83 RFU sec^{-1} , which is 53% of the optimum velocity.

In order to have the reactions synchronized in droplets, it is necessary to lyse the cells at the moment of encapsulation or as close as possible to that moment.

There are many different ways to lyse bacterial cells [113], with the efficiency and

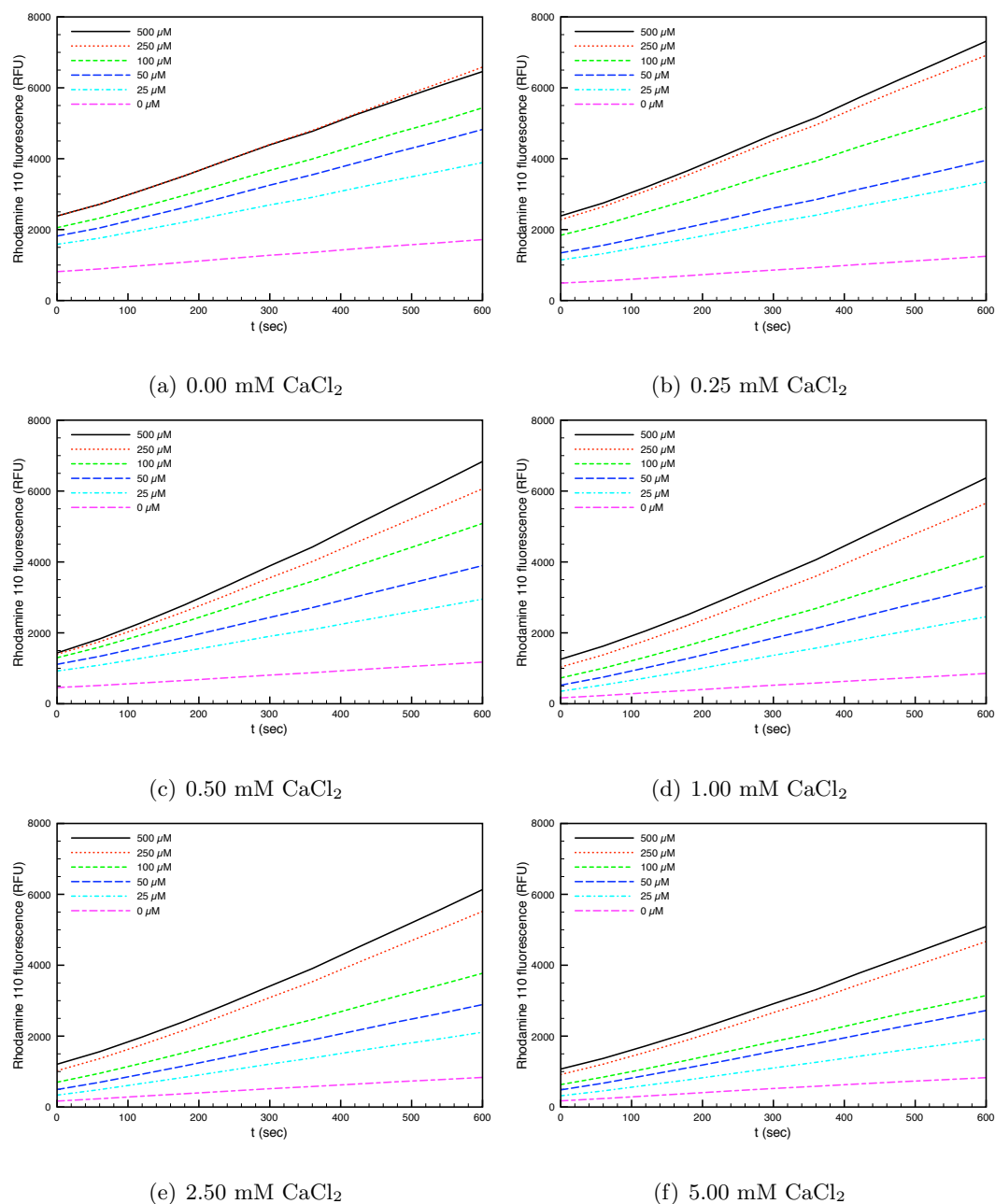


Fig. 3.4: SGAP peptidase activity as a function of Zn²⁺ and Ca²⁺ concentrations. Measurements were performed with 0.25 ODU₆₀₀ *E. coli* K12 TB1 pKB4-SGAP-his cells in 1 × PBS, 1 g l⁻¹ protease-free BSA, 2 mg ml⁻¹ polymyxin B, 120 μM L2R, pH 7.4 with different zinc and calcium concentrations. Reaction velocities were averaged between three samples.

timescale varying between them. Lysozyme [114], for example, is highly efficient, but slow. Several other ways exist to make pores in bacterial cell walls, such as CaCl_2 and EDTA. EDTA was not a viable option in this case because it deactivates SGAP. CaCl_2 can also disrupt bacterial membranes, but would need to be added in high concentrations to do so, also affecting SGAP activity.

Methods that would be more suitable for the envisaged microfluidic method (figure 3.5) include detergent-based lysis, solvent-based lysis and antibiotics.

In detergent-based lysis the membrane dissolves in the detergent, leading to the release of periplasmic and intracellular proteins. Examples of this method are the commercially-available BugBuster solutions (Novagen, EMD chemicals, San Diego, CA, USA) and a solution called PopCulture (Novagen, EMD chemicals, San Diego, CA, USA).

Another general method that will rapidly lyse bacterial cells immediately is the use of solvents. Isopropanol has already been shown to permeabilize small colonies of bacteria that were confined in beads [115]. Similarly, chloroform has been used to lyse colonies to allow detection [116]. Finally, ethanol is commonly used in the laboratory as a disinfectant. These three lytic agents were chosen for further examination.

Additionally, an interesting molecule that is very efficient in the permeabilization of gram-negative bacterial cells is polymyxin B (figure 3.6; [113, 117–122]). This molecule was included in the measurements of lytic efficiency for the proposed system.

An experiment was setup using washed cells (section 2.4.4) in PBS Assay Mixture (section 2.3.17) for fluorescence-based assays (section 2.4.12), except that the lytic agent was varied. The final concentrations used in this experiment were $1\times$ for all the detergent-based lysis solutions (BugBuster, BugBuster PAF (primary amine-free) and PopCulture), 10% (v/v) for the solvents (isopropyl alcohol, ethanol and chloroform) and 2 mg ml^{-1} polymyxin B (K. Blank, personal communication). The reaction velocities were

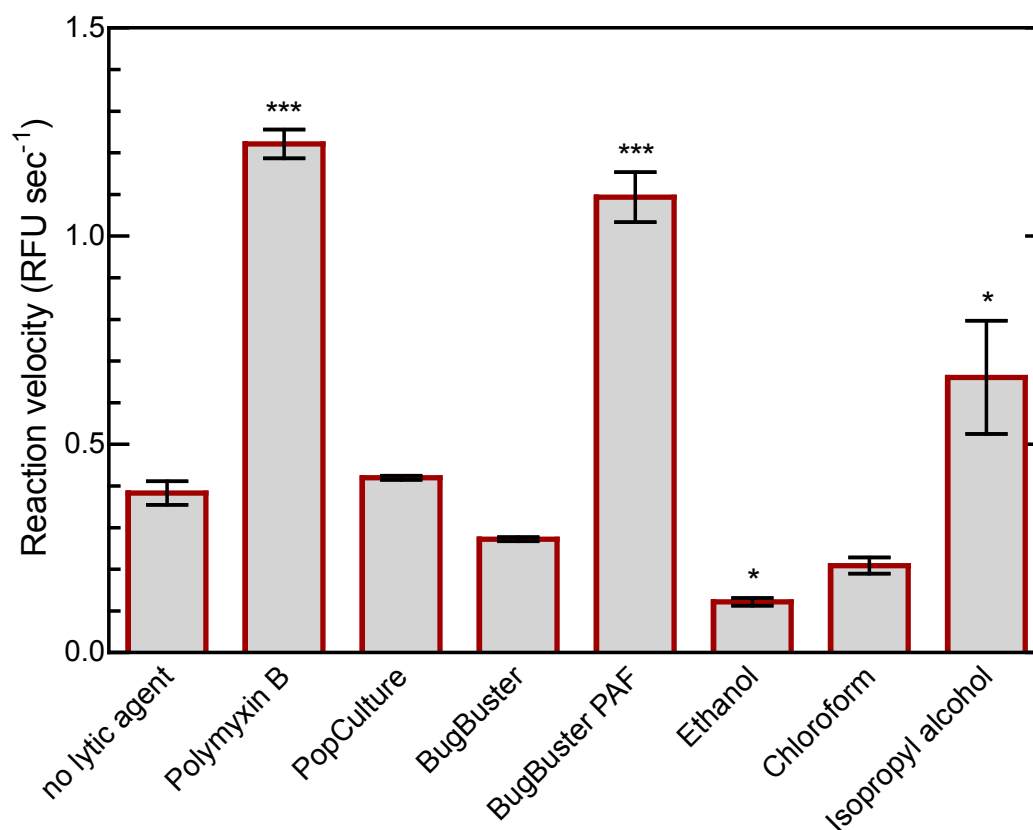


Fig. 3.5: The effects of different methods of cell lysis on SGAP peptidase activity in a cell suspension. The reactions were performed with a 0.025 ODU₆₀₀ *E. coli* K12 TB1 pKB4-mCherry-SGAP-his suspension in PBS Assay Mixture without polymyxin B (section 2.3.17). The initial reaction velocities in relative fluorescence units per second (RFU sec⁻¹) were determined in triplicate. The final concentrations were 2 mg ml⁻¹ for polymyxin B, 1× for PopCulture, BugBuster and BugBuster Primary Amine-Free (BugBuster PAF) and 10% (v/v) for ethanol, chloroform and isopropyl alcohol. Compared to the sample without lytic agent ('no lytic agent'), polymyxin B, BugBuster Primary Amine-Free ('Bugbuster PAF') and isopropyl alcohol increase the reaction velocity. Ethanol decreases the SGAP activity and the other samples ('BugBuster', 'PopCulture', and 'Chloroform') did not affect the reaction velocity.

* $P < 0.05$

*** $P < 0.0001$

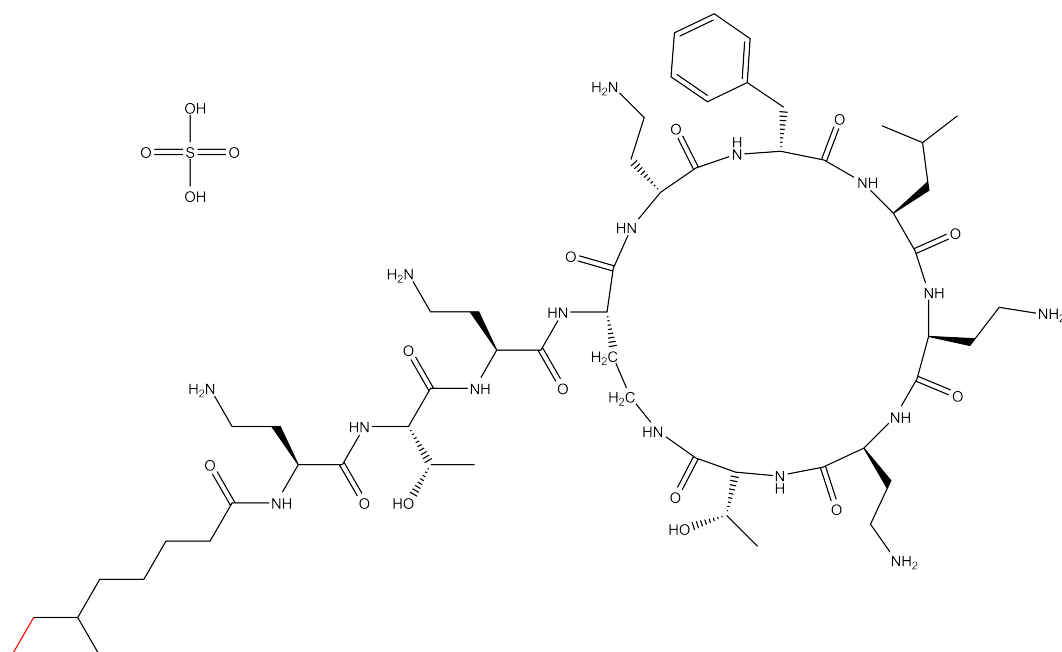


Fig. 3.6: The chemical structure of polymyxin B. Polymyxin B consists of a mixture of polymyxin B₁ and B₂, the difference being indicated by the red group: polymyxin B₁ contains it, while polymyxin B₂ does not [122]. The molecule contains a fatty acid tail (bottom left) and a nonapeptide head group. It is supplied in the form of a sulfate salt.

averaged over three samples and the standard error of the mean was calculated.

When comparing the different methods of lysis to a sample in which there is no lytic agent added, polymyxin B, BugBuster PAF (primary amine-free) and isopropyl alcohol significantly increase reaction velocity (from 0.383 ± 0.028 RFU sec^{-1} to 1.221 ± 0.035 RFU sec^{-1} , 1.094 ± 0.060 RFU sec^{-1} , and 0.661 ± 0.136 RFU sec^{-1} , respectively). Only ethanol significantly decreased the reaction velocity when compared to the sample without lytic agent (0.122 ± 0.009 RFU sec^{-1}). The other agents did not affect the reaction velocity.

Of all the lysis methods, polymyxin B yielded the greatest reaction velocity. Therefore, this molecule was chosen for the microfluidic experiments. The mechanism of action of polymyxin B has been studied [117, 122]. Briefly, the molecule is amphiphatic because of a non-polar tail and a polar nonapeptide headgroup. The different features of the molecule allow interaction with both lipopolysaccharides and phospholipids, as well as interference with the divalent ions in the membrane. Following these interactions, the hexapeptide head probably buries itself in the membrane, thereby destabilizing it.

After confirming the assay conditions (1 mM CaCl_2 , 100 μM ZnCl_2 , 1 g l^{-1} protease-free BSA and 2 mg ml^{-1} polymyxin B) it was important to determine the Michaelis constant (K_M) of SGAP for L2R. Determining this constant is necessary for subsequent directed evolution experiments, because, to evolve k_{cat} , the substrate concentration must not be limiting [9].

This experiment was performed with commercial SGAP. It was diluted to 1.2 U μl^{-1} to give an activity comparable to the lyzed cells. The L2R concentration was varied between 0 μM and 500 μM while maintaining 5% (v/v) DMSO in all reactions. Fluorescence was measured in triplicate. The results of this experiment are plotted in figure 3.7.

With an R^2 of 0.9590 the K_M was determined to be 60.11 μM . Consequently a final

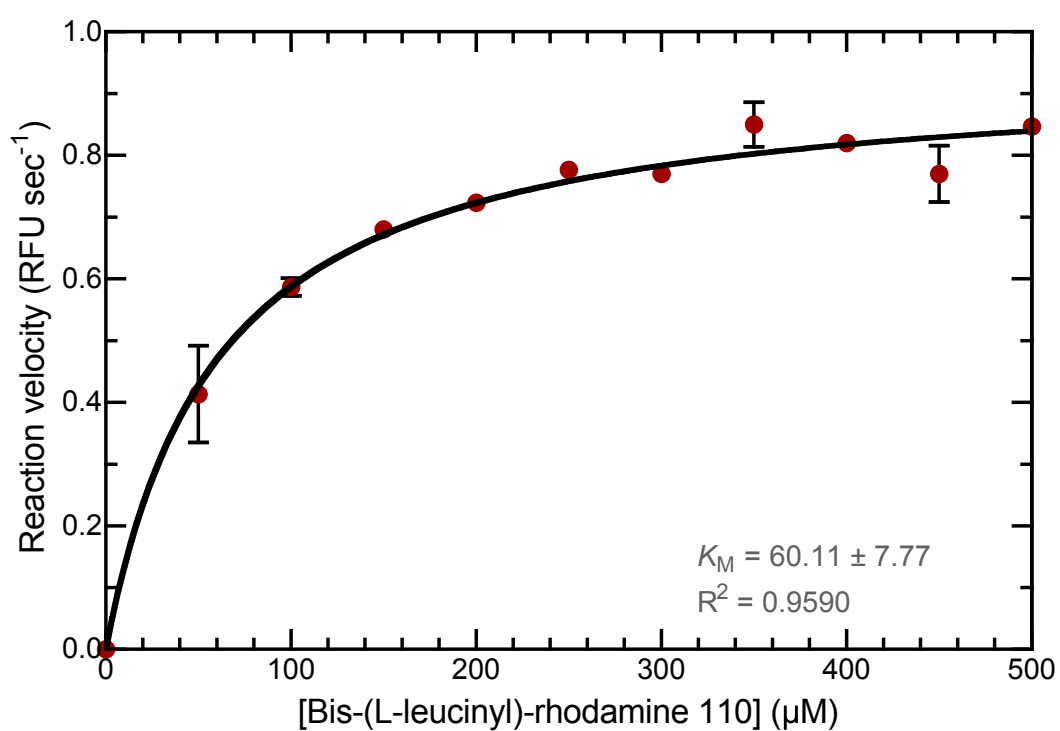


Fig. 3.7: Effect of substrate concentration on SGAP peptidase activity. The Michaelis constant (K_M) of SGAP for L2R when using 50 U of pure protein in 1× PBS, 100 μM ZnCl₂, 1 mM CaCl₂, 1 g l⁻¹ protease-free BSA, pH 7.4 was measured to be 60.11 ± 7.77 μM.

concentration of 120 μM was used in the assays.

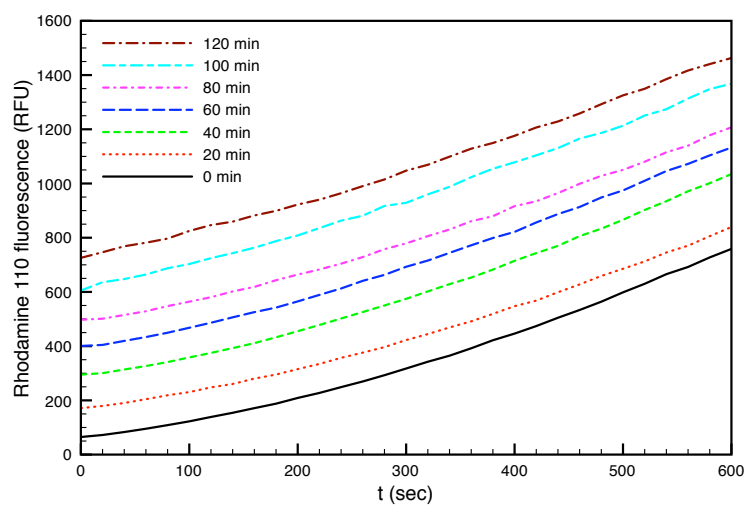
This result is not conclusive, since the analysis is severely limited by the solubility of L2R in PBS. In the higher range of concentrations ($> 200 \mu\text{M}$), the solution became hazy, indicating incomplete dissolution of the substrate. Consequently the real K_M may be higher in reality.

The final aspect of the reaction that needed to be determined before shifting to microfluidics was whether the reaction can be stopped and started by regulating the temperature. This would make it possible to synchronize the reactions in many droplets off-chip: the droplets would be collected on ice, incubated for a certain period of time at 25°C , and then reinjected at ice temperature. Consequently, it needed to be verified that the peptidase reaction would not be affected by incubating PBS Assay Mixture (section 2.3.17) mixed with washed cells (section 2.4.4) on ice for a relatively long time (figure 3.8). To do this, a complete reaction mixture was kept on ice and every 20 minutes aliquots were taken, heated to 25°C , and placed in the spectrophotometer. For each time point, 10 minutes of kinetic data were recorded to determine the initial rate of reaction.

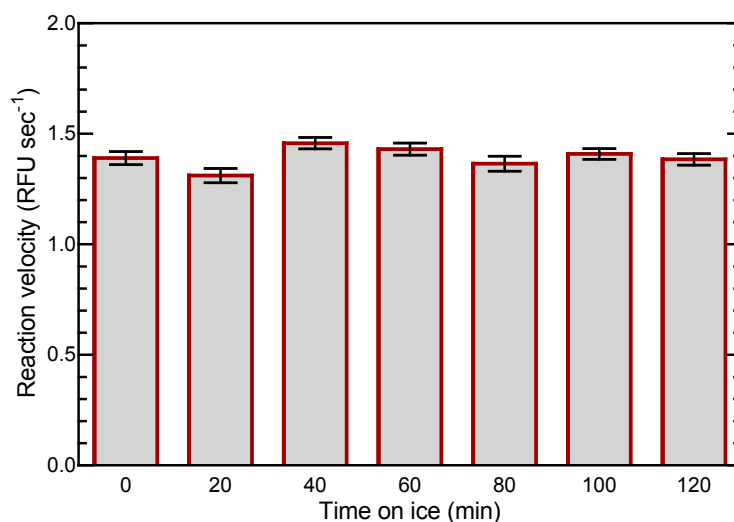
Over 120 minutes the initial reaction velocities of reheated reactions remained constant, which meant that the reaction is not affected by incubating the assay mixture on ice.

However, it was observed that the reaction continues to advance, even though it is incubated on ice (see figure 3.8a). The initial RFUs that were measured at each timepoint rose from 50 RFU at the outset of the experiment to approximately 750 RFU after 120 minutes of incubation on ice. These values correspond to 0.008 μM and 0.041 μM , respectively, in a reaction where 120 μM of L2R was added.

Though effect is not substantial, it is something that may need to be kept in mind when doing selections in microfluidics, as these can take a long time. The time a selection



(a) Reaction profiles



(b) Reaction velocities

Fig. 3.8: The effect of ice-incubation and reheating on SGAP peptidase activity. The reactions were performed with a 0.25 ODU₆₀₀ suspension of washed *E. coli* K12 TB1 pKB4-mCherry-SGAP-his (section 2.4.4) in PBS Assay Mixture (section 2.3.17) on ice. (a) The reaction profiles of the reactions. The values were averaged from three samples for each timepoint. (b) The initial reaction velocities were determined in triplicate by cutting off the first 200 seconds of the kinetics measurement in order to allow the samples to heat up to 25°C.

takes depends on the combination of λ (number of bacteria per droplet) and ϵ (ratio of positive versus negative events) for experiments. The duration of a selection is inversely proportional to the values of λ and ϵ .

3.4 Conclusions

In this chapter it has been demonstrated that periplasmically expressed SGAP peptidase activity can be measured using a fluorescence-based assay. The conditions were optimized to be $1\times$ PBS, 1 mM CaCl_2 , 100 μM ZnCl_2 , 1 g l^{-1} protease-free BSA, 2 mg ml^{-1} polymyxin B, 120 μM L2R, pH 7.4.

Different direct methods of lysis were tested, showing that the preferential order of testing in microfluidics was (i) polymyxin B, (ii) BugBuster Primary Amine Free and (iii) isopropyl alcohol. Ethanol cannot be used, since it inhibits SGAP activity. The other methods do not significantly impact activity relative to unlyzed cells.

Finally, it has been shown that SGAP activity is not decreased when incubating a complete reaction on ice for extended periods of time, which should allow synchronization of droplet reactions during long selections of up to 2 hours.

In short, after the assay development, SGAP is ready to continue on to microfluidic experiments, which will be explained in the following chapter.

4. MICROFLUIDICS WITH SGAP

4.1 Introduction

In the previous chapter the optimal conditions for a fluorescence-based assay for SGAP peptidase activity were determined. The validation of these conditions in droplet-based microfluidics is described in this chapter.

However, before that, some basic microfluidic experiments were performed.

The surfactant concentrations in the EA/HFE 7500 emulsions generated on-chip are above the critical micellar concentration of the surfactant. As a consequence, there can be exchange of solutes between the aqueous phases of the droplets [123]. It was, therefore, necessary to determine whether rhodamine 110 is exchanged or not, as exchange would impair the accurate determination of enzyme activity in each droplet.

Next, it was necessary to determine the relationship between the OD_{600} of *E. coli* TB1 K12 cells and λ (the initial mean number of cells per droplet [22]). This relationship was needed in order to tune the enrichment value in a FADS experiment.

The third point of validation was to measure the reaction rate of the SGAP peptidase assay in droplets. It was necessary to know if either the EA surfactant or the HFE 7500 oil inhibited the SGAP peptidase assay. Ideally, droplets containing wildtype SGAP would be clearly distinguishable from inactive droplets in order to allow activity-based selections.

After addressing all of these points, a model selection using FADS [22] was performed.

In this chapter it is reported that, although rhodamine 110 shows considerable leakage from droplets made in fluorinated oil with a surfactant, it is on a timescale that permits the analysis of SGAP peptidase activity in microdroplets. Polymyxin B was found to be the best lytic agent. Finally, the model selection proved to be successful

4.2 Materials and methods

The optical setup, data acquisition and control system, as well as mould, chip and microfluidic device preparation were the same as described by Baret *et al.* [22]. The channel depth for all devices was 25 μm , except the sorting device, where it was 21 μm .

4.2.1 Testing the exchange of free rhodamine 110 between droplets

Two Omnifix-F 1 ml disposable syringes (B. Braun Medical AG, Boulogne Bilancourt, France) were filled with 40 mM HEPES, pH 8.5 containing 10 μM or 100 μM rhodamine 110, to serve as aqueous phases in microfluidic droplets. Droplets were formed in a T-junction-based dual emulsifier (supplementary information, figure 9.1(a)) with HFE 7500 oil containing 2% (w/w) EA surfactant using a flowrate (Q_{surf}) of 700 $\mu\text{l hr}^{-1}$ and a total aqueous flowrate (Q_{aq}) of 200 $\mu\text{l hr}^{-1}$. Droplets were formed at a frequency of ~ 1 500 Hz (37 pl droplets with a diameter of ~ 41 μm when spherical) and collected for 10 minutes through poly(ethylene terephthalate) (PET) PE 20 tubing (Becton, Dickinson and Company, Le Pont de Claix, France) into a glass capillary filled with surfactant-free HFE 7500 oil [24]. After incubation, the droplets were reinjected into a different microfluidic device (supplementary information, figure 9.1(c)) with a flowrate (Q_{em}) of 25 $\mu\text{l hr}^{-1}$ and spaced with surfactant-free HFE 7500 oil ($Q_{oil} = 150$ $\mu\text{l hr}^{-1}$). Fluorescence

was measured after 30 minutes, 60 minutes, 90 minutes and 100 minutes. The RFUs were calculated from the output of the PMTs in Volts (V) using the formula $\text{RFU} = V/(\text{Gain}^{pc})$, where pc is the PMT constant, which was 7.2 for this specific PMT.

4.2.2 Occupancy

E. coli TB1 pKB4-SGAP-his cells were grown overnight (section 2.4.2) and washed (section 2.4.4) with SB. Next, the cells were re-suspended to 0.25 ODU₆₀₀ and serially diluted to 0.025 ODU₆₀₀ and 0.0025 ODU₆₀₀. The suspensions were supplemented with 1 μM fluorescein ($\lambda_{ex} = 488 \text{ nm}$, $\lambda_{em} = 525 \text{ nm}$) to allow droplet detection. Three Omnifix-F 1 ml disposable syringes were filled with the bacterial suspensions, serving as the aqueous phases for three emulsions. Q_{aq} was 100 $\mu\text{l hr}^{-1}$. Q_{surf} was adapted so that droplets were generated at a frequency of $\sim 2\text{--}300 \text{ Hz}$, making 12 pl droplets ($\sim 28 \mu\text{m}$ diameter when spherical). The emulsions were collected off-chip through PET tubing into 1.5 ml microcentrifuge tubes, overlaid with 200 μl SB/cam⁺ and incubated for 14 h at 25°C before reinjecting them according to the previously described technique [22] with Q_{em} at 5 $\mu\text{l hr}^{-1}$. When the droplets arrived on chip, photographs were taken every 20 seconds for 300 seconds. Each photograph was counted manually for the total number of droplets (n_{total}) and the total number of occupied droplets ($n_{occupied}$). The occupancy was then determined ($n_{occupied}/n_{total}$) with the standard deviation ($\sqrt{n_{occupied}}/n_{total}$). The number of bacteria per droplet (at encapsulation) was $\lambda = -\ln(P(X = 0))$, in which ($P(X = 0)$) represents $(1 - n_{occupied})$, or the probability that a droplet is empty [22].

4.2.3 Screening

E. coli TB1 pKB4-SGAP-his cells, pKB4-SGAP-E131A-his cells or pKB4-mCherry-SGAP-his cells were grown (section 2.4.2), induced (section 2.4.3), washed (section 2.4.4)

and re-suspended to 0.052 ODU₆₀₀ before being loaded into an Omnifix-F 1 ml disposable syringe (aqueous phases 1 (SGAP) and 2 (SGAP-E131A)). PBS Assay Mixture was prepared without the lytic agent but with 0.1 μM rhodamine 110 or 50 μM resorufin (section 2.3.17). 2 mg ml⁻¹ polymyxin B, 1 \times BugBuster Primary Amine Free or CHCl₃-saturated PBS were used as lytic agents. Omnifix-F 1 ml disposable syringes were filled with PBS Assay Mixture as necessary (aqueous phases 3 (polymyxin B), 4 (BugBuster PAF), 5 (CHCl₃-saturated PBS) and 6 (without lytic agent)). Aqueous phases 1 and 2 (input port 1) and 3-6 (input port 2) were both injected at $Q_{aq} = 100 \mu\text{l hr}^{-1}$ into a co-flow microfluidic chip (supplementary information, figure 9.1(b)), making 5 different emulsions (aqueous phases 1+3, 1+4, 1+5, 1+6 and 2+3). Q_{surf} was adapted so that droplets were generated at a frequency of $\sim 4\ 600$ Hz, making 12 pl droplets ($\sim 28 \mu\text{m}$ diameter when spherical). Emulsions were collected through PET tubing for 10 minutes into a glass capillary filled with surfactant-free HFE 7500 oil [24]. Emulsions were re-injected into a single inlet microfluidic device (supplementary information, figure 9.1(c)) at $Q_{em} = 25 \mu\text{l hr}^{-1}$ and spaced with $Q_{oil} = 150 \mu\text{l hr}^{-1}$. Fluorescence was measured 20 minutes, 40 minutes and 60 minutes after emulsification. The RFUs were calculated from the output of the PMTs in Volts (V) using the formula $\text{RFU} = V/(\text{Gain}^{pc})$, where pc is the PMT constant, which was 7.2 for this specific PMT. Epifluorescence photos were taken with TB1 pKB4-mCherry-SGAP-his cells, except for E131A with polymyxin B lysis. TB1 pKB4-SGAP-E131A-his cells were used since mCherry::SGAP-E131A was unavailable. Green fluorescence was detected by excitation through a 479/40 filter and emission through a 530/43 filter, red fluorescence was detected by exciting through a 540/25 filter and detecting emission through a 605/55 filter. A green fluorescence photograph was merged with a red fluorescence photograph using NIS Elements BR 3.0 software (Nikon France S.A.S., Champigny sur Marne, France). For the epifluorescence image with E131A, a bright light photograph was merged with a green fluorescence photograph. When taking epifluorescence photographs, the droplets contained 0.1 μM

rhodamine 110 for droplet detection. When measuring fluorescence intensities, resorufin was used to detect droplets.

4.2.4 Sorting

E. coli TB1 pKB4-SGAP-his cells and TB1 pKB4- Δ SGAP-his cells were grown (section 2.4.2), induced (section 2.4.3), washed (section 2.4.4) and re-suspended to 0.52 ODU₆₀₀. A 1:9 mixture of SGAP: Δ SGAP cells ($\epsilon = 0.1$) was prepared and diluted to 0.052 ODU₆₀₀ (aqueous phase 1). PBS Assay Mixture was made with 50 μ M resorufin (section 2.3.17; aqueous phase 2). Two Omnifix-F 1 ml disposable syringes were filled with aqueous phases 1 and 2 and injected into a co-flow microfluidic chip at $Q_{aq} = 100 \mu\text{l hr}^{-1}$ each. Q_{surf} was adapted to generate droplets at a frequency of ~ 4 600 Hz, making 12 pl droplets ($\sim 28 \mu\text{m}$ diameter when spherical). The emulsion was collected through PET tubing into a glass capillary filled with surfactant-free HFE 7500 oil that was cooled to 4°C in a Peltier cooling system throughout the experiment. The emulsion was reinjected at $Q_{em} = 15 \mu\text{l hr}^{-1}$ and spaced out at $Q_{oil} = 500 \mu\text{l h}^{-1}$. Subsequently droplets were sorted as a function of rhodamine 110 fluorescence, selecting the top 0.3% most fluorescent droplets. The RFUs were calculated from the output of the PMTs in Volts (V) using the formula $\text{RFU} = V/(\text{Gain}^{pc})$, where pc is the PMT constant, which was 7.2 for this specific PMT. The sorting parameters, using the notation of Baret *et al.* [22], were: $F = 30$ kHz, $\tau_{sort} = 0.8$ ms, $U_{sort} = 1.3$ kV_{*p-p*}. 2 000 sorted droplets were collected in PET tubing, which was drained into a 1.5 ml microcentrifuge tube. The tubing was then flushed with 30 μ l of Droplet Destabilizer (RainDance Technologies, Lexington, MA, USA), followed by 70 μ l of 1 \times Pfu Buffer. The emulsion was broken by vortexing at maximum velocity for 30 seconds and then centrifuged for 3 seconds in a table-top centrifuge. 35 μ l of the supernatant was used in a 50 μ l PCR reaction (section 2.4.10; colony PCR program in table 2.1) of which 10 μ l was subsequently digested with

SalI and separated by gel electrophoresis (section 2.4.8).

4.3 Results and discussion

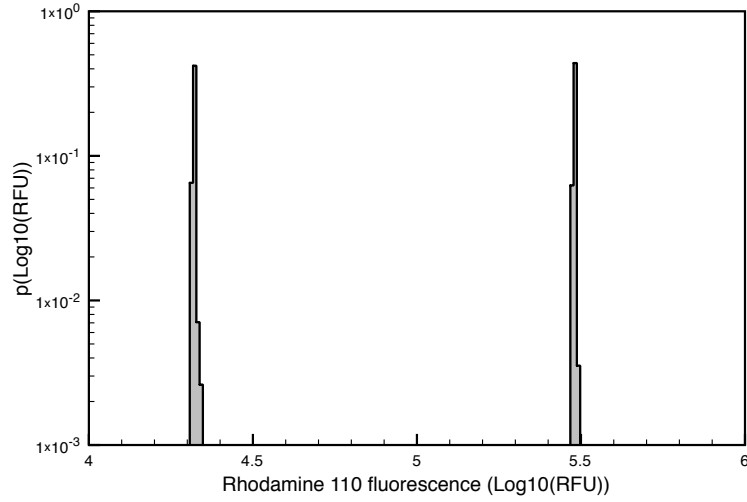
A high concentration of surfactant, far above the critical micellar concentration, is necessary to make stable emulsions in our setups. Consequently, two factors needed to be examined: (i) whether the surfactant inhibits the SGAP peptidase assay and (ii) since exchange between droplets is, among other things, dependent on micellar transport [123–130], the exchange rate of free rhodamine 110 between droplets.

2% (w/w) EA surfactant—a PEG-PFPE amphiphilic block copolymer [109]—in HFE 7500 oil was found to not inhibit the SGAP peptidase assay in microtitre plate (data not shown).

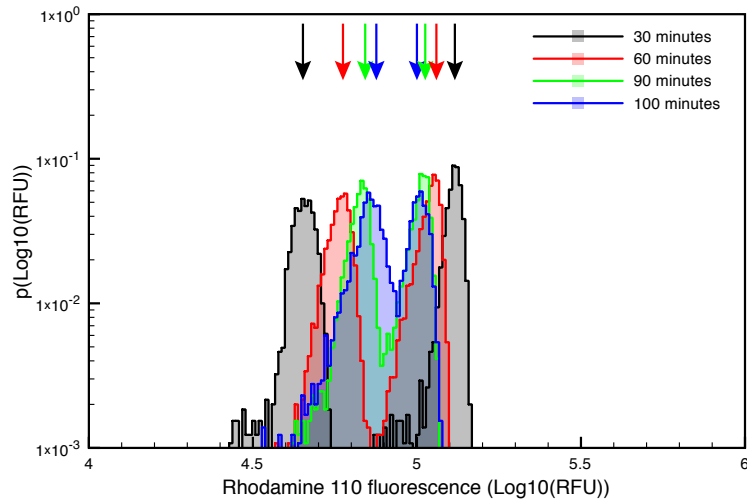
In order to assess the rapidity of exchange of rhodamine 110 in microdroplets, a dual emulsifier (supplementary information figure 9.1(a)) was used to simultaneously encapsulate 10 μM rhodamine 110 and 100 μM rhodamine 110. The emulsion was incubated off-chip in a glass capillary [24] and reinjected into a different device. The fluorescence profile of the droplet population was measured after 30 minutes, 60 minutes, 90 minutes and 100 minutes (see figure 4.1).

Upon emulsification, the fluorescence signals of the 10 μM and 100 μM rhodamine 110 droplets were found to differ by $\sim 1 \log_{10}$ units (slightly more than 10-fold). After 30 minutes (black histogram) the two peaks were separated by $\sim 0.4 \log_{10}$ units (2.5-fold). At each subsequent timepoint the peaks came approached each other until they overlapped after 100 minutes (blue histogram). The last timepoint where the peaks were still separate was 60 minutes. Reactions liberating free rhodamine 110, therefore, should not proceed for >60 minutes.

Another factor that needed to be verified was the relationship between OD_{600} and λ .



(a) Fluorescence profile upon droplet generation



(b) Fluorescence profile upon reinjection

Fig. 4.1: The exchange rate of rhodamine 110 in microfluidic droplets. Droplets created with a dual emulsifier (supplementary information, figure 9.1(a)) contained either 10 μM rhodamine 110 or 100 μM rhodamine 110 in 40 mM HEPES pH 8.5. The emulsion was incubated in a glass capillary and reinjected. The fluorescence was measured (a) upon creation (b) after 30 minutes (black histogram), 60 minutes (red histogram), 90 minutes (green histogram) and 100 minutes (blue histogram). $p(\log_{10}(\text{RFU})) = \frac{\text{number of droplets at } x \log_{10}(\text{RFU})}{\text{total number of droplets}}$, which denotes the probability a droplet is at $x \log_{10}(\text{RFU})$.

However, λ can only be determined indirectly after assessing droplet occupancy. Occupancy depends on the Poisson distribution [22, 131–133], which means that even when using suspensions at high ODs, not all droplets will be occupied, but multiple bacteria will be encapsulated per droplet. Experimentally, this means that using suspensions of bacteria at different ODs should lead to a linear increase in λ , but not in occupancy. Occupancy is defined as

$$\text{occupancy} = \frac{n_{\text{occupied}}}{n_{\text{total}}}$$

in which n_{occupied} denotes the number of occupied droplets and n_{total} denotes the total number of droplets. λ is calculated as

$$\lambda = -\ln(P(X = 0))$$

with $P(X = 0) = 1 - n_{\text{occupied}}$, or the probability that a droplet is empty [22].

0.25 ODU₆₀₀, 0.025 ODU₆₀₀ and 0.0025 ODU₆₀₀ suspensions of TB pKB4-SGAP-his were emulsified in 12 pl droplets and left to grow overnight at 25°C. The following day 15 photographs were taken of each emulsion and n_{occupied} and n_{total} were determined for each photograph. The results are shown in figure 4.2.

The inset graph shows that the occupancy did not increase linearly over all OD₆₀₀s. The maximum occupancy was ~ 0.6 . Contrastingly, λ increased linearly to nearly 1 at the highest OD₆₀₀. The relationship between OD₆₀₀ and λ is $\lambda = 3.7832 \times \text{ODU}_{600}$.

Knowing the λ of an emulsion to be used in FADS, which was chosen to be 0.1, the enrichment can be finetuned. For example, using ϵ s (being the ratio of positive to negative) of 0.1 (1/10 positive events), 0.01 (1/100 positive events) or 0.001 (1/1000 positive events) can lead to enrichment factors of 110.5, 1010 and 10010, respectively [22].

Following these microfluidic determinations, the SGAP peptidase assay was tested in

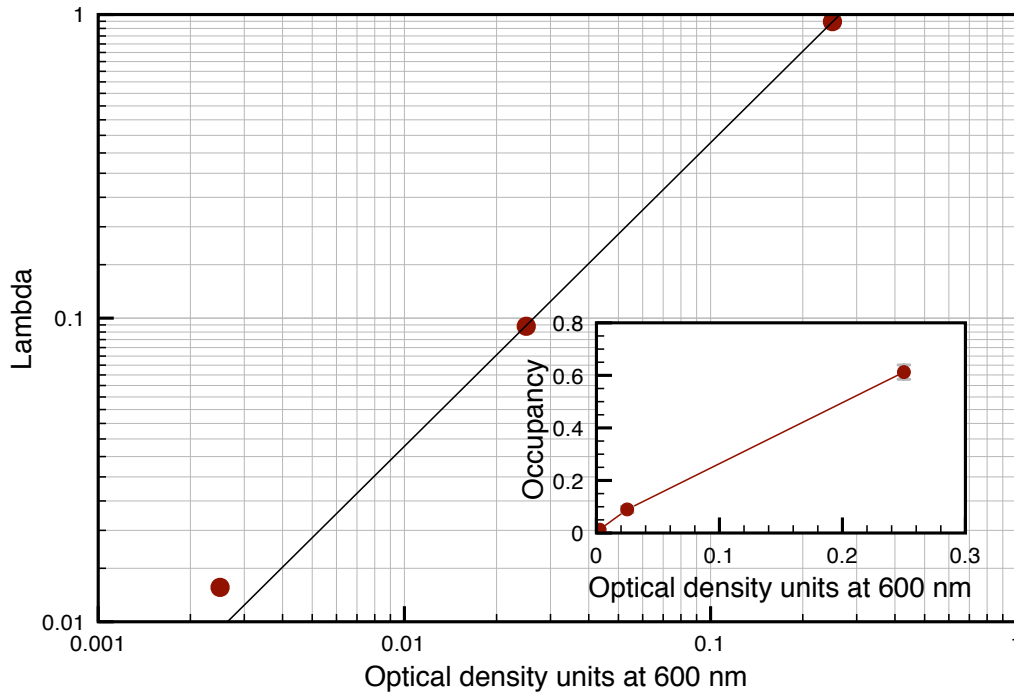


Fig. 4.2: Determination of droplet occupancy and initial mean number of cells per droplet (λ [22]). 15 photographs were made of each emulsion and n_{total} as well as $n_{occupied}$ were determined by eye. Droplet occupancy (inset) was calculated ($n_{occupied}/n_{total}$) with the standard deviation ($\sqrt{n_{occupied}}/n_{total}$). λ is defined as $\lambda = -\ln(P(X = 0))$, in which $P(X = 0)$ is the probability that a droplet is empty. The graph for lambda is fitted with the formula $\lambda = 3.7832 \times ODU_{600} + 0.016$.

microfluidic droplets. The first two aspects investigated were to verify the efficacy of polymyxin B in microfluidic droplets and to monitor the SGAP peptidase assay (see figure 4.3).

It was found that polymyxin B did not lyse all the bacteria (figure 4.3(i)). Therefore, the next best lytic agents from the microplate optimization were tested: BugBuster Primary Amine-Free and chloroform, in the form of chloroform-saturated PBS. From figure 4.3(f)-(h) it becomes clear that none of the lytic agents completely lysed the cells. However, with each lytic agent, except polymyxin B, there were more bacteria visible than there were fluorescent droplets.

These results were then compared to the fluorescence profiles obtained from the different reactions (figure 4.3(a)-(d)). All conditions, including the absence of any lytic agent, showed a small, separate population of fluorescent droplets, which was smaller than the expected 10% of the total population. However, with polymyxin B, this fluorescent population was $\sim 10\%$ of the total population. When E131A was encapsulated in droplets, no increase in fluorescence was observed, as expected (figure 4.3(e)).

So, polymyxin B remained the best lytic agent and a model selection using this agent was performed by FADS (see figure 4.4) [22]. The conditions of the experiment were: $\lambda = 0.1$ and $\epsilon = 0.1$ (ratio of positive versus negative of 1/10). Solving the equation

$$\eta_m = \frac{1}{1 - e^{-\left(\frac{\epsilon\lambda}{1+\epsilon}\right)}}$$

for the maximal theoretical enrichment (η_m) [22] with the aforementioned conditions yields a theoretical enrichment of $\eta_m = 110.5$.

Even though the droplets containing SGAP did not create a separate population compared to empty droplets and droplets containing Δ SGAP, the top 0.3% most fluorescent droplets were selected (indicated by the sorting gate in transparent red).

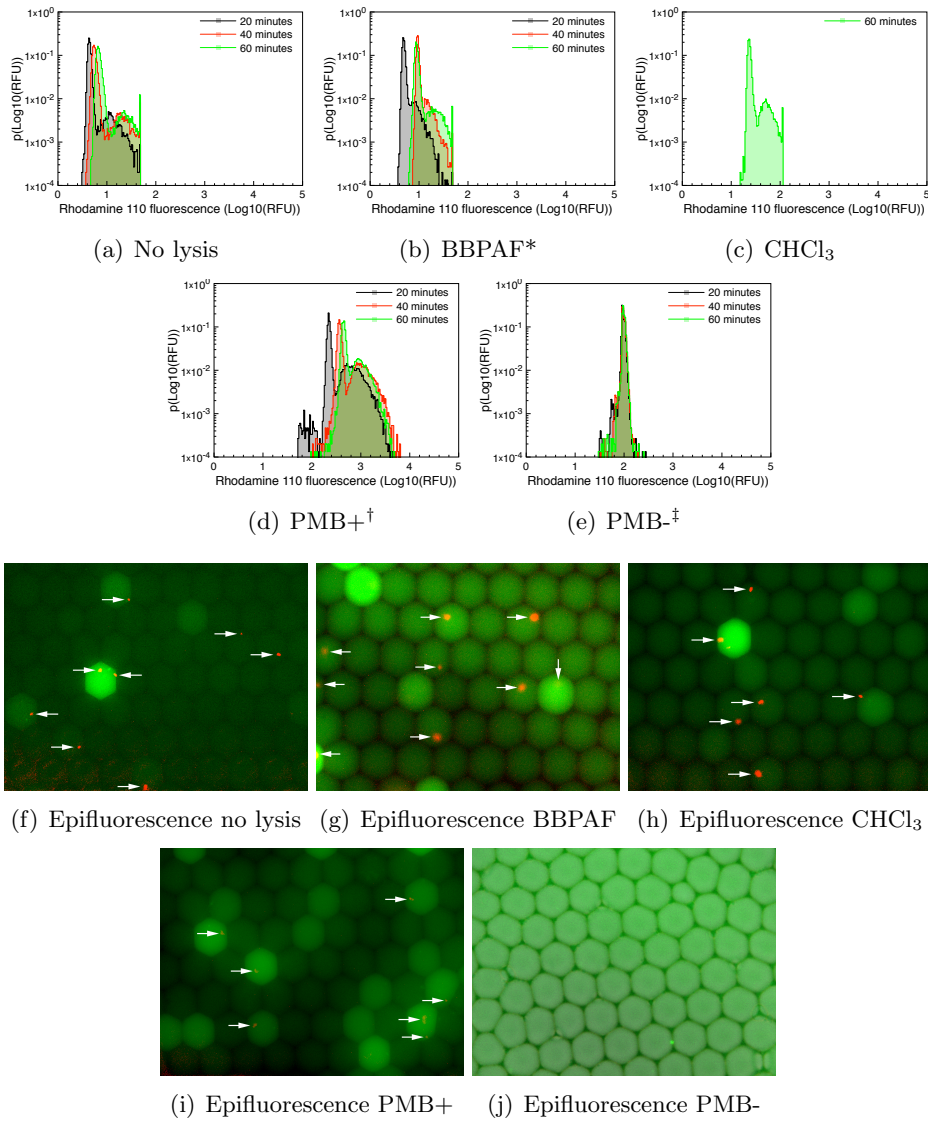
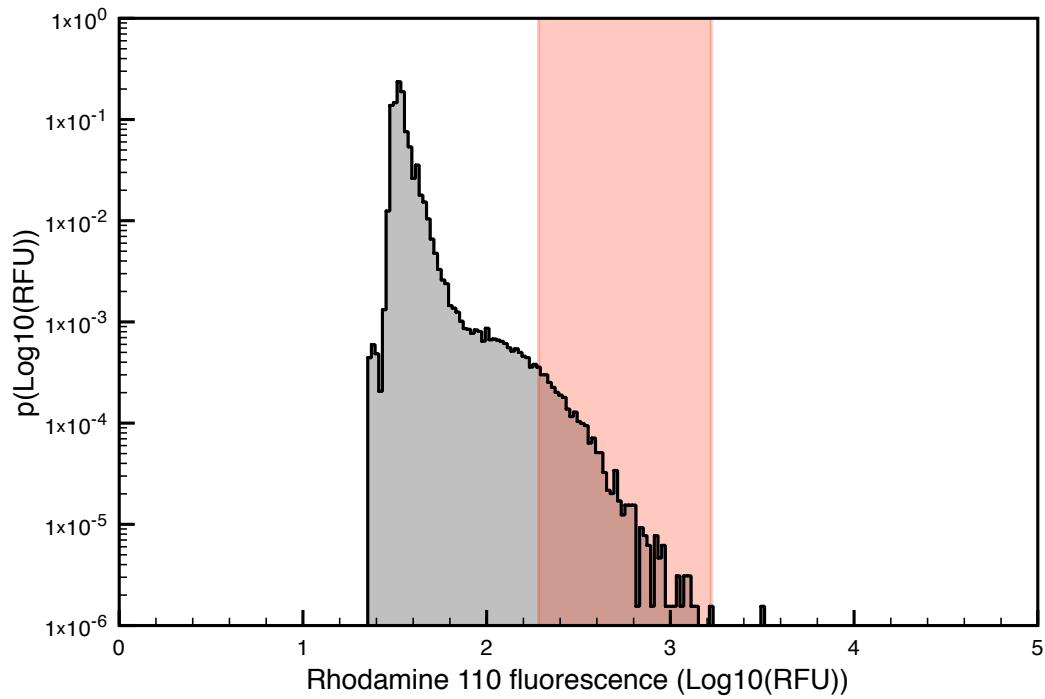


Fig. 4.3: The effect of different lytic agents on bacterial lysis and the SGAP peptidase assay in microfluidics. (a–j) 12 pL droplets were made using a co-flow with an 0.026 ODU₆₀₀ suspension of TB1 pKB4-mCherry-SGAP-his and PBS Assay Mixture without polymyxin, but with 0.1 μ M free rhodamine 110 or 50 μ M resorufin (section 2.3.17). Droplets were incubated in a glass capillary before reinjection. (a–e) Fluorescence profiles for PBS Assay Mixture (a) without lytic agent or PBS Assay Mixture supplemented with (b) 1 \times BugBuster Primary Amine Free, (c) CHCl₃-saturated PBS or (d,e) polymyxin B after 20 minutes (black histograms), 40 minutes (red histograms) and 60 minutes (green histograms). $p(\log_{10}(\text{RFU})) = \frac{\text{number of droplets at } x \log_{10}(\text{RFU})}{\text{total number of droplets}}$, which denotes the probability a droplet is at $x \log_{10}(\text{RFU})$. (f–j) Merged epifluorescence photos, in which bacteria have been indicated by white arrows.

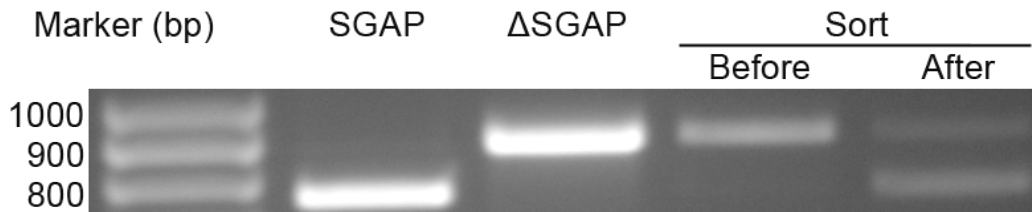
* BugBuster Primary Amine Free

[†] Polymyxin B with TB1 SGAP cells

[‡] Polymyxin B with TB1 E131A cells



(a) Sorting histogram



(b) Agarose gel after sorting

Fig. 4.4: Results from a FADS-based model selection of SGAP from a mixture of SGAP and Δ SGAP. (a) Fluorescence profile of the model selection. $p(\log_{10}(\text{RFU})) = \frac{\text{number of droplets at } x \log_{10}(\text{RFU})}{\text{total number of droplets}}$, which denotes the probability a droplet is at $x \log_{10}(\text{RFU})$. The sorting gate, comprising the top 0.3% most fluorescent droplets, is indicated in transparent red. (b) 1.5% agarose gel containing the restricted samples demonstrating enrichment of SGAP over Δ SGAP.

After the model selection, the droplets were recovered in $1\times$ Pfu Buffer, amplified by PCR, and restricted with SalI to distinguish SGAP (cut once, yielding fragments of 755 bp and 127 bp) and Δ SGAP (not cut, yielding a single 882 bp fragment).

The agarose gel (figure 4.4(b)) shows that SGAP was not detectable before the model selection. But, after the model selection, SGAP became detectable, indicating successful enrichment. Quantitating the intensity of the bands on the gel (section 2.4.8) indicated an $\epsilon_0 = 0.1$ before the model selection and an $\epsilon_1 \approx 2.89$ after the model selection, yielding $\eta_{exp} = \frac{\epsilon_1}{\epsilon_0} = 28.9$.

The experimental enrichment, η_{exp} was found to be lower than the theoretical enrichment η_m , but the ~ 3.8 -fold difference falls within the 5-fold error margin of the model for predicting enrichment [22]. In conclusion, the model selection was successful.

This experiment demonstrated that SGAP peptidase activity can be selected, at a frequency of ~ 300 Hz, by FADS. Compared to microtitre plate assays the analysis was ~ 300 -fold faster than can be achieved even with a robotic system, while using far smaller volumes (8.4 μ l of aqueous phase in FADS compared to 700 ml of aqueous phase in microtitre plate assays). The throughput is lower than in FACS [2], but it was straightforward to select for activity and the equipment is $\sim 10\times$ less expensive.

There remain some outstanding issues that need to be resolved in the microfluidics system described here. Firstly, the model selection was performed while incubating the droplets for 60 minutes, which means that the endpoint was late in the reaction. For directed evolution, when k_{cat} needs to be evolved, the endpoint should be in the initial, linear stage. Using capillaries, it is technically difficult to have reactions lasting less than 20 minutes. An integrated device with a droplet maker, delay line [25] and sorting module at the end is probably the best solution for this issue.

In addition, there was a large distribution in fluorescence signals from droplets contain-

ing SGAP. For example, in the model selection the sorting gate nearly spans 1 \log_{10} unit, which is less than the entire fluorescent population. If this distribution is due to variations in expression level of SGAP [106], the population could be tightened by normalizing for this expression level. One method to investigate this is creating a fluorescent fusion protein. The fluorescent signal of the fused protein could then be used to normalize for expression level. A fusion protein between mCherry and SGAP was made to this effect, which is discussed in the next chapter.

Another issue that needs to be addressed is the lysis. When adding polymyxin B to the reaction mixture, often droplets containing SGAP formed a separate population. This separate population has a higher fluorescence that is completely distinct from droplets containing either no bacteria or an inactive variant of SGAP. This was, however, not the case, for example, in the model selection. This ‘shoulder’ has been observed before in the case of incomplete lysis (O.J. Miller, personal communication). Perhaps lysis would be completed if the droplets were subjected to shear inside the droplets or a combination of lytic agents.

4.4 *Conclusions*

After developing a fluorescence-based SGAP peptidase assay, this chapter showed the feasibility of this assay in microfluidics. It was demonstrated that the assay achieved completion in less than 60 minutes, in 2% (w/w) EA surfactant in HFE 7500 oil. Consequently the exchange of free rhodamine 110 between droplets, though present, should not impede selections for SGAP peptidase activity.

Polymyxin B proved to be the best lytic agent in droplets, even though not all cells were lysed, leading to incomplete separation of the populations of SGAP droplets and inactive droplets (empty, E131A or Δ SGAP).

Finally, it was shown that SGAP can be selectively enriched from a mixture of SGAP and Δ SGAP by FADS with an η_{exp} of 28.9.

5. NORMALIZATION FOR EXPRESSION LEVEL OF SGAP — FUSION PROTEIN WITH MCHERRY

5.1 Introduction

One experiment in the development of the fluorescence-based SGAP peptidase assay showed that SGAP activity correlated with the optical density of a bacterial suspension expressing SGAP (see figure 3.3). These measurements, however, only took bacterial populations into account. When the scale was brought down to single cells in individual microfluidic droplets, there was a distribution in apparent activities covering at least one \log_{10} step (see, for example, figures 4.3(d) and 4.4(a)).

The two sources of variation are, probably: incomplete lysis and varying levels of SGAP expression in individual bacteria (e.g. [106, 116, 134–138]). The former can be addressed by optimizing the lysis strategy while the latter can, perhaps, be ameliorated by normalizing activity for protein expression levels. The approach described in this chapter—to fuse SGAP to a fluorescent protein called mCherry (see figure 5.1) [107]—is one possible way to achieve this.

mCherry, a red-fluorescent protein ($\lambda_{ex} = 587$ nm, $\lambda_{em} = 610$ nm), was obtained after directed evolution of mRFP1 and resembles GFP structurally (see figure 5.1(c) and (d)) [107, 140]. It was chosen for several reasons [107, 141]:

1. It folds easily and is stable when used in fusion proteins.
2. It is a small, monomeric protein.

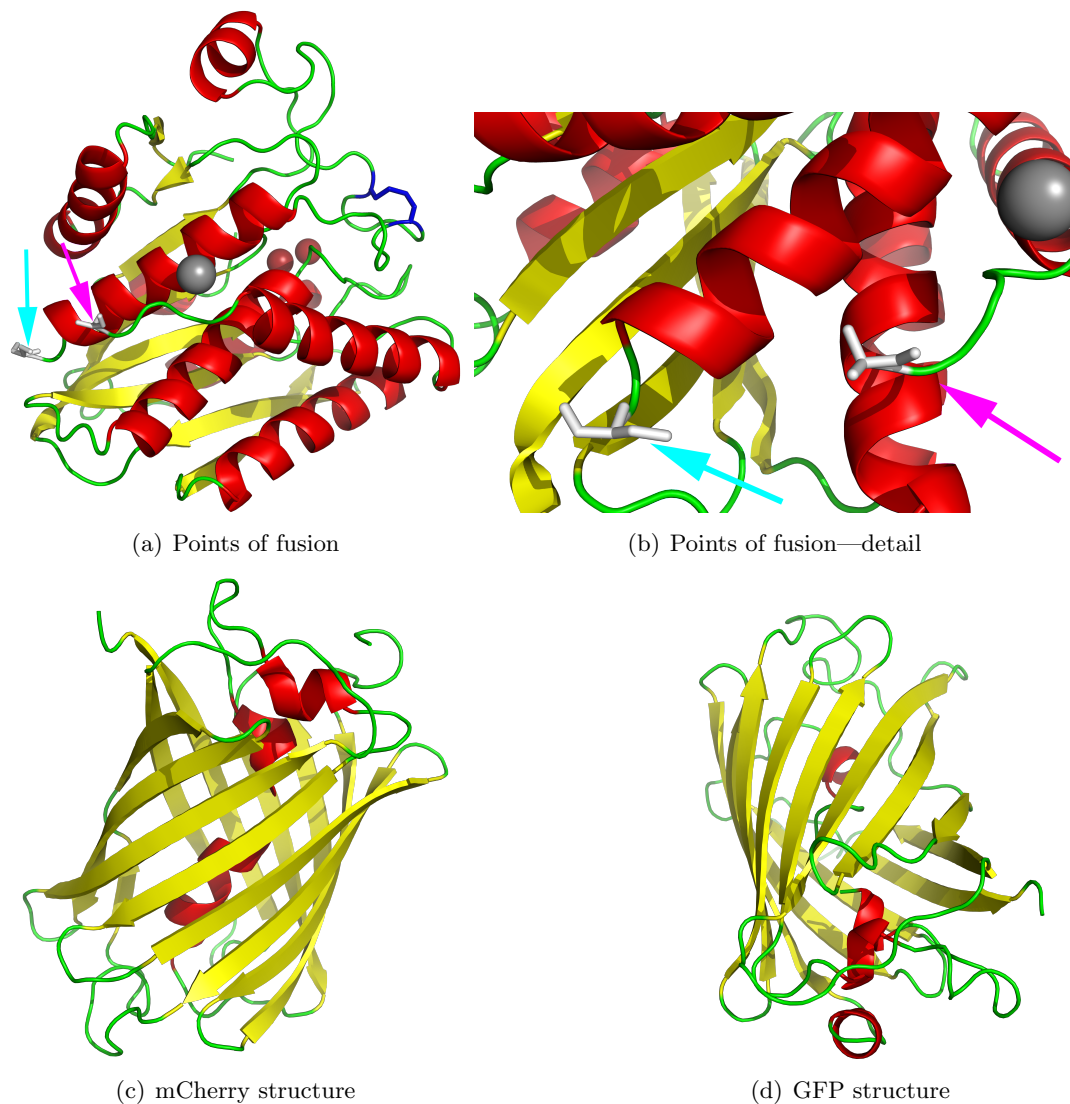


Fig. 5.1: Structural visualization of fusion sites and mCherry. β -sheets are drawn in yellow, α -helices in red and random coils in green. (a,b) The fusion sites on SGAP are indicated by the white residues in stick representation. The cyan arrow points towards the C-terminus of SGAP and the magenta arrow points towards the N-terminus of SGAP. (a) The sites as seen on the full-length SGAP protein. (b) The same image as before zoomed into the specific area where the termini are located. The protein structures were visualized from PDB file 1F2O [51]. Crystal structures of (c) mCherry at 1.36 Å resolution (PDB file 2H5Q [139]) and (d) *Aequorea victoria* green fluorescent protein (GFP; PDB file 1EMA [140]) at 1.90 Å resolution. Both proteins have a β -barrel structure with 12 anti-parallel β -sheets. GFP has four small α -helices, whereas mCherry has three.

3. The excitation and emission spectra (see figure 5.2) indicate that it would suffer little from spilling of rhodamine 110 fluorescence.

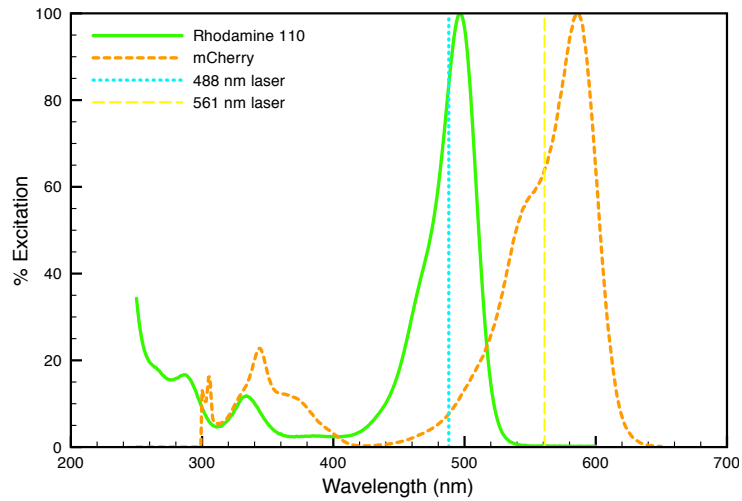
Both a C-terminal (SGAP::mCherry) and an N-terminal (mCherry::SGAP) fusion between mCherry and SGAP were constructed with the linker: SGLRSRA [107].

In this chapter the synthesis of both mCherry::SGAP and SGAP::mCherry will be discussed with the results that were obtained. mCherry::SGAP showed far higher SGAP activity than SGAP::mCherry but is, unfortunately, not yet detectable in droplets (data not shown). In addition, mCherry fluorescence correlates with SGAP peptidase activity.

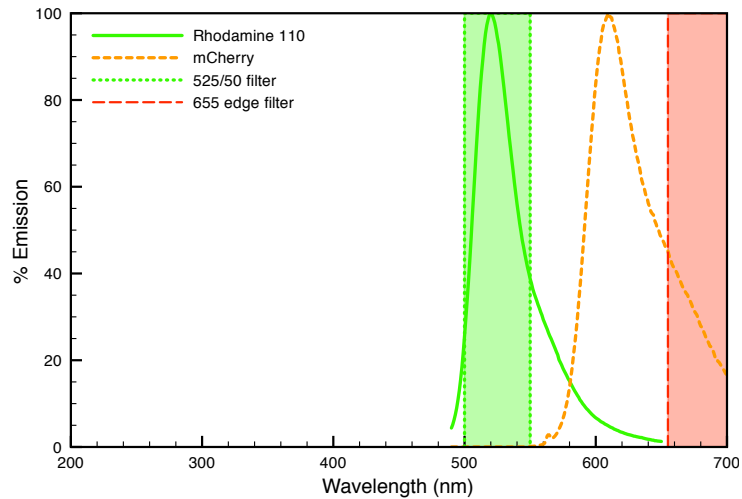
5.2 Materials and methods

5.2.1 Cloning

For the different plasmids involved in this protocol, see figure 5.3. Components affecting the C-terminal fusion (*SGAP::mCherry*) are indicated in red, slanted text whereas components affecting the N-terminal fusion (mCherry::SGAP) are written in black. V424, a plasmid containing the mCherry gene, was kindly donated by M. Erhardt (Universität Konstanz). The gene encoding mCherry was amplified with either a primer combination of *090113_pKB4_C_FW* and *090107_pKB4_C_BW* or *090107_pKB4_N_FW* and *090113_pKB4_N_BW* (table 2.2). The PCR reaction mixtures (section 2.4.10) were supplemented with 5% (v/v) DMSO. A Normal PCR program was run (table 2.1) with an annealing temperature of 68°C. The amplicons were restricted with *EcoRI* or BglII, gel purified (section 2.4.8) and ethanol-precipitated (section 2.4.9). pKB4-SGAP-his was restricted with *EcoRI* or BglII and ethanol-precipitated (section 2.4.9). Restricted plasmid and restricted amplicon were ligated in equimolar quantities (section 2.4.15). Single colonies were grown (section 2.4.2), induced (section 2.4.3) and washed (section 2.4.4).



(a) Excitation spectra for rhodamine 110 and mCherry



(b) Emission spectra for rhodamine 110 and mCherry

Fig. 5.2: Excitation and emission spectra for rhodamine 110 and mCherry. (a) Excitation spectra of rhodamine 110 (green) and mCherry (orange). The vertical cyan line represents a blue laser (λ_{488}) and the vertical yellow line represents a yellow laser (λ_{561}). Rhodamine 110 is excited for $\sim 84\%$ at λ_{488} and mCherry is excited for $\sim 64\%$ at λ_{561} . Rhodamine 110 is excited 100% at λ_{497} and mCherry at λ_{587} . (b) Emission spectra of rhodamine 110 (green) and mCherry (orange). The translucent green area indicates a 525/50 filter for green fluorescence. The translucent red area represents a 655 edge filter for red fluorescence. Rhodamine 110 has 100% emission at λ_{520} and mCherry emission is 100% at λ_{610} .

The suspensions were checked for SGAP peptidase activity with the fluorescence-based assay using HEPES Assay Mixture containing 10 μ M L2R (sections 2.3.17 and 2.4.12), while simultaneously measuring mCherry fluorescence ($\lambda_{em} = 587$ nm, $\lambda_{em} = 610$). Interesting plasmids were purified via midi prep (section 2.4.9) and sent for sequencing (section 2.4.13). mCherry::SGAP was found to contain an inactivating nonsense mutation, which was negated by site-directed mutagenesis using the primers 090406_NAct_fw and 090406_NAct_bw (section 2.4.11; tables 2.2 and 2.1). Next, several clones were grown (section 2.4.2), induced (section 2.4.3), washed (section 2.4.4) and checked in dual fluorogenic measurements as before. The plasmid DNA of interesting clones were purified by midi prep (section 2.4.9) and verified again by sequencing (section 2.4.13).

5.2.2 Correlating mCherry fluorescence to SGAP activity

E. coli K12 TB1 pKB4-mCherry-SGAP-his cells and *E. coli* K12 TB1 pKB4-SGAP-mCherry-his cells were grown (section 2.4.2), induced (section 2.4.3), washed (section 2.4.4), and adjusted to a final OD₆₀₀ of 2.00 ODU. Serial dilutions were then made, diluting to 1.00, 0.50, 0.10, 0.050 and 0.025 ODU₆₀₀. Using the different suspensions a fluorescence-based assay was performed (section 2.4.12) using PBS Assay mixture containing 10 μ M L2R (section 2.3.17), while simultaneously measuring mCherry fluorescence ($\lambda_{ex} = 587$, $\lambda_{em} = 610$ nm) in triplicate for all samples. Initial reaction velocities were determined over the first 600 seconds of the measurements using SoftMax Pro V5.2 software. For each suspension the average reaction velocity and mCherry fluorescence were determined alongside the standard errors of the mean for both types of measurement.

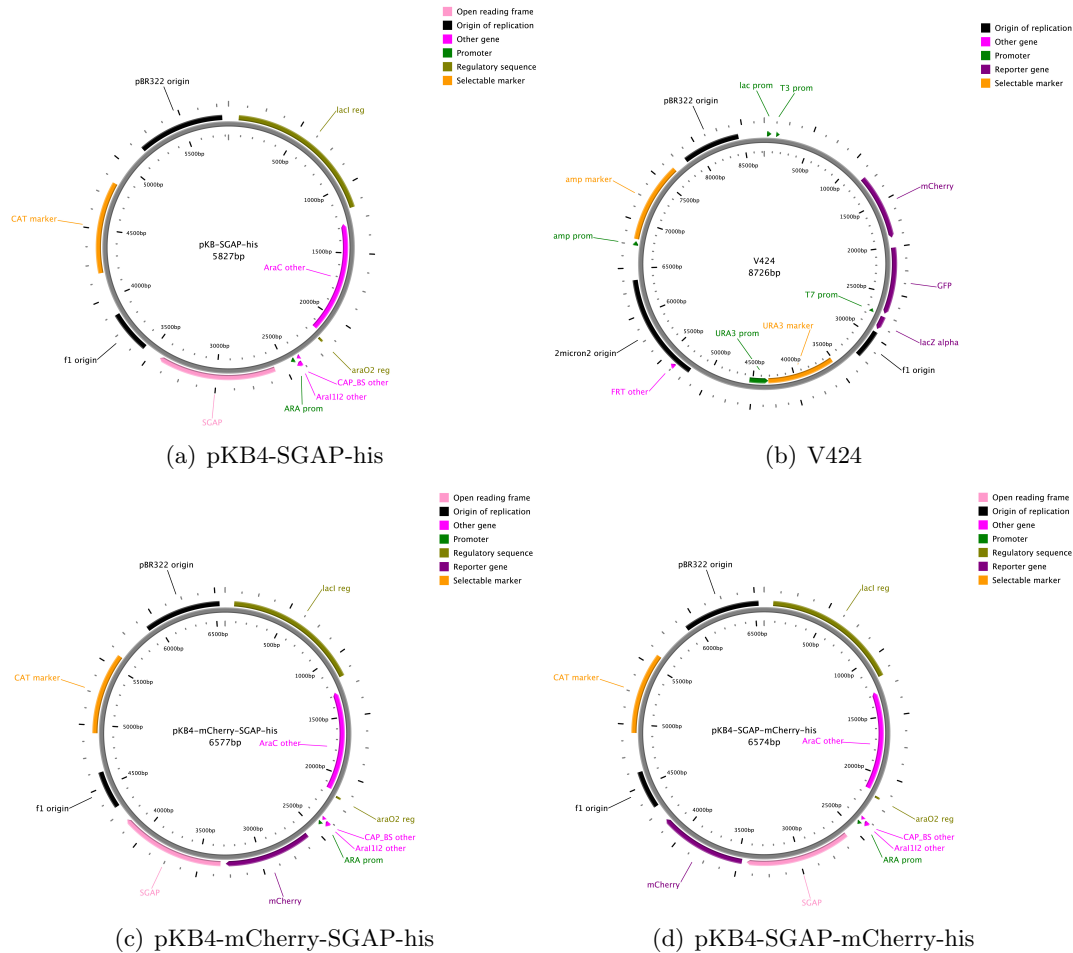


Fig. 5.3: (a) pKB4-SGAP-his was the basic SGAP-expressing plasmid for this project. It contains a chloramphenicol resistance gene (orange; resistance marker), is induced by the addition of arabinose (magenta; other gene) and contains SGAP (light pink; open reading frame) as well as a hexahistidine tag (not shown) to allow purification of the expressed proteins. (b) V424 is a plasmid that was kindly donated by M. Erhardt (Universität Konstanz), containing the mCherry gene (purple; reporter gene [107]). After cloning the theoretical plasmids (c) pKB4-SGAP-mCherry-his (encoding SGAP::mCherry with a hexahistidine tag) and (d) pKB4-mCherry-SGAP-his (encoding mCherry::SGAP with a hexahistidine tag) were obtained. The plasmid maps were made using PlasMapper [142].

5.2.3 Comparison of SGAP peptidase activity between mCherry::SGAP and SGAP::mCherry

E. coli K12 TB1 pKB4-SGAP-mCherry-his cells and *E. coli* K12 TB1 pKB4-mCherry-SGAP-his cells were grown (section 2.4.2), induced in triplicate (section 2.4.3) and washed (section 2.4.4). HEPES Assay Mixture was used with 10 μM L2R and 100 $\mu\text{g ml}^{-1}$ polymyxin B (section 2.3.17) in a fluorescence-based assay over 1.5 h (section 2.4.12). 100 $\mu\text{g ml}^{-1}$ polymyxin B did not show any difference in activity in microtitre plate assays compared to 2 mg ml^{-1} (data not shown). Each induced culture was measured in triplicate. Reaction velocities were determined with SoftMax Pro V5.2 software. The average reaction velocities for mCherry::SGAP and SGAP::mCherry were compared using an unpaired *t*-test.

5.3 Results and discussion

Generally, fluorogenic peptidase substrates are based on rhodamine 110 (blue/cyan excitation, green fluorescence) or aminocoumarin (UV excitation, blue fluorescence). A fluorescent protein should, therefore, be red-shifted. In addition, the protein must retain its fluorescence without interfering with SGAP activity. Therefore, the fluorescent protein should be small—preferably monomeric—and fold readily. mCherry was identified as the most promising for all these aspects, with its excitation (λ_{587} , yellow/orange) and emission (λ_{610} , red) wavelengths sufficiently red-shifted [107, 141].

mCherry has a β -barrel structure, much like GFP. It descends from mRFP1, which itself is a direct descendant of *Discosoma sp* red fluorescent protein (DsRed) and has been used in a fusion protein before with a linker consisting of seven amino acids (SGLRSRA) [107, 139, 140, 143, 144].

Both N-terminal and C-terminal variants were constructed, since it was impossible to

know beforehand whether SGAP activity would be affected.

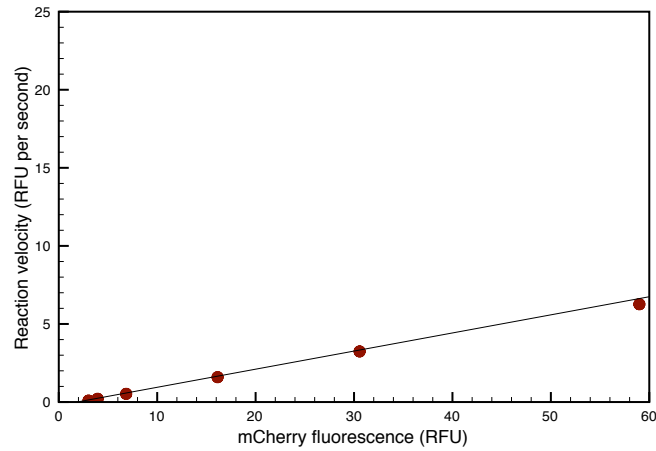
V424 was used as the template from which mCherry was amplified. During this amplification the linker was introduced as well. Consequently, the primers were long and thus secondary structures were more likely, which in turn meant that the PCR conditions had to be changed. DMSO was added to a final concentration of 5% (v/v) and the annealing temperature was increased to 68°C. Without DMSO there was no amplification and at lower annealing temperatures the amplification lead to an unknown amplicon, half the size of mCherry (supplementary information, figure 9.9).

Both fusion proteins, SGAP::mCherry (C-terminal) and mCherry::SGAP (N-terminal) were verified via fluorescence-based assays (data not shown) and sequencing.

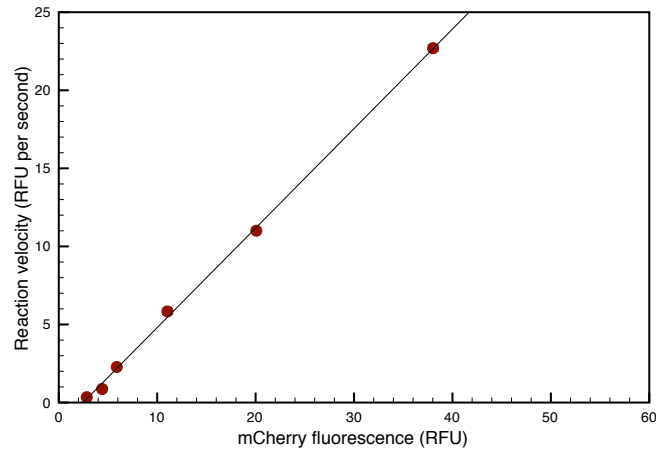
To confirm whether mCherry could be used as a fluorescent marker to normalize for expression, first a dilution experiment was performed similar to that in chapter 3 (see figure 5.4). When assuming that bacterial suspensions were at certain OD_{600s}, a fit was obtained of $R^2 = 0.988$. The addition of an empirical value (mCherry fluorescence) was expected to improve the fit.

When correlating SGAP activity with mCherry fluorescence in different dilutions, the R^2 values are 0.9997 and 0.9991 for SGAP::mCherry and mCherry::SGAP, respectively. The different points on the graphs have the standard errors of the mean included for both mCherry fluorescence and reaction velocity of SGAP peptidase activity.

In order to quantitatively determine which of the two fusion proteins showed the highest SGAP peptidase activity a direct comparison was made. Three different induced cultures were measured in triplicate in a fluorescence-based measurement (section 2.4.12). The measurements were directly compared via an unpaired *t*-test (see figure 5.5). The experiment was performed using only 100 µg ml⁻¹ polymyxin B instead of the usual 2 mg ml⁻¹, but on microplate this lower concentration did not make a difference in the



(a) Correlation for SGAP::mCherry



(b) Correlation for mCherry::SGAP

Fig. 5.4: Correlation between mCherry fluorescence ($\lambda_{ex} = 587$ nm and $\lambda_{em} = 610$ nm) and SGAP reaction velocity for (a) SGAP::mCherry and (b) mCherry::SGAP fusion proteins. Several dilutions of *E. coli* K12 TB1 pKB4-SGAP-mCherry-his or *E. coli* K12 TB1 pKB4-SGAP-mCherry suspensions were used while measuring both mCherry fluorescence and the increase in rhodamine 110 fluorescence. Reaction velocities (RFU sec^{-1}) were determined over the first 600 seconds. The plots include the standard error of the mean for reaction velocities as well as mCherry fluorescence. In both fusion proteins there is a linear correlation between the reaction velocity of SGAP and mCherry fluorescence (R^2 values of 0.9997 and 0.9991 for SGAP::mCherry and mCherry::SGAP, respectively). Neither line goes exactly through the origin.

reaction profiles (data not shown).

mCherry::SGAP showed a higher SGAP peptidase activity than SGAP::mCherry in the same experimental conditions, either because of better expression or better specific activity. In any case, mCherry::SGAP was chosen for further development.

This was the reason why in the microfluidics experiments mCherry::SGAP was used to visualize the lysis of the cells (figure 4(g)-(i)). However, mCherry has not been detectable in microfluidics so far due to the limited sensitivity of the current optical setup (data not shown). It has, therefore, not been possible to normalize SGAP activity for the expression level of SGAP::mCherry.

mCherry is described as one of the brightest fluorescent proteins in the red spectral class [141]. However, if the brightness does not suffice in the long run for detection, there are many more fluorescent proteins in the orange, red and far-red spectra that could potentially be used (listed in [141, 145]). Many of these proteins fall into the original mFruit series of fluorescent proteins [107], but many others have recently been developed.

5.4 Conclusions

In this chapter the construction of two fusion proteins between SGAP and mCherry was described: a C-terminal fusion (SGAP::mCherry) and an N-terminal fusion (mCherry::SGAP). The N-terminal fusion showed higher SGAP peptidase activity than the C-terminal fusion under the same experimental conditions and so was chosen to continue experiments with.

Assays investigating the correlation between SGAP peptidase activity and mCherry fluorescence, found a nearly perfect correlation for this relationship in both fusion proteins ($R^2 = 0.9991$ and $R^2 = 0.9997$ for mCherry::SGAP and SGAP::mCherry, respectively),

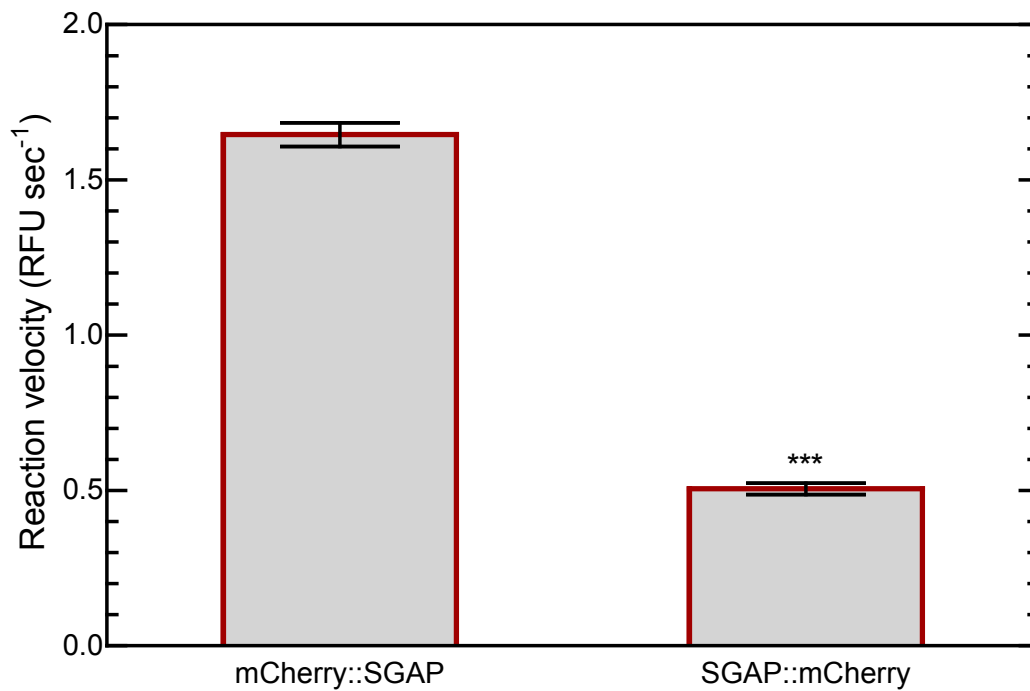


Fig. 5.5: Quantitative comparison of SGAP peptidase activity between the fusion proteins mCherry::SGAP and SGAP::mCherry. Suspensions at 0.25 ODU₆₀₀ of *E. coli* K12 TB1 pKB4-mCherry-SGAP-his or *E. coli* K12 TB1 pKB4-SGAP-mCherry-his in HEPES Assay Mixture with 100 $\mu\text{g ml}^{-1}$ polymyxin B and 10 μM L2R (section 2.3.17) from three different induced cultures were measured in triplicate for 1.5 h. The reaction velocities were determined over the entire measurement of 1.5 h. The mCherry::SGAP fusion protein showed a higher SGAP peptidase activity than the SGAP::mCherry fusion protein (***) $P < 0.0001$, unpaired t -test).

compared to a fit of $R^2 = 0.988$ when correlating the measured $\text{OD}_{600\text{s}}$ with SGAP peptidase activity. This is promising with respect to the desired normalizations in microfluidic droplets.

mCherry was chosen because it was marked as one of the best fluorescent proteins in the red spectrum [107, 141, 145]. However, mCherry fluorescence has not yet been detectable in droplets. The equipment does not seem to be sensitive enough to detect mCherry fluorescence at the concentration of 1 bacterial cell per 12 pl droplet.

6. SYNTHESIS OF 7-AMINOCOUMARIN-4-METHANESULFONIC ACID

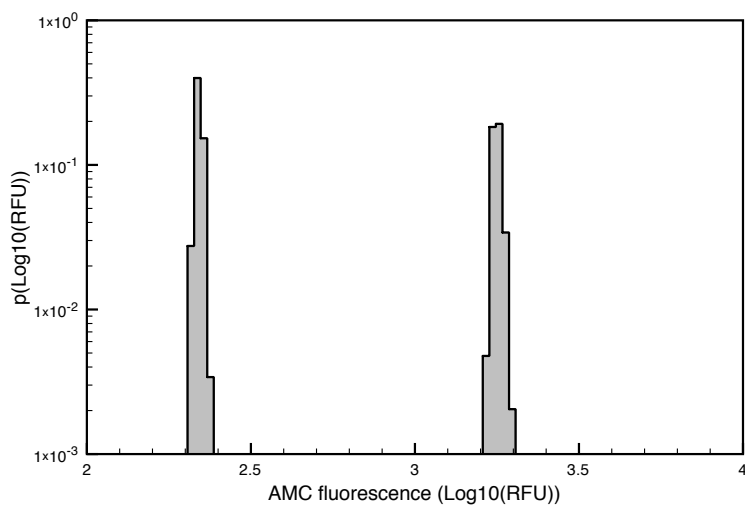
6.1 *Introduction*

The possible long-term goals of the project involving directed evolution of SGAP have been discussed in section 1.3. Briefly, some of the options were: (i) checking how genetic drift functions, (ii) investigating the effect of negative selection on directed evolution of a protein, (iii) determining the difference between selecting specifically for a generalist or a specialist and (iv) testing whether evolvability can be evolved.

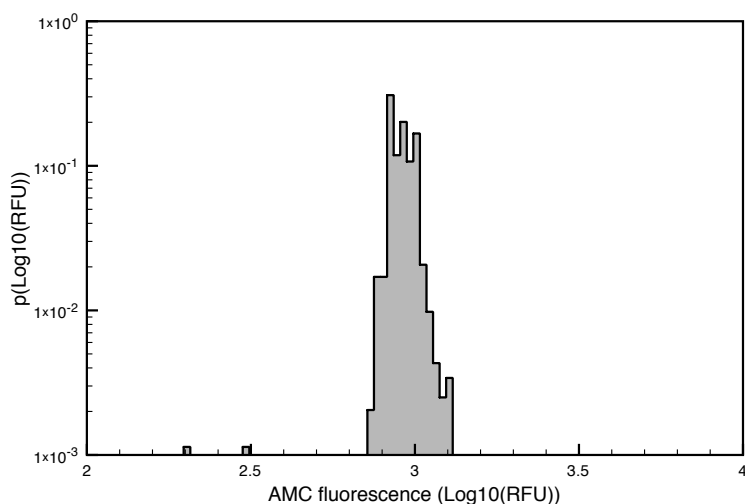
All of these goals are critically dependent on the specific selection or counterselection of a second activity of SGAP. At the outset of the project there were no functional fluorogenic substrates for the phosphodiesterase or catechol oxidase activities of SGAP, so a new substrate for the aminopeptidase activity was needed.

Generally, fluorogenic peptidase substrates are based on rhodamine 110 or 7-aminocoumarin. The excitation and emission spectra of aminocoumarin supplement the different colors already used in this project. However, the exchange of aminocoumarin between microfluidic droplets is very rapid (L. Granieri, personal communication, figure 6.1).

Hydrophilicity is one of the factors believed to influence exchange between droplets [130]. More hydrophilic substances are expected to remain inside the droplets longer. Synthesis of an aminocoumarin that is more hydrophilic than the commonly-used 7-amino-4-methylcoumarin would, perhaps, decrease the exchange between droplets.



(a) Fluorescence profile upon droplet generation



(b) Fluorescence profile 60 minutes after droplet generation

Fig. 6.1: Determination of the exchange rate of 7-amino-4-methylcoumarin (AMC) between droplets. Droplets containing 20 μM or 200 μM AMC were produced in 2% (w/w) AEH24 surfactant in FC40 fluorinated oil. The experimental methods have been described by L. Granieri ([146]). Fluorescence profiles (a) when droplets were generated and (b) after 60 minutes of incubation. RFUs were calculated from the output of the PMTs in Volts (V) using the formula $\text{RFU} = V/(\text{Gain}^{pc})$, where pc is the PMT constant, which was 7.2 for this specific PMT. $p(\log_{10}(\text{RFU})) = \frac{\text{number of droplets at } x \log_{10}(\text{RFU})}{\text{total number of droplets}}$, which denotes the probability a droplet is at $x \log_{10}(\text{RFU})$. Graphs plotted with data from L. Granieri.

The molecule that was chosen to be synthesized was 7-aminocoumarin-4-methanesulfonic acid (ACMS) [147]. The synthesis strategy employed is indicated schematically in figure 6.2. Briefly, the idea was to use the building blocks 3-aminophenol and ethylchloroformate together in order to protect the amine moiety of the aminophenol (step 1). Subsequently, a Pechmann condensation between the product of step 1 and ethyl-4-chloroacetoacetate yielded a protected aminocoumarin (step 2). Next, a sulfonation reaction was performed in order to replace the $-Cl$ of the 4-chloromethane group with a sulfonate ($-SO_3^-$) (step 3). When the ACMS molecule was obtained, the $-NH_2$ group needed to be deprotected (step 4). Grafting an amino acid moiety, using an acyl chloride, onto ACMS would then be the final step (step 5). Steps 1-4 have been described [147–149], but were adapted slightly.

In this chapter the synthesis of ACMS, which was done in collaboration with Gabrielle Woronoff (Université Catholique de Louvain-la-Neuve, Biochemistry Unit, Patrice Soumillon laboratory), will be explained and the results obtained will be discussed. In addition, some preliminary experiments with ACMS will be discussed. The excitation and emission spectra of this molecule were measured and matched those reported in the literature [147]. Additionally, the exchange of ACMS between microfluidic droplets was measured.

6.2 Materials and methods

In sections 2.2.1-2.2.4 ‘eq’ denotes equivalent. Unless otherwise stated, all chemicals used in the synthesis came from Sigma and were chemical grade. The general protocols have been described [147–149], but have been adapted slightly.

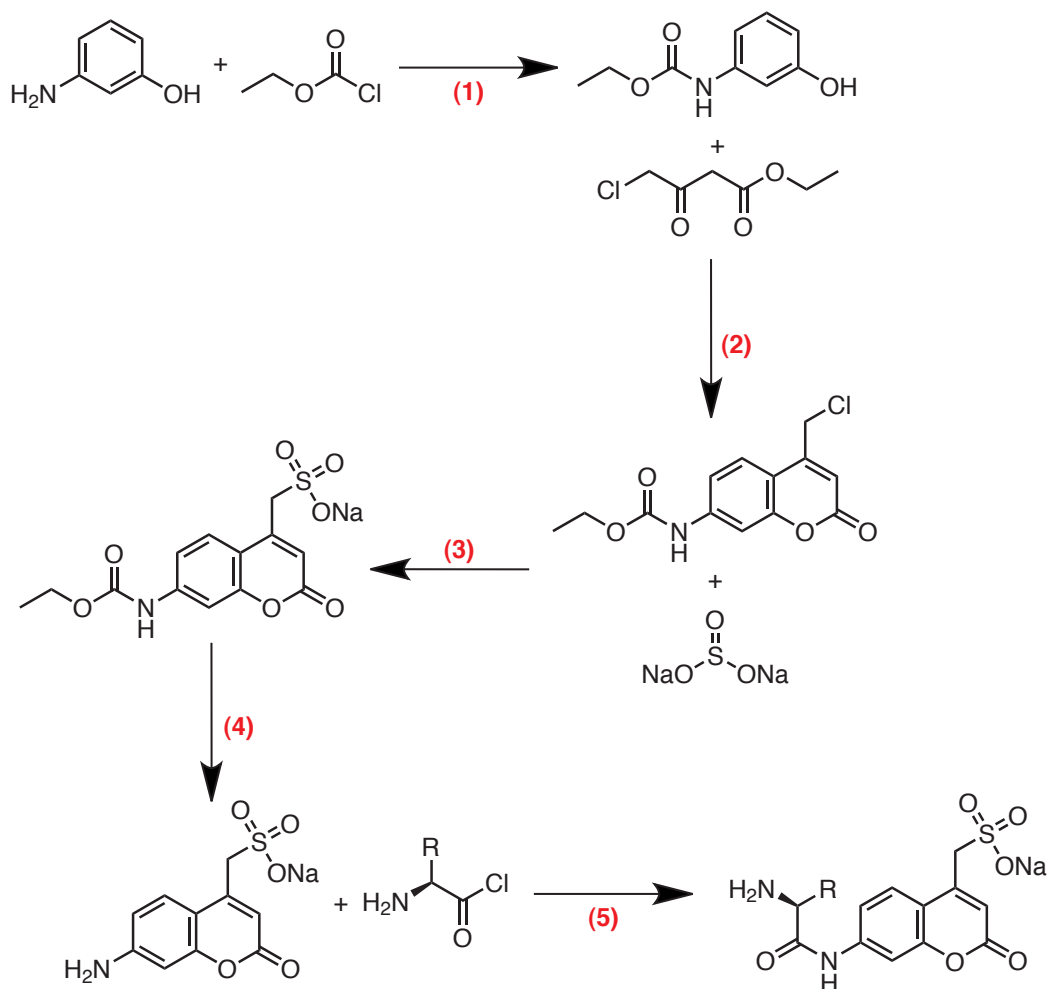


Fig. 6.2: Synthesis strategy to obtain a substrate for SGAP based on 7-aminocoumarin. (1) Protection of 3-aminophenol. 3-aminophenol and ethylchloroformate are the building blocks for a protected molecule. (2) Formation of a protected 7-aminocoumarin by way of a Pechmann condensation starting with protected aminophenol and ethyl-4-chloroacetoacetate. (3) Sulfonation of the protected aminocoumarin. Ammoniumsulfite and the protected aminocoumarin are used as the starting product of this reaction. (4) Deprotection of the sulfonated and protected aminocoumarin. (5) Creation of an aminopeptidase substrate based on ACMS. Taking ACMS and acyl chloride form of an amino acid together, an aminopeptidase substrate is synthesized. Steps 1-4 were done as described in the literature [147–149], with slight adaptations.

6.2.1 Protection of 3-aminophenol

20 g of 3-aminophenol (184 mmol; 2 eq) was dissolved in 500 ml dry diethyl ether and 100 ml dry tetrahydrofuran in an inert environment. Ethylchloroformate (1 eq) in 100 ml dry diethyl ether was added dropwise. The mixture was left to react for 3.5 h at room temperature. The suspension was filtered through a number 4 porosity filter. The flow-through was dried under vacuum at 30°C and re-dissolved in 500 ml dry diethyl ether. Liquid-liquid extractions were performed: 2× in 0.1 M HCl, 2× in saturated NaHCO₃ and 2× in ddH₂O (until neutral pH was obtained). The organic phase was dried under vacuum and re-suspended in 100 ml chloroform. The solution was brought to reflux until complete dissolution of the product occurred. The product was recrystallized on ice and then filtered through a number 4 porosity filter and washed with ice-cold chloroform. The obtained crystals were dried in a vacuum dessicator before determining the ¹H-NMR in DMSO. This reaction yielded ~95%.

6.2.2 Pechmann condensation with protected 3-aminophenol

2.5 g of protected aminophenol (13 mmol; 1 eq) were dissolved in 70 ml 70% (v/v) H₂SO₄ under vigorous agitation while keeping the mixture cooled in an ice bath. Ethyl 4-chloroacetoacetate (1 eq) was added and the reaction was left to return to room temperature overnight. The following day, the reaction mixture was poured onto 100 ml ice water (ddH₂O) and agitated for another 30 minutes on ice. The yellowish suspension was filtered through a cold number 4 porosity filter and washed twice with 50 ml of ice-cold dry diethyl ether. The filtrate was dissolved in 320 ml of acetone at reflux and subsequently left to cool down to room temperature before being placed on ice and leaving recrystallization to occur for 1 h. The suspension was filtered through a cold number 4 porosity filter. The flowthrough was evaporated until crystals started forming and put back on ice for 30 minutes to recrystallize. The suspension was also filtered through a

cold number 4 porosity filter. $^1\text{H-NMR}$ was measured in DMSO. This reaction yielded $\sim 48\%$.

6.2.3 Sulfonation of protected 7-aminocoumarin

3.5 g of protected aminocoumarin (12.4 mmol; 1 eq) were dissolved in 140 ml pure ethanol and 20 ml of dimethylformamide (DMF) were added. Sodium sulphite (1.2 eq) was dissolved in 20 ml ddH₂O and added to the other solution before bringing the entire mixture to reflux. Then another 20 ml DMF were added and the whole was incubated for another 4 h at reflux. The entire mixture was cooled off to room temperature before drying under vacuum. The product was dissolved in 200 ml ddH₂O at reflux temperature and filtrated warm through a number 4 porosity filter while washing twice with ddH₂O at reflux temperature. The flow-through was dried under vacuum again and dissolved in methanol at reflux temperature. The methanol solution was filtered warm as well before vacuum drying the flow-through. $^1\text{H-NMR}$ was measured in DMSO. This reaction yielded $\sim 60\%$.

6.2.4 Deprotection of protected 7-aminocoumarin

2.5 g of protected 7-aminocoumarin-4-methanesulfonic acid were taken. 5.5 ml of concentrated sulfuric acid were mixed with 5.5 ml of concentrated acetic acid. This acid mixture was used to dissolve the 2.5 g of reaction product. The mixture was incubated overnight at 100°C while agitating. The following day, the mixture was poured onto 50 ml of ethanol, after which the solution was adapted to 100 ml with ethanol. The mixture was cooled off to allow recrystallization and filtered through a number 4 porosity filter. The filtrate was dried in a vacuum dessicator before measuring the $^1\text{H-NMR}$ in DMSO. This reaction yielded $\sim 95\%$.

6.2.5 Measurement of excitation and emission spectrum

ACMS was diluted to 1 μM in 40 mM HEPES pH 8.5. Excitation and emission spectra were measured in triplicate in a black 384-well plate with a final volume of 40 μl per sample. For the excitation spectrum the emission detection was fixed at λ_{462} [147] and the excitation was varied between λ_{250} and λ_{440} with 1 nm increments. Conversely for the emission spectrum the excitation was fixed at λ_{362} [147] and the emission was varied between λ_{385} and λ_{650} with 1 nm increments. Subsequently the average values for the different reads were normalized based on the maximum signal for the respective spectrum.

6.2.6 Testing the exchange of free 7-aminocoumarin-4-methanesulfonic acid between droplets

This experiment was done as described in chapter 4.2.1, except that the droplets were produced with either 10 μM or 100 μM ACMS in 40 mM HEPES, pH 8.5.

6.3 Results and discussion

The results of the synthesis are described in section 9.2 with all the $^1\text{H-NMR}$ spectra in figures 9.2 for the protection of 3-aminophenol, 9.3 for the Pechmann condensation, 9.4 for the sulfonation of the protected 7-aminocoumarin, and 9.5 for the deprotection of ACMS, respectively.

The final step in the synthesis to obtain ACMS itself was the deprotection of the molecule. This was done under highly acidic conditions at 100°C overnight, with a distinctive coloration happening in the reaction, going from colourless to green to dark brown. The $^1\text{H-NMR}$ showed the following δ (see figure 9.5): 1.05 (ethanol residual

[150]), 2.50 (DMSO residual [150]), 3.44 (ethanol residual [150]), 3.88 (2H, s, $-\underline{\text{CH}_2}-\text{SO}_3\text{H}$), 5.95 (1H, s, 3-H), 6.18 (5H, s, $-\text{NH}_2$, $-\text{CH}_2-\text{SO}_3\text{H}$ and ethanol residual [150]), 6.43 (1H, d, 8-H), 6.55 (1H, dd, 6-H), 7.57 (1H, d, 5-H). This reaction yielded approximately 95%.

The number of peaks in this ^1H -NMR spectrum, the big peak around $\delta = 6.18$ ppm and the clear peak at $\delta = 3.88$ ppm indicated ACMS had been obtained. The latter peak indicates methanesulfonic acid moiety. The broad peak at $\delta = 6.18$ ppm probably contains a residue of ethanol as well as the $-\text{NH}_2$ and $-\text{SO}_3\text{H}$ groups. The total number of peaks as well as their integrals were in line with the expected number of hydrogens.

The excitation and emission spectra of the synthesized molecule (see figure 6.3), with reported maxima of $\lambda_{ex} = 362$ nm and $\lambda_{em} = 462$ nm [147], were measured to characterize the molecule. The maximum measured values for the synthesized ACMS were $\lambda_{ex} = 360$ nm and $\lambda_{em} = 460$ nm.

However, amenability of ACMS in microfluidics was still critically dependent on the exchange profile or the leakage from the droplets. 7-amino-4-methylcoumarin (AMC) is generally used as the basis for fluorogenic peptidase substrates, but leaks from the droplets rapidly (figure 6.1).

The leakage of ACMS from microfluidic droplets was determined by conducting an experiment that was analogous to the leakage test performed for rhodamine 110 but with 10 μM ACMS or 100 μM ACMS (see figure 6.4). The fluorescence was measured 50 minutes, 70 minutes and 180 minutes after droplet formation. Upon droplet creation there was a tenfold difference between the fluorescence intensities of the two types of droplets and this difference remained up to 180 minutes after droplet formation. The 180-minute measurement is slightly shifted because the microscope stage moved between measurements or because the laser power was different. ACMS does not seem to measurably leak from the droplets or exchange between them. Consequently, it would be suitable

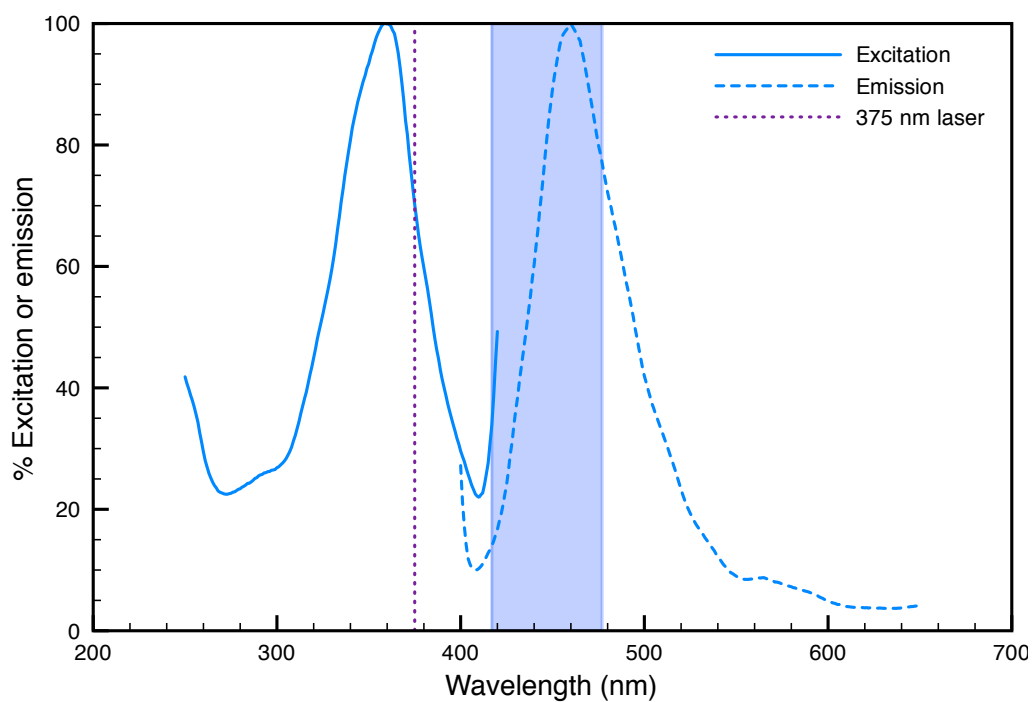


Fig. 6.3: Excitation and emission spectra of synthesized ACMS. The solid blue line represents the excitation spectrum and the dashed line represents the emission spectrum. Each of the spectra was normalized on the maximum fluorescence. The vertical, dark purple, line is the wavelength for the UV laser that was used for subsequent experiments (λ_{375}). The light blue area on the graph represents the filter that was subsequently used for the detection of ACMS (447/60).

for use in droplet microfluidics, in contrast to AMC, which had only one population of droplets after 60 minutes (figure 6.1).

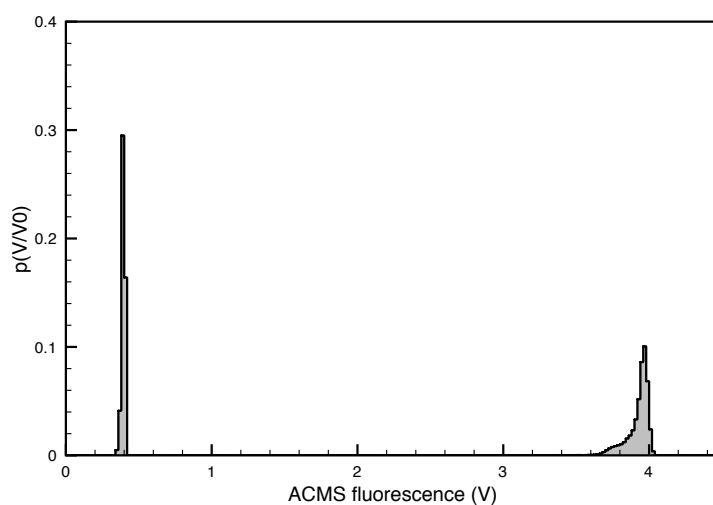
No ACMS-based substrate for SGAP has, so far, been synthesized. However, using an acyl chloride [151] a substrate for penicillin G acylase (EC 3.5.1.11) was successfully synthesized. This substrate functions correctly in both microplate assays and microfluidic assays (G. Woronoff, personal communication). Synthesis of L-leucinyl-7-aminocoumarin-4-methanesulfonic acid, to serve as a substrate for SGAP peptidase activity, is currently underway.

6.4 Conclusions

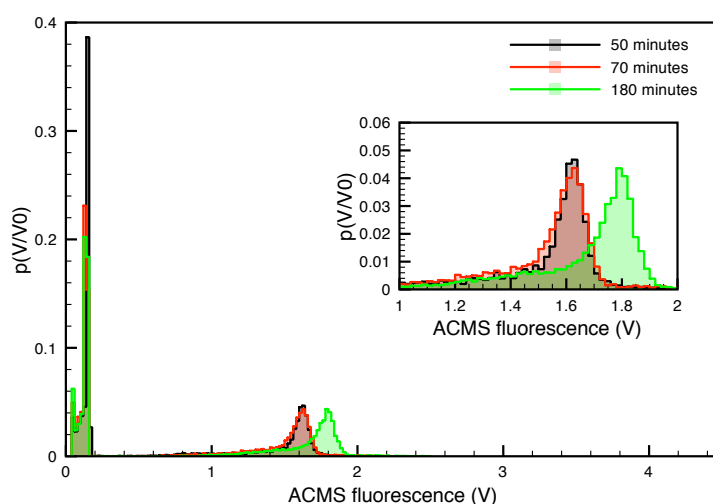
In this chapter the synthesis of ACMS was described, which was performed as a combination of syntheses described by Atkins and Bliss [148], Sato and colleagues [147] and Pianowski and Winssinger [149] with small adaptations to the protocols. The different steps of the synthesis had yields varying between 48% and nearly 100%, with an overall yield of $\sim 25\%$. The obtained product shows the same excitation and emission spectra as were previously reported [147].

In contrast with AMC, ACMS did not exchange between microfluidic droplets. This does not mean that all combinations of surfactant and fluorinated oil will show the same pattern, but the combination of EA surfactant and HFE 7500 oil is widely used and important.

One substrate has already been synthesized with ACMS: a substrate for penicillin G acylase. This substrate works in both microplate assays and microfluidic assays (G. Woronoff, personal communication). This synthesis strategy is now being used to prepare substrates for SGAP, coupling ACMS to L-leucine, L-valine and L-glutamate.



(a) Fluorescence profile upon creation



(b) Fluorescence profile upon reinjection

Fig. 6.4: Leakage assay of ACMS in microfluidics. In analogy to the leakage tests that were performed with rhodamine 110, a dual droplet maker was used to simultaneously create droplets containing either 10 μM ACMS or 100 μM ACMS. (a) Upon droplet formation a tenfold difference was measured in the signals. (b) The droplets were incubated in a glass capillary at ambient temperature throughout the experiment. Fluorescence was measured after 50 minutes (black histogram), 70 minutes (red histogram) and 180 minutes (green histogram). The inset is zoomed in to the second population, which contains 100 μM ACMS. $p(\log_{10}(V/V_0)) = \frac{\text{number of droplets at } x \log_{10}(V/V_0)}{\text{total number of droplets}}$, which denotes the probability a droplet is at $x \log_{10}(V)$. V_0 is a reference voltage of 1 V. The 180 minute histogram is slightly shifted compared to the other two because the microscope stage moved slightly before the measurement or because the laser power varied.

7. FLAT AND CRYSTALLIZABLE EMULSIONS

7.1 *Introduction*

This project was performed in collaboration with Julien Sylvestre from Jérôme Bibette's laboratory at the École Supérieure de Physique et de Chimie Industrielles (ESPCI) in Paris. There are some advantages of these flat and crystallizable, or 2D, emulsions. For one, they facilitate the use of fluorescent substrates to screen for activity. Secondly, they allow simpler selections than in typical IVC selections [9]. Thirdly, they do not require an expensive FACS machine.

The emulsions are crystallizable because the formulation of oil and surfactant used (decane containing 2.5% (w/v) Span 60 and 2.5% (w/v) cholesterol) solidifies when kept at temperatures below 37°C [152]. Using fluorescent beads, it has been demonstrated that 2D emulsions exhibited a linear increase in the number of fluorescence counts, dependent on the number of beads introduced, over four orders of magnitude [152]. In addition, it has been demonstrated that fluorescence kinetics can be monitored in real-time over a period of 90 minutes with minimal mobility of the droplets [152].

Until the point of our collaboration, however, this system, which is different from previously published double emulsions [9] both in the creation of droplets as well as the oil/surfactant formulation, had never been used to monitor enzymatic activity in a library. If it was possible to identify single genes in a large library that were capable of catalyzing a specific reaction, this approach would be useful for isolating genes by

function from genomic or metagenomic libraries. The model system chosen was *in vitro* transcription and translation (IVTT) of *lacZ*, which encodes β -galactosidase.

The interest in being able to screen metagenomic libraries—libraries containing fragments of DNA from many microorganisms in an environmental sample [153]—is that only between 0.1-1.0% of microorganisms can be cultivated in laboratory cultures [154]. The microorganisms that have been cultivated, have proved to be an important source of, for example, antibiotics and biocatalysts [155]. So there is a plethora of possibly interesting genetic material still to be discovered in metagenomic libraries. As an example, soil metagenomic libraries can contain $\sim 10\,000$ *E. coli* genomes [156, 157]. *In vivo* expression is not suitable for screening (meta)genomic libraries, as it may be severely limited by the toxicity of specific genes. Besides, transformation efficiency is another limiting factor.

A goal for the 2D emulsions was to work with a model genomic library, which was based on random fragments of DNA from *E. coli* BL21 DE3 pLysS cells. All BL21 strains are descendents of the *E. coli* B strain, which has a genome size of approximately 4 megabases (Mb), according to the Genomes On Line Database (GOLD [158]). *E. coli lacZ* is approximately 3 kb long, so if random fragments of ~ 3 kb are created by shearing the whole genome, only 1 sequence out of ~ 4 million will be *lacZ*. In practice, however, the number of positives will be higher because some *lacZ* truncates and extended fragments will still be functional.

Assuming 1 active sequence in 4 million sequences, and considering that the maximum sorting speeds for FACS and FADS are 7×10^4 and 2×10^3 events per second, respectively [2, 22], to obtain one positive sample from a genomic library would take 57 seconds or 2 000 seconds, respectively. Visualizing millions of reactions simultaneously would allow the library to be screened more completely and in less time.

The IVTT-expressed *lacZ* model system was used to check several aspects of the 2D

emulsion system. For one, it would be checked for biocompatibility of the oil/surfactant combination. Secondly, the sensitivity of the system could be verified, to know whether working with genomic or even metagenomic libraries would be feasible in 2D emulsions.

IVTT was used to express *lacZ* from the plasmid pIVEX2.2EM-*lacZ* (see figure 7.1 [9]). This plasmid is suitable for IVTT reactions, as it contains a T7 promoter and terminator. The manufacturer's guidelines for the IVTT kit used, EcoPro T7 System (Roche Applied Science, Mannheim, Germany) indicates that a PCR product is preferred over plasmids for IVTT. Primers were chosen to produce a PCR fragment that contained both the T7 promoter and terminator from the plasmid.

In this chapter, the application of 2D emulsions in identifying *lacZ* fragments is discussed. In the end, a high dilution of initial PCR product lead to a number of positive events that was within the range of expectation. However, the negative samples included several false positives. The possible causes for this observation and potential remedies are also discussed.

7.2 Materials and methods

The reader is referred to the PhD thesis by Julien Sylvestre [152] for additional details. Unless specified otherwise, all chemicals came from Sigma.

7.2.1 *In vitro* transcription and translation

pIVEX2.2EM-LacZ-his (see figure 7.1) was used as the template in a PCR reaction. Expand long template system (Roche Applied Science, Mannheim, Germany) was used. PCR mixture was made up of $1 \times$ LT buffer 1, $0.35 \mu\text{M}$ dNTPs, $0.3 \mu\text{M}$ LMB-11E, $0.3 \mu\text{M}$ pIVB-8 (sequences: $5' - \text{GCCCGATCTTCCCCATCGG} - 3'$ and $5' - \text{CACACCCGTCCTGTGGA} - 3'$,

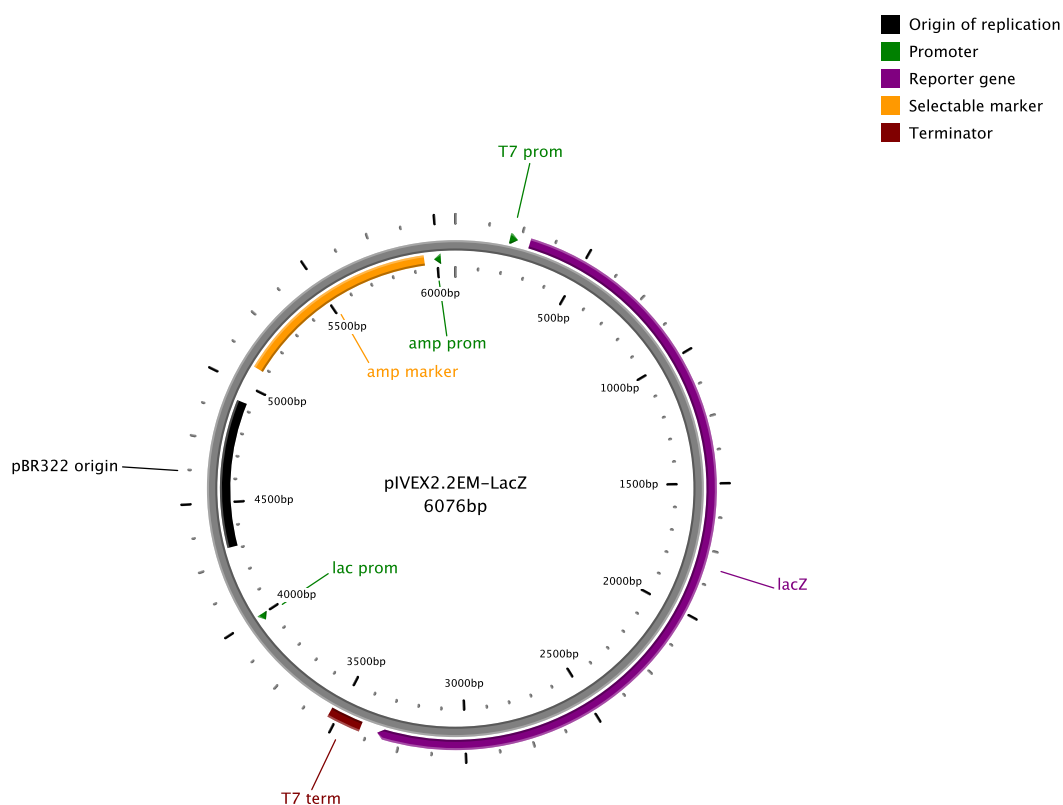


Fig. 7.1: pIVEX2.2EM-LacZ, as described by Mastrobattista *et al.* [9]. This plasmid is the basic plasmid used in the *in vitro* transcription and translation of *lacZ* via the T7 promoter, yielding β -galactosidase. β -galactosidase can be detected through the hydrolysis of fluorescein-di- β -D-galactopyranoside (FDG). Hydrolysis of FDG yields fluorescein, which shows similar excitation and emission features as rhodamine 110. Bacteria containing this plasmid were always grown in Amp⁺ media. The plasmid map was created using PlasMapper [142].

respectively [9]), 3.75 U LT enzyme mix and 2.5 ng of template in a final volume of 50 μl . The PCR was run as follows: incubate at 95°C for 2 minutes, cycle 10 times (95°C for 30 seconds, 50°C for 30 seconds, 68°C for 2 minutes), cycle 20 times (95°C for 30 seconds, 50°C for 30 seconds, 68°C for 2 minutes + 10 additional seconds per cycle), 68°C for 7 minutes and store at 4°C. Following the PCR amplification, the reactions were purified with a QIAquick PCR purification kit (QIAGEN S.A., Courtabœuf, France), after which they were purified further by isopropanol precipitation. The PCR fragment was diluted to 60 ng μl^{-1} and served as the template for the *in vitro* transcription and translation (IVTT) reactions.

Just before starting an IVTT reaction, the template was diluted 10⁴-fold in yeast total RNA, to a final concentration of 6 pg μl^{-1} . FDG was prepared in 8:1:1 H₂O:DMSO:EtOH, according to the manufacturer's guidelines. IVTT was performed using the EcoPro T7 System (Novagen, Merck KGaA, Darmstadt, Germany). Each IVTT reaction was performed in a final volume of 100 μl and contained 70 μl of EcoPro extract, 0.2 mM methionine, 200 μM fluorescein-di- β -D-galactopyranoside (FDG) and 6 pg PCR template. The IVTT mix was encapsulated as soon as possible after mixing the components together. Upon encapsulation, the entire mix was incubated for 2.5h at 30°C.

7.2.2 Emulsification and plating of emulsion

Standard microscopic slides (75 mm \times 25 mm) were cut in half with a diamond pen as necessary. 2.5% (w/v) Span 60, 2.5% (w/v) cholesterol in decane was prepared and stored at room temperature. Before creating an emulsion this mixture was heated to 40°C and mixed to homogeneity. Per sample, 45 μl of oil/surfactant mixture was pipetted into a 1.8 ml round-bottom cryotube (Nalge Nunc, Thermo Fisher Scientific, Illkirch, France) to which a 8 mm \times 3 mm magnetic stirring bar was added. The oil/surfactant mix was stirred vigorously while adding the 95 μl of the IVT mix dropwise over the course of 1

minute. Next, the emulsion was left to stir for an additional 30 seconds before plating. The emulsion was put at 37°C immediately afterwards to prevent recrystallization before spreading.

Two thermocouple wires with a diameter of 12.5 μm (Omega Engineering Inc., Manchester, UK) were taped over the length of a standard microscopic slide. The microscopic slide, as well as the cut slides, were pre-heated to 37°C. When spreading an emulsion, the slide was kept at 37°C continuously. 20 μl of emulsion was pipetted onto the center of the microscopic slide, between the two wires. A cut microscopic slide was placed on top of the emulsion and then moved back and forth over the length of the slide with wire 30 times, without breaking the wire. After spreading the emulsion the final IVTT incubation was performed.

7.2.3 Analysis of flat emulsion

At 20 \times magnification, a microscope with a robotic stage was used to make a grid of 25 photos of an emulsion. The emulsions were excited using a blue filter and detected with a green filter. The photographs were fused using NIS elements AR 2.3 software. An algorithm was then used to bin the pixels and count the fluorescent droplets within pictures based on the relative fluorescence.

7.3 Results and discussion

Before actually starting the experiments, it was necessary to know the DNA concentration needed to mimic a genomic or metagenomic library screen. Based on previous observations, the following parameters in the calculation were used:

- The PCR fragment was 3 500 bp long.
- One basepair has an average molecular weight of 660 g mol⁻¹.

- The DNA concentration was 60 ng μl^{-1} .
- The average droplet diameter was 3 μm .
- The total volume of the emulsion was 140 μl .

Based on these values, a rough estimate of the maximum number of droplets that can be created in a 2D emulsion, as well as the number of droplets per gene, are calculated as follows:

$$\begin{aligned}
 3\,500 \text{ bp} \times 660 \text{ g mol}^{-1} &= 2.31 \times 10^6 \text{ g mol}^{-1} = 2\,310 \text{ ng pmol}^{-1} \\
 \frac{60 \text{ ng } \mu\text{l}^{-1}}{2\,310 \text{ ng pmol}^{-1}} &= 0.026 \text{ pmol } \mu\text{l}^{-1} = 0.16 \times 10^{11} \text{ genes } \mu\text{l}^{-1} \\
 \frac{4}{3} \times \pi \times (1.5 \text{ } \mu\text{m radius})^3 &= 4.79 \text{ } \mu\text{m}^3 = 4.79 \text{ fl droplet}^{-1} \\
 \frac{1.40 \times 10^{-4} \text{ l}}{4.79 \times 10^{-15} \text{ l}} &= 2.92 \times 10^{10} \text{ droplets} \\
 \frac{2.92 \times 10^{10} \text{ droplets}}{0.16 \times 10^{11} \text{ genes}} &= \mathbf{1.83 \text{ droplets gene}^{-1}}
 \end{aligned}$$

So, when using undiluted PCR template (at 60 ng μl^{-1}), approximately 1 in 2 droplets contains a gene. This prediction is supported when looking at figure 7.2(a). This sample was prepared without diluting the DNA, so a high fraction of the droplets was fluorescent. The droplets were quite small, in the range of 3 μm diameter, but with a high degree of polydispersity. In addition, the completely black areas clearly indicate that the emulsion was not tightly packed over the entire slide. There are quite a lot of open areas, which cover approximately 50% of the slide's area.

After seeing this sample and establishing that the surfactant/oil mixture was biocompatible, it was necessary to dilute the DNA template further in order to investigate the sensitivity of the technique.

An experiment was conducted with the PCR fragment that was diluted 10^4 -fold compared to the first experiment. On average 1 in $\sim 18\,300$ droplets contained a gene. The

negative sample was an IVTT reaction without DNA. The results are presented in figure 7.2(b-d). Note that 1 μl of DNA was used in a final volume of 100 μl of IVTT, thus yielding a final dilution factor of 10^6 .

The first major question was then how many positive events were expected in a large image, consisting of 25 individual photographs fused together. In order to calculate this, two assumptions were made:

- Each individual photograph covers an area of $300 \mu\text{m} \times 300 \mu\text{m}$.
- Approximately 50% of the photographed area is droplets (the rest is empty).

This yields the following calculation:

$$\begin{aligned}
 300 \mu\text{m} \times 300 \mu\text{m} \times 12.5 \mu\text{m} &= 1.125 \times 10^6 \mu\text{m}^3 = 1.125 \times 10^{-3} \mu\text{l} \\
 25 \times (1.125 \times 10^{-3} \mu\text{l}) &= 0.028 \mu\text{l} \\
 0.028 \mu\text{l} \times 50\% \times \frac{95}{140} &= 0.0087 \mu\text{l} \\
 \frac{0.16 \times 10^{11} \text{ genes } \mu\text{l}^{-1}}{10^6 \text{ dilution}} &= 1.6 \times 10^4 \text{ genes } \mu\text{l}^{-1} \\
 0.0087 \mu\text{l} \times (1.6 \times 10^4 \text{ genes } \mu\text{l}^{-1}) &= \mathbf{152 \text{ genes}}
 \end{aligned}$$

The expectation was, then, to detect 152 positive droplets in the *lacZ* emulsion and 0 positive droplets in the negative emulsion. In practice, when using a cut-off of 600 RFUs, 110 positive droplets were detected in the positive emulsion and 4 positive droplets in the negative emulsion. These results closely match the anticipated numbers. As it stands, the PCR product could be diluted another 10- to 100-fold and droplets would still be detected. This would make 1 gene per $\sim 1\,830\,000$ droplets. According to the earlier estimate, several fused images would need to be analyzed to identify the *lacZ* in an *E. coli* genomic library.

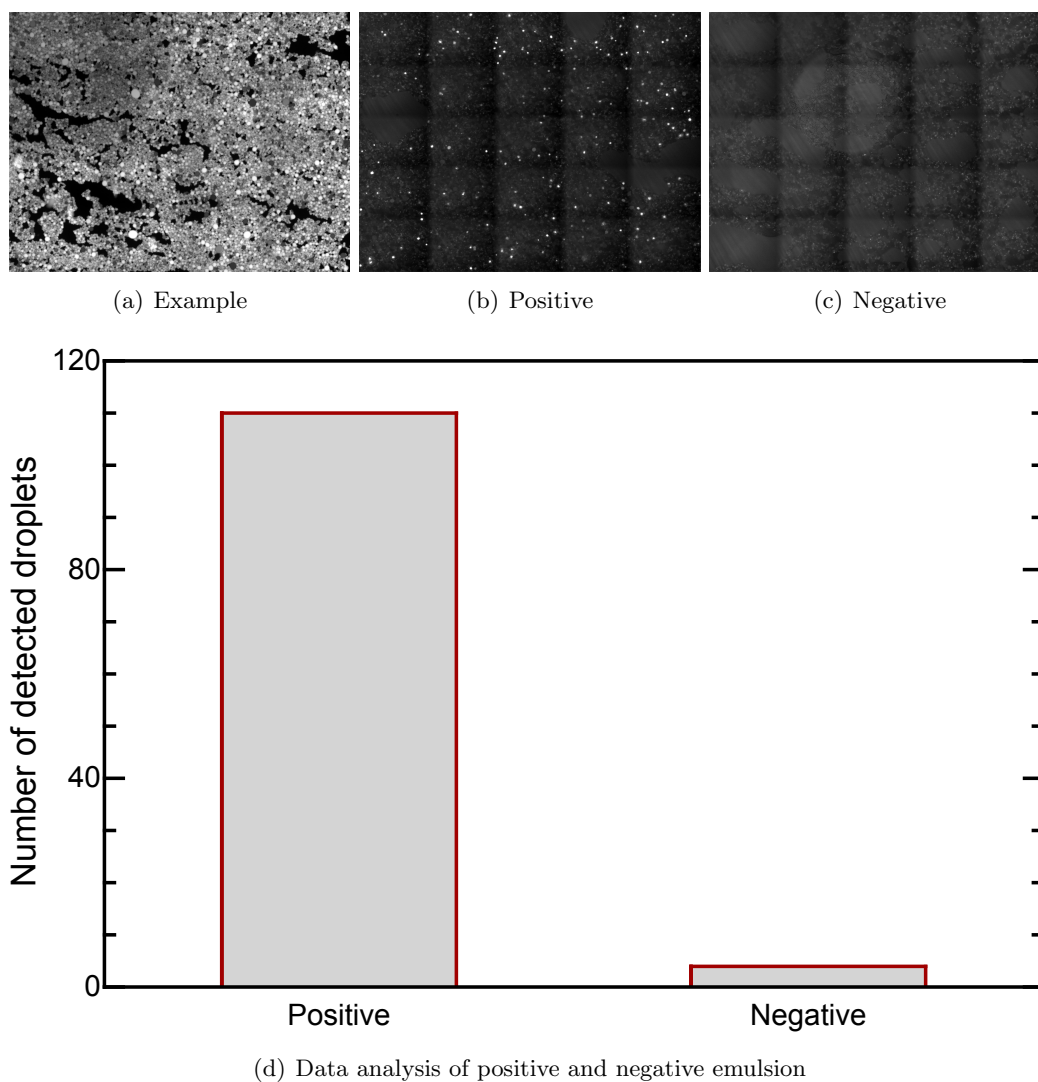


Fig. 7.2: Analysis data for 2D emulsions. (a) Photograph of an emulsion in which 60 ng of PCR template was used for the IVTT reaction, which means that on average 1 in 2 droplets expressed β -galactosidase. (b) Photograph of a positive emulsion containing β -galactosidase after IVTT with 6 pg of PCR template and (c) a negative emulsion. Photographs (b) and (c) are zoomed out 25 \times compared to photograph (a) and contain on average 2 781 600 droplets. (d) Quantitative comparison between the positive and negative emulsion shown in (b) and (c), respectively. An in-house algorithm was created that could bin the pixels and allow quantification of the number of positive events based on the relative fluorescence. The cut-off point for this analysis was 600 RFU, showing 110 events in the positive emulsion and 4 events in the negative emulsion.

Initially, $\Delta lacZ$ [9] was used as a negative sample. This nonsense mutation of *lacZ* encodes a completely inactive variant of β -galactosidase by introducing a stop codon early on in coding sequence of the enzyme. However, distinctly positive droplets were observed in emulsions containing only this inactive variant, in addition to a high background fluorescence (figure 7.3). This, in combination with the absence of a high background fluorescence in positive emulsions, rules out autofluorescence [159] possibly originating from the IVTT kit, as this should not be confined to distinct droplets.

Since these fluorescent droplets would hamper the screening of (meta)genomic libraries, one of the main focuses in the development of the technique was to reduce the frequency of these false positives.

Possible sources of these false positives were: (i) accidentally compartmentalized microbes exhibiting β -galactosidase activity, (ii) contamination by *lacZ* fragments of DNA, (iii) precipitation or crystallization of the substrate or product in certain droplets. It proved impossible to completely eliminate the false positives.

Even in the setup that was used in our experiments, which is far from automated maximally, the speed of the analysis nearly matches what can be achieved in FACS. The entire process of taking pictures and subsequent analysis took 2-3 minutes, which means that the screening throughput is currently at 1.5×10^4 - 2.3×10^4 droplets s^{-1} . This is along the same speed as FACS and exceeds the current maximum of FADS [22]. However, a difference between 2D emulsions and FACS/FADS on the other side is the ease of the experiment. Preparing 2D emulsions is very simple and quick.

In contrast, both FACS and FADS allow the selection of droplets of interest. There is still a lot of work to be done before the 2D emulsions will be at this point as well. One possibility is that a micromanipulator could be used to select active droplets from the emulsion. One big hurdle to overcome before addressing this point is accessing the droplets: currently, emulsions are covered with a glass slide and removing this glass slide

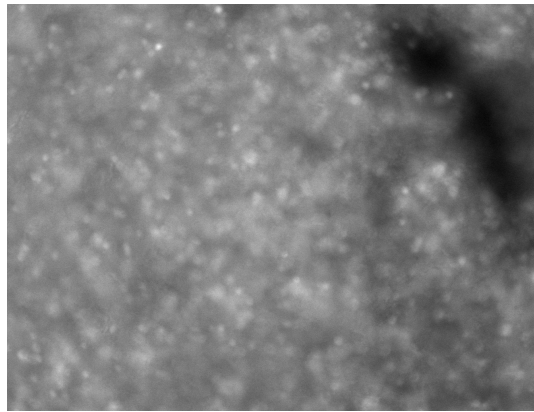


Fig. 7.3: Photograph of a 2D emulsion containing $\Delta lacZ$.

means that half of the created emulsion is lost, sticking to the upper slide. However, it may be possible to freeze the droplets *in situ* to stop this from happening.

7.4 Conclusions

In this chapter a new technique for rapid screening of gene libraries has been described. It was demonstrated that biologically active genes can be detected in 2D emulsions at a speed comparable to FACS analysis. The sensitivity is in the range necessary to screen genomic libraries.

The main issue that remains to be resolved is droplet selection, which is not possible yet.

8. GENERAL DISCUSSION

8.1 *Overall summary*

SGAP, having detectable aminopeptidase, phosphodiesterase and catechol oxidase activities, is considered to be an evolutionary intermediate [84]. As such, it is an enzyme that is well-placed to answer some fundamental, yet outstanding, questions in evolution. One of the most pertinent questions that remains to be answered is whether evolvability can be evolved. Evolvability is one of the most contentious issues in evolutionary biology.

Evolvability itself is defined as the potential of an entity to evolve. The open question is then whether an enzyme can possess an increased potential to evolve: to have a higher evolvability. One way to answer this question is to evolve an enzyme between at least two different activities. Since SGAP, in its wildtype form, is already capable of catalyzing different types of reaction to some degree, it is a good starting point for answering this question.

The aim of this PhD project was to develop a system for selecting SGAP mutants based upon at least one of its three activities. Such a system could then be used to perform selections of SGAP in order to answer questions about evolution.

Microfluidics experiments with SGAP were envisioned to have as few steps as possible, as fewer manipulations of the droplets would reduce the number of complicating factors. It was, therefore, chosen that the microfluidic droplets would be produced containing all

of the assay components from the beginning.

The first step of the process was to create a fluorescence-based assay for SGAP peptidase activity that could work in droplets (chapter 3). The simplest approach was chosen: bacterial expression of SGAP (or a mutant), followed by lysis and the addition of a fluorogenic substrate. After optimizing the reaction conditions in microplate, polymyxin B was identified as the best lytic agent, since it increased the SGAP activity most with respect to unlyzed cells.

The next step was to validate the approach in microfluidic droplets (chapter 4), in which polymyxin B was found to be the best lytic agent once again. A sorting experiment was performed and an experimental enrichment factor of nearly 29 was achieved, compared to a theoretical value of 110.5: well within the error margin of the model.

Unfortunately, a wide distribution of peptidase activities was observed in droplets containing compartmentalized bacteria expressing SGAP. mCherry, a monomeric red fluorescent protein, was used to make a fusion protein with SGAP (chapter 5) in order to normalize these activities for SGAP expression. Although there was a strong correlation between mCherry fluorescence and SGAP peptidase activity in microplate, it has proved impossible so far to detect this fluorescence in droplets due to the nature of the optical setup.

The long-term goals described in chapter 1 require the facility to detect at least two activities simultaneously, whether they are peptidase activities with different substrates or two completely different activities, such as peptidase activity and catechol oxidase activity. Aminocoumarins exhibit blue fluorescence, which fits in with the green and red fluorescences produced by rhodamine 110 and mCherry, respectively. However, they leak from droplets rapidly and are, therefore, not suitable for droplet-based selections. A hydrophilic derivative (ACMS) was successfully synthesized at $\sim 25\%$ yield and was shown not to leak between droplets (chapter 6). This molecule is an excellent starting

point for new peptidase substrates and has recently been coupled to L-leucine.

Finally, some work was done on 2D emulsions (chapter 7). The interesting property of these emulsions is the very high throughputs achievable for detecting activities in droplets, enabling genomic and metagenomic screens. Using a model system of *lacZ* in IVTT, expressing β -galactosidase, it has been demonstrated that this technique is as rapid as FACS, but there are a number of technical hurdles that must be overcome in order to allow selection of specific droplets, rather than just analysis.

8.2 Overall conclusions

The following conclusions were reached while optimizing the assay for SGAP peptidase activity:

- SGAP requires the presence of both zinc and calcium for activity. With bacterial expression of SGAP, the optimum concentrations of ZnCl_2 and CaCl_2 were found to be 500 μM and 0.25 mM, respectively.
- The K_M of SGAP with L2R was shown to be approximately 60 μM . This analysis allowed the $2 \times K_M$ value of L2R to be identified, facilitating selection of SGAP for improvements in k_{cat} .
- When comparing polymyxin B, BugBuster, BugBuster Primary Amine Free, Pop-Culture, isopropanol, ethanol and chloroform for lysis of SGAP-expressing bacteria, polymyxin B was demonstrated to be the most effective form of lysis in microtitre plate assays.
- Assuming that droplets could be synchronized by incubating them on ice during production, it was checked on microtitre plate whether the SGAP peptidase assay would be affected by an incubation on ice. Although initial reaction velocity

remains the same over a period of two hours, initial fluorescence increases. This should be taken into account if a screening and selection experiment takes a long time, for instance with a very low number of positive events (droplets containing SGAP) versus negative events (empty droplets or droplets containing Δ SGAP or E131A).

The following conclusions were reached during the reformatting of the SGAP peptidase assay for droplets:

- In order to tune the enrichment values in SGAP selections, the relationship between the OD_{600} of *E. coli* K12 TB1 cells and λ (the initial mean number of cells [22]) was determined. The relationship was found to be $\lambda = 3.7832 \times ODU_{600} + 0.016$.
- After validating the assay in droplets, a sorting experiment was performed. SGAP was selectively enriched from a population of SGAP and Δ SGAP using $\lambda = 0.1$ and $\epsilon = 0.1$. The experimental enrichment factor ($\eta_{exp} = 28.9$) was close to the maximal predicted enrichment ($\eta_m = 110.5$), indicating that the selection was successful. Therefore, the current assay permits the selection of active SGAP from a population of negative mutants.
- The variation in activities observed in a population of bacteria expressing wildtype SGAP suggests that directed evolution of SGAP will be difficult without further optimizing the assay. It is likely that this variation results from incomplete lysis (chapter 4) and/or variation in the expression level of SGAP.

The following conclusions were reached for a fusion protein between mCherry and SGAP that was created to normalize SGAP peptidase activity for expression level:

- In microplate, it was found that bacterial density, as measured by optical density, and peptidase activity correlated in a linear fashion with an R^2 value of 0.988 for the fit (chapter 3). Fusing mCherry to SGAP allowed peptidase activity to

be normalized by red fluorescence, rather than optical density. This improved the correlation: an R^2 of 0.9991 was observed for mCherry::SGAP and an R^2 of 0.9997 was observed for SGAP::mCherry.

- The red fluorescence of mCherry::SGAP could not be detected in droplets. The most likely explanation for this is the low sensitivity of the optical setup used. It has not, therefore, been possible so far to normalize SGAP peptidase activity for SGAP expression in droplets.

The following conclusions were reached after synthesizing a blue fluorophore (ACMS) as the basis for new fluorogenic substrates for SGAP peptidase activity:

- ACMS was successfully synthesized, as determined by $^1\text{H-NMR}$, with a yield of $\sim 25\%$. Fluorescence analysis revealed an excitation maximum of 360 nm and an emission maximum of 460 nm.
- The main reason to synthesize ACMS was because 7-amino-4-methylcoumarin exchanges between droplets very rapidly. It was hoped that the sulfonic acid moiety at the 4-position would render the entire molecule more hydrophilic and so reduce the exchange. ACMS was found to not exchange between the droplets at all within 3 h, facilitating the use of coumarin-based substrates in droplets.
- ACMS has recently been used to synthesize the first droplet-compatible coumarin-based peptidase substrate, but the substrate needs to be verified by $^1\text{H-NMR}$.

The following conclusions were reached when working with 2D emulsions for the directed evolution or screening of large libraries:

- The established mixture of oil and surfactant that is used when creating the emulsions had not been tested previously with a biological system. IVTT of *lacZ* was chosen as the model system to check whether this might work. The oil/surfactant mixture was found to be biocompatible, as it allowed IVTT with *lacZ*, yielding

β -galactosidase, which hydrolyzed FDG.

- Initial analyses have allowed the detection of active *lacZ* genes at a throughput similar to a FACS. However, there is no way yet to recover active droplets, so the technique is restricted to analysis only.

8.3 Future work

It has been demonstrated that lysis or permeabilization of bacterial cells is necessary to obtain detectable SGAP activity in droplets. However, even using a polymyxin B concentration 1000 \times greater than what should be necessary to kill cells [113, 119–122], it does not lead to complete lysis of the bacterial cells in droplets. This could be a reason for not always having a separate population of active droplets. One of the first things that should be done as this project continues, is optimize the lysis protocol further. An option to do this would be to increase the internal shear force of the microfluidic droplets to add to the lytic effect of polymyxin B.

A second point to improve is the sensitivity of the optical setup to allow detection of mCherry fusion proteins released from bacterial cells. One approach would be to replace the PMTs with avalanche photo diodes, which are more sensitive.

When the sorting experiment was performed, the off-chip incubation of the droplets lasted for approximately 60 minutes before the actual selection, which meant that the reaction was in the plateau phase. In order to do directed evolution experiments, the sorting and selection should be based on initial reaction velocity. The reaction profile for SGAP in droplets, in analogy to what is seen in microtitre plate assays, would need to be determined. It is most reasonable to attempt this by way of a delay line that will allow multiple measurement points [25]. When a reaction profile for SGAP in droplets has been ascertained, the ideal incubation time can be determined. It seems likely that

an integrated microfluidic device will be used that contains a droplet maker, delay line and sorting module.

When these optimizations (lysis, reaction time and normalization) have been effected, the directed evolution of SGAP can commence. Genetic libraries should be made and cloned into pKB4 and then transformed into TB1 cells. The mutational load for the libraries should be determined, as should the transformation efficiency.

Producing acyl chloride from an amino acid should permit the synthesis of fluorogenic substrates using ACMS. Therefore, finishing the synthesis of ACMS to create some different SGAP fluorogenic substrates should facilitate achievement of several of the possible long-term goals of this project, as described in chapter 1.3. The synthesis of fluorogenic substrates is envisaged using leucine as a verification and to permit precise kinetic determinations of wildtype and variants of SGAP. In addition, two more fluorogenic substrates could be synthesized based on the hydrolytic activity of SGAP on these groups. Valine and glutamic acid represent amino acids that are hydrolyzed with medium and low reaction rates, respectively, compared to leucine.

The main issue remaining to be resolved for the 2D emulsions is a method to pick droplets of interest. Currently, with a glass slide on top of the emulsions, there is no way of accessing the droplets. A possible approach would be to freeze the droplets *in situ* after analysis, remove the cover slide, and use a microdissection apparatus to pick droplets of interest.

9. SUPPLEMENTARY INFORMATION

9.1 *Computer-aided design (CAD) files of microfluidic devices*

In this section the different computer-aided design (CAD) files of the three different devices used in this project are shown (figure 9.1). One that was used as a double emulsifier in the leakage assays, to encapsulate two different aqueous phases simultaneously. The second device is a co-flow device, which was used to encapsulate the bacterial cells together with assay mixture for the assays, as well as the sorting experiment. Finally, the general reinjection device is displayed that was used in the basic assays. For the sorting experiment the reinjection was done into a different device, but this device is described in the FADS paper by Baret *et al.* [22].

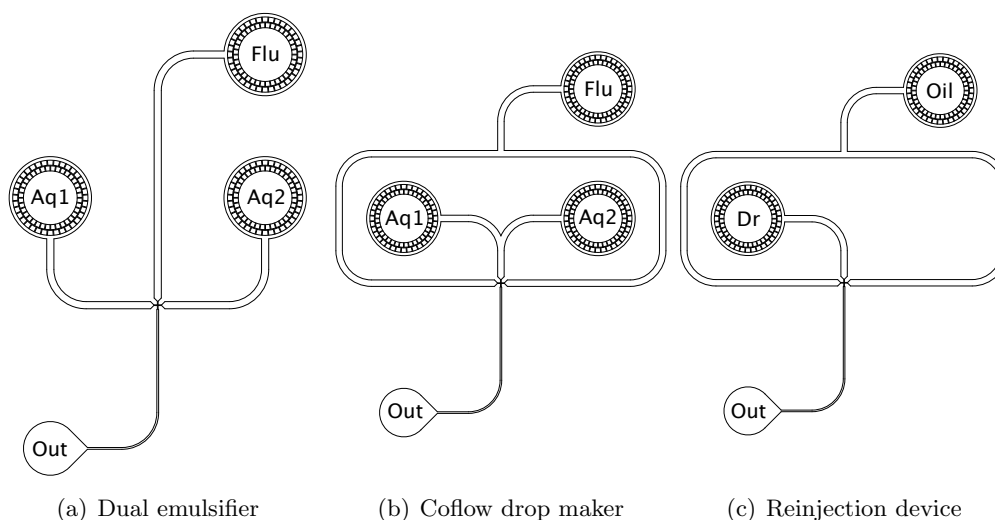


Fig. 9.1: CAD designs of the devices used in this project. (a) A dual emulsifier, (b) a coflow droplet maker and (c) a reinjection module. (a,b) A mix of fluorinated oil and surfactant ('Flu') and two aqueous solutions ('Aq1' and 'Aq2') enter the device through the circular ports with integrated filters. After emulsification the droplets are collected via the outlet ('Out') in a glass capillary. In (a) the aqueous solutions, coming in from the left and right of the nozzle, are encapsulated into separate droplets by the fluorinated oil/surfactant mix, coming in from the top of the nozzle. The nozzle of the device is $25\ \mu\text{m} \times 100\ \mu\text{m}$. In (b) the aqueous solutions combine at the nozzle ($20\ \mu\text{m} \times 100\ \mu\text{m}$) and are emulsified in the oil. (c) Surfactant-free fluorinated oil ('Oil') and microfluidic droplets ('Dr') enter the device through the circular ports with integrated filters. At the nozzle ($30\ \mu\text{m} \times 100\ \mu\text{m}$) the surfactant-free oil spaces the droplets to allow proper fluorescence detection. In all devices the wide channels before the nozzles are $200\ \mu\text{m}$ wide and the channel width after the nozzles is $50\ \mu\text{m}$. The depth of the channels, following fabrication, was $25\ \mu\text{m}$.

9.2 ACMS synthesis

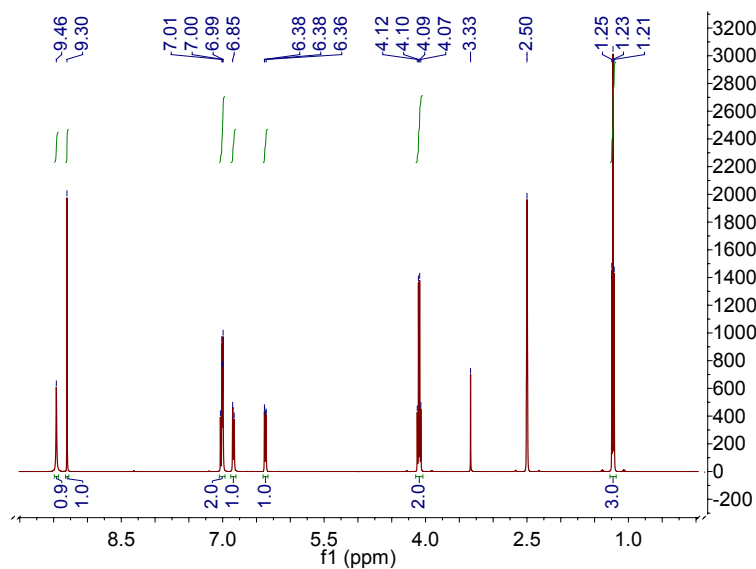
In this section the different $^1\text{H-NMR}$ spectra are showed and described.

The protection of the $-\text{NH}_2$ group of 3-aminophenol by ethyl chloroformate was performed and lead to the following $^1\text{H-NMR}$ peaks (figure 9.2), δ : 1.23 (3H, t, $-\text{O}-\text{CH}_2-\text{CH}_3$), 2.50 (DMSO residual [150]), 3.33 (H_2O residual [150]), 4.10 (2H, q, $-\text{O}-\text{CH}_2-\text{CH}_3$), 6.37 (1H, d, 6-H), 6.84 (1H, d, 4-H), 7.02 (2H, m, 2-H and 5-H), 9.30 (1H, s, $-\text{OH}$), 9.46 (1H, s, $-\text{NH}$). This reaction yielded approximately 95%.

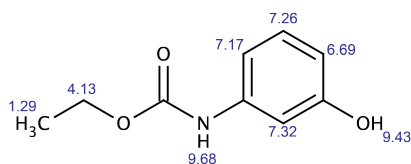
The following step of the synthesis, the Pechmann condensation (figure 9.3), shows $^1\text{H-NMR}$ δ : 1.27 (3H, t, $-\text{O}-\text{CH}_2-\text{CH}_3$), 2.50 (DMSO residual [150]), 3.32 (H_2O residual [150]), 4.17 (3H, q, $-\text{O}-\text{CH}_2-\text{CH}_3$), 4.98 (2H, s, $-\text{CH}_2-\text{Cl}$), 6.52 (1H, s, 3-H), 7.43 (1H, d, 6-H), 7.60 (1H, s, 5-H), 7.76 (1H, d, 8-H), 10.20 (1H, s, $-\text{NH}$). This reaction yielded approximately 48%.

Then the product of the sulfonation reaction (figure 9.4) shows $^1\text{H-NMR}$ δ : 1.26 (3.6H, t, $-\text{O}-\text{CH}_2-\text{CH}_3$), 2.50 (DMSO residual [150]), 3.17 (methanol residual [150]), 3.33 (H_2O residual [150]), 3.99 (2H, s, $-\text{CH}_2-\text{SO}_3^-$), 4.15 (3H, m, $-\text{O}-\text{CH}_2-\text{CH}_3$ and methanol residual [150]), 6.23 (1H, s, 3-H), 7.33 (1H, d, 6-H), 7.55 (1H, s, 5-H), 7.84 (1H, d, 8-H), 10.12 (1H, s, $-\text{NH}$). The yield of this reaction was approximately 60%.

One of two indications coming from the sulfonation reaction is the change in the chemical shift from $\delta = 4.98$ ppm of $-\text{CH}_2$ in the chloromethane moiety to $\delta = 3.99$ ppm of $-\text{CH}_2$ in the methanesulfonic acid moiety. In addition, the 3-H peak in 7-aminocoumarin shifts from $\delta = 6.52$ to $\delta = 6.23$.

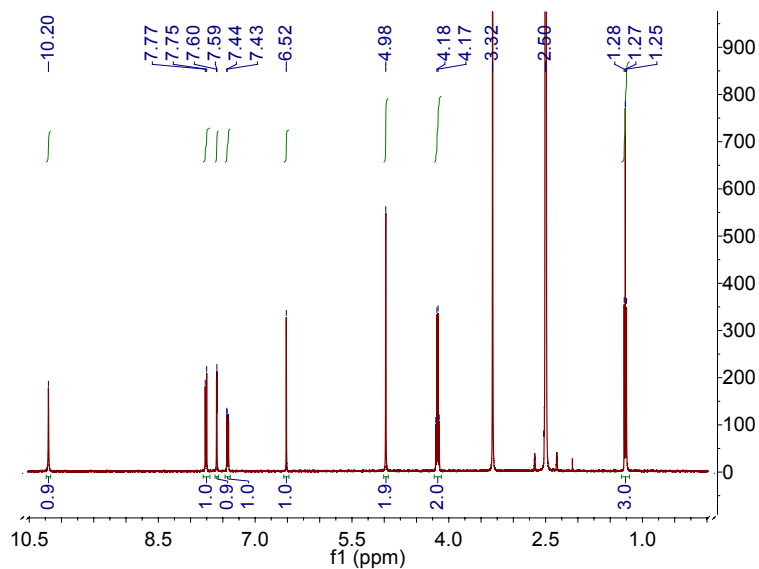


(a) NMR spectrum

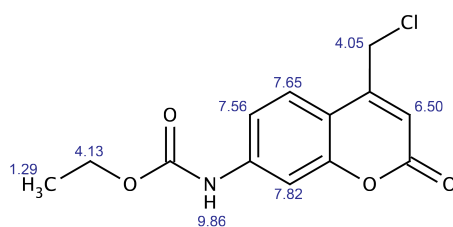


(b) Final molecule

Fig. 9.2: Representative $^1\text{H-NMR}$ spectrum and molecular structure with predicted $^1\text{H-NMR}$ peaks for the product of the first reaction in the synthesis of ACMS. The peaks at 2.50 and 3.33 ppm are the residual peaks for DMSO and H_2O , respectively [150]. The blue numbers at the different hydrogen atoms in the molecular structure indicate that all peaks should be well-defined.

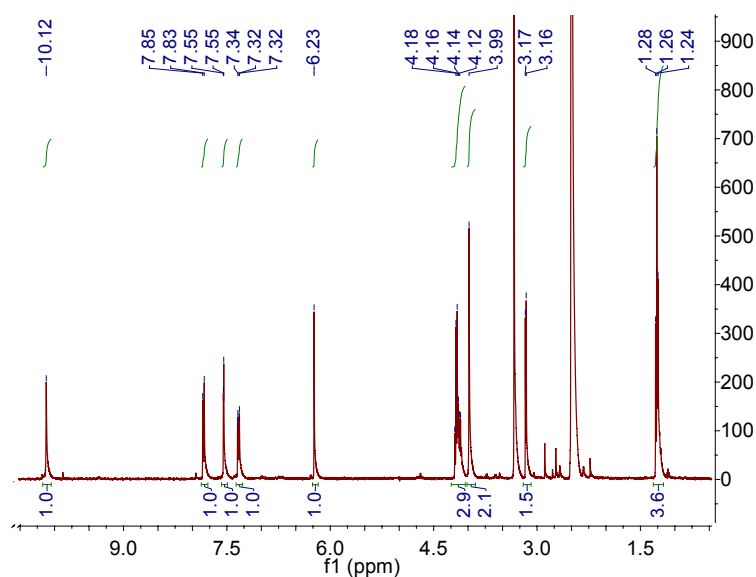


(a) NMR spectrum

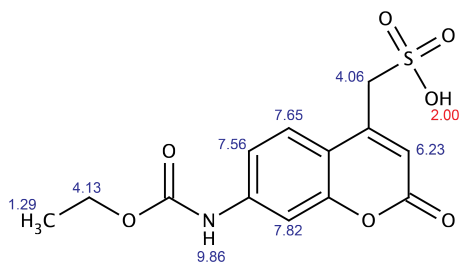


(b) Final molecule

Fig. 9.3: Representative $^1\text{H-NMR}$ spectrum and molecular structure with predicted $^1\text{H-NMR}$ peaks for the product of the Pechmann condensation in the synthesis of ACMS. The peaks at 2.50 and 3.33 ppm are the residual peaks for DMSO and H_2O , respectively [150]. The blue numbers at the different hydrogen atoms in the molecular structure indicate that all peaks should be well-defined.



(a) NMR spectrum



(b) Final molecule

Fig. 9.4: Representative $^1\text{H-NMR}$ spectrum and molecular structure with predicted $^1\text{H-NMR}$ peaks for the product of the sulfonation reaction in the synthesis of ACMS. The peaks at 2.50 and 3.32 ppm are the residual peaks for DMSO and H_2O , respectively [150]. The blue numbers at the different hydrogen atoms in the molecular structure indicate that all peaks should be well-defined. The red number at the hydrogen of the sulfonic acid moiety indicates that the hydrogen peak of this atom will not be clearly defined.

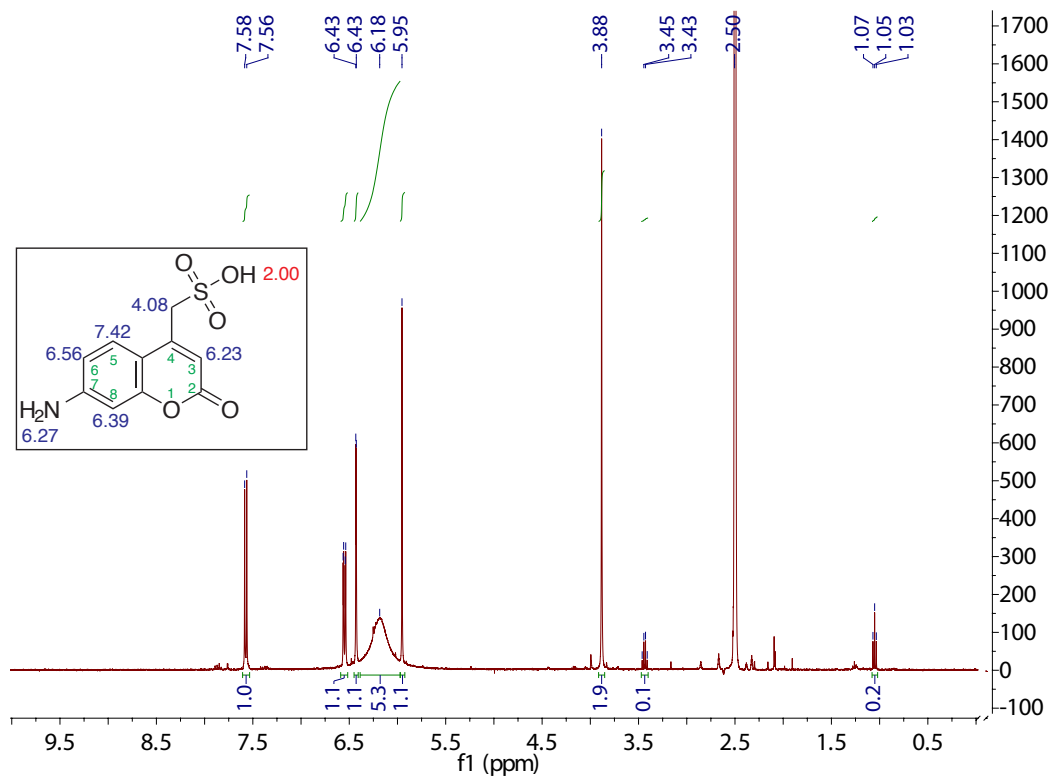


Fig. 9.5: The $^1\text{H-NMR}$ spectrum obtained after the synthesis of 7-aminocoumarin-4-methanesulfonic acid (ACMS). The chemical shift is visible on the x-axis (in ppm). Directly underneath the peaks is the integration value, indicative of the relative intensity of the peak, and above the peaks are the ppm-shifts. The inset is the chemical structure of ACMS and the predicted NMR peaks for the different units. When the numbers are blue, the peak should be well-defined around the mentioned chemical shift, the red number at the sulfonic acid moiety indicates that this peak most likely is not clearly defined. Finally, the green numbers inside the structure are for referencing.

9.3 DNA and amino acid sequence of wildtype *Streptomyces griseus* aminopeptidase

In the following set of figures two sequences will be given. The first sequence (figure 9.6(a)) is the DNA sequence of the wildtype SGAP variant that has been used in the entire project. Figure 9.6(b) shows the amino acid sequence of wildtype SGAP.

```

1 GCGCCGGACA TCCCCTGGC GAACGTCAAG GCCCACCTCA CGCAGCTCTC
51 GACGATCGCC GCGAACAACG GCGGCAACCG CGCCCACGGC CGCCCCGGCT
101 ACAAGGCGTC CGTCGACTAC GTGAAGGCCA AGCTCGACGC GGCCGGATAC
151 ACCACCACGC TCCAGCAGTT CACCTCGGGC GGGGCCACCG GCTACAACCT
201 GATAGCCGAC TGGCCCCGGC GCGACCCCAA CAAGTCCTG ATGGCCGGGG
251 CCCACCTCGA CTCGGTCTCC TCCGGCGCCG GGATCAACGA CAACGGCTCC
301 GGCTCGGCCG CCGTGCTGGA GACCGCGCTC GCCGTCTCC GCGCCGGGTA
351 CCAGCCCGAC AAGCACCTGC GGTTCGCCTG GTGGGGCGCG GAGGAGCTGG
401 GCCTGATCGG CTCGAAGTTC TACGTTAACA ACCTGCCGTC CGCCGACCGC
451 TCCAAGCTCG CCGGATATCT CAACTTCGAC ATGATCGGCT CGCCCAACCC
501 CGGTTACTTC GTCTACGACG ACGACCCGGT CATCGAGAAG ACCTTCAAGG
551 ACTACTTCGC CGGCCTGAAC GTCCCAGCCG AGATCGAGAC CGAGGGCGAC
601 GGCCGCTCCG ACCACGCCCC GTTCAAGAAC GTCGGCGTCC CCGTCGGCGG
651 ACTCTTCACC GGCGCCGGCT ACACCAAGTC CGCCGCCAG GCGCAGAAGT
701 GGGGCGGGAC GGCCGGGCAA GCCTTCGACC GCTGCTACCA CTCCTCGTGC
751 GACAGCTGA GCAACATCAA CGACACCGCC CTCGACC GCA ACAGCGATGC
801 AGCAGCACAT GCCATTTGGA CCCTGAGCAG C

```

(a) DNA sequence SGAP

```

1 APDIPLANVK AHLTQLSTIA ANNGGNRAHG RPYKASVDY VKAKLDAAGY
51 TTTLQQFTSG GATGYNLIAD WPGGDPNKVL MAGAHLDSVS SGAGINDNGS
101 GSAAVLETAL AVSRAGYQPD KHLRFWWGA EELGLIGSKF YVNNLPSADR
151 SKLAGYLNFD MIGSPNPGYF VYDDDPVIEK TFKDYFAGLN VPTEIETEGD
201 GRSDHAPFKN VGVVPVGLFT GAGYTKSAAQ AQKWGGTAGQ AFDRCYHSSC
251 DSLSNINDTA LDRNSDAAAH AIWTLSS

```

(b) Amino acid sequence SGAP

Fig. 9.6: DNA sequence and amino acid sequence of wildtype SGAP. Both sequences have been grouped by ten and the number of the nucleotides or amino acids with which each respective line begins are indicated in blue at the left-hand side.

9.4 Additional figures

The first image (figure 9.7) is a graphical representation of a double assay for SGAP peptidase activity with fluorogenic substrates based on rhodamine 110 and ACMS.

Figures 9.8 and 9.9 illustrate two different agarose gels. The first demonstrates that when using agarose gels to demonstrate enrichment of SGAP over Δ SGAP, the detection limit lies at approximately 1/1. If the proportion of Δ SGAP is higher (for example 1/10), the SGAP variant is no longer visible. The second image demonstrates why DMSO is necessary and a higher annealing temperature is recommended for the amplification of mCherry from V424.

Figure 9.10 depicts a graphical representation of a selection system based on two fluorogenic substrates and the theoretical differences between applying or not applying a counterselection for a second activity.

Figure 9.11 indicates what is hypothesized to happen when the fluorescent signal coming from L2R hydrolysis in microdroplets could be normalized based on mCherry expression.

Finally, figure 9.12 illustrates the introduction of the arabinose inducible cassette into pKB3-CalB-his, the parental plasmid to pKB4-SGAP-his.

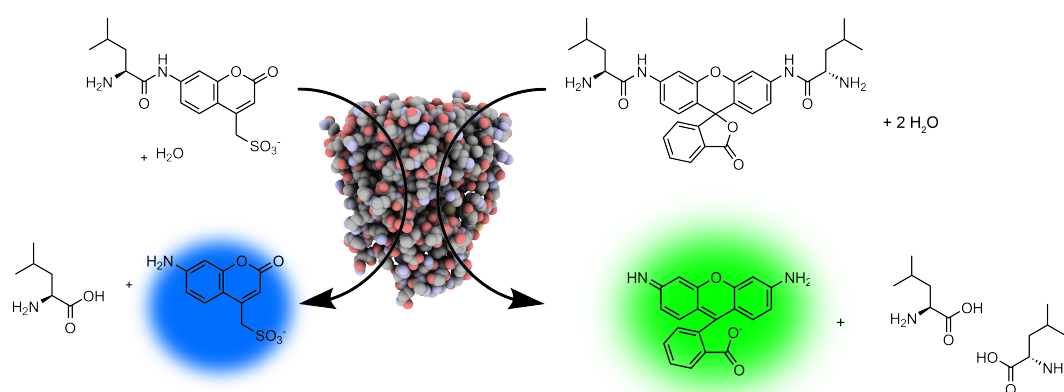


Fig. 9.7: Graphical representation of an assay system for measuring two SGAP peptidase activities simultaneously using two fluorophores. On the left is drawn L-leuciny-7-aminocoumarin-4-methanesulfonic acid, which can be hydrolyzed to L-leucine and ACMS by SGAP. ACMS can then be detected by $\lambda_{ex} = 362$ nm and $\lambda_{em} = 462$. On the right is drawn bis-(L-leuciny)-rhodamine 110, which can be hydrolyzed to $2 \times$ L-leucine and rhodamine 110, detectable via $\lambda_{em} = 488$ nm and $\lambda_{em} = 525$ nm. Both substrates have been substituted with L-leucine in this image for illustrative purposes.

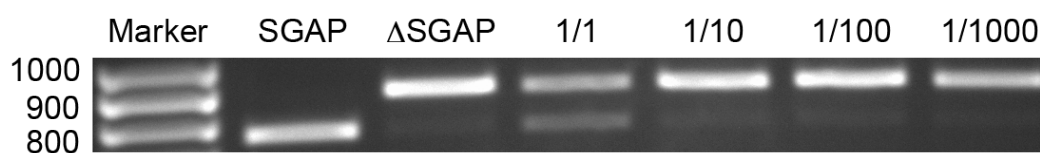


Fig. 9.8: Assessment of the detection limit of SGAP in various dilutions in comparison to Δ SGAP. The cells were washed before use, comparable to when cells are prepared for fluorescence assays. Suspensions were made in 10 mM PBS, 1 g l⁻¹ protease-free BSA, pH 7.4 to a final concentration of 1 000 cells μ l⁻¹ (assuming that 1 ODU₆₀₀ contains 1 \times 10⁹ bacterial cells). Various suspensions were made: pure SGAP; pure Δ SGAP; 1/1, 1/10, 1/100 and 1/1 000 of SGAP/ Δ SGAP. A colony PCR was run using 1 000 cells of each sample. After the PCR reaction 10 μ l of the reaction was used in a restriction containing 5 U of SalI, 1 \times NEBuffer 3 and 100 μ g ml⁻¹ BSA. The restriction was incubated for 1 hour at 37°C, after which the samples were purified by ethanol precipitation. 300 ng of each sample was put onto a 1.2% (w/v) agarose gel containing EDTA in TAE buffer and migrated for 70 minutes at 60 V.

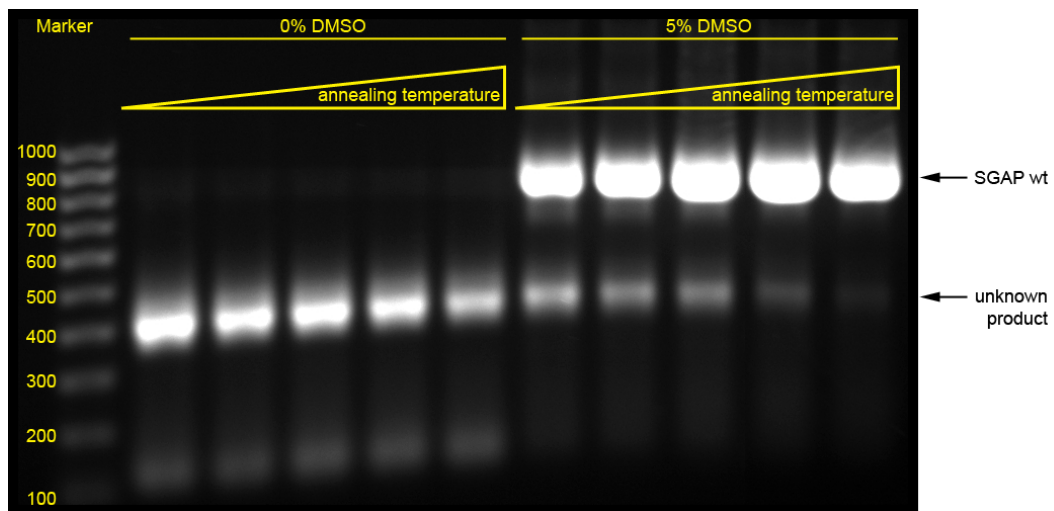


Fig. 9.9: Optimization of PCR conditions for PCR of mCherry from the plasmid V424. The PCR (section 2.4.10) was adapted to (i) running 30 cycles, (ii) having a final volume of 20 μ l, (iii) the inclusion of 5% (v/v) DMSO in some samples and (iv) having a temperature gradient for the annealing temperature. The reactions were run with 0.4 ng of V424 per reaction. The samples on the left did not contain DMSO whereas the samples on the right did. In both of the conditions from left to right the annealing temperature increases (60.0°C, 62.3°C, 63.5°C, 66.0°C and 68.0°C for the respective samples). Without DMSO there is only amplification of an unknown fragment approximately half the size of SGAP wt. At all annealing temperatures containing 5% (v/v) DMSO the SGAP wt amplicon is present, but with increasing annealing temperature the quantity of unknown product decreases.

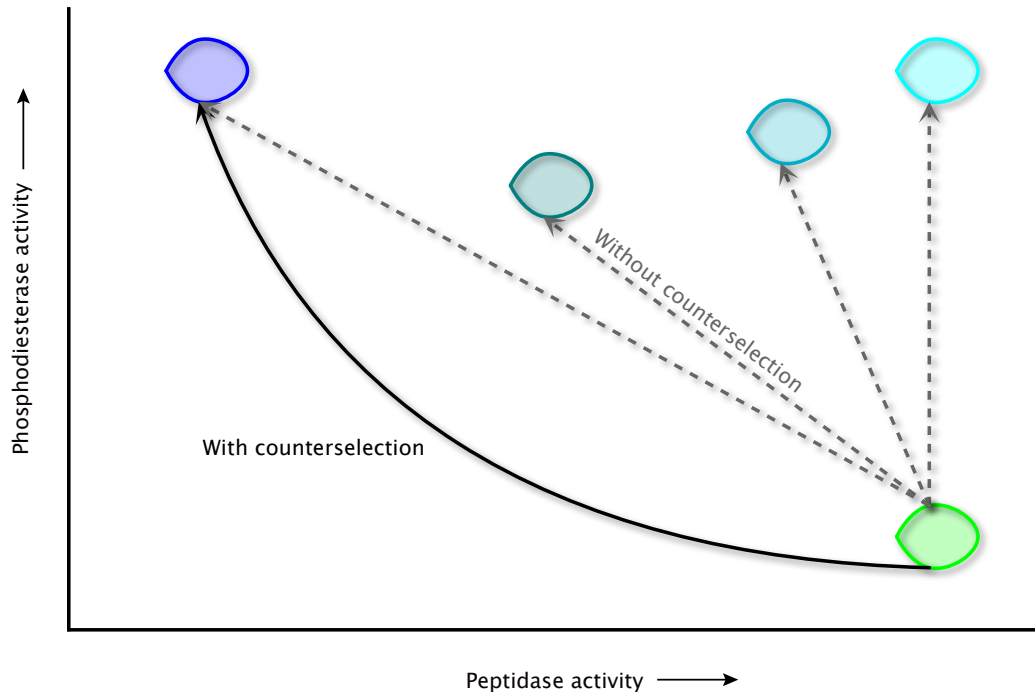


Fig. 9.10: Theoretical graph indicating the possible scenarios when selecting for a secondary activity for SGAP with and without counterselection. The x-axis represents peptidase activity (green color) and the y-axis represents phosphodiesterase activity (blue color). In the wildtype, the peptidase activity will be high. When phosphodiesterase activity is then selected in directed evolution, the phosphodiesterase activity will increase. When a counterselection is performed against the initial activity (black solid arrow), the protein would no longer be a peptidase. Consequently, the population would go from the lower right (low blue fluorescence, high green fluorescence) to the upper left (high blue fluorescence, low green fluorescence) corner of this hypothetical 2D plot. However, if there is no specific counterselection against the initial activity (grey dashed arrows), the only demand is that phosphodiesterase activity increases. This means that the protein can retain the original activity (cyan color, upper right), completely lose the original activity (blue color, upper left) or anything in between.

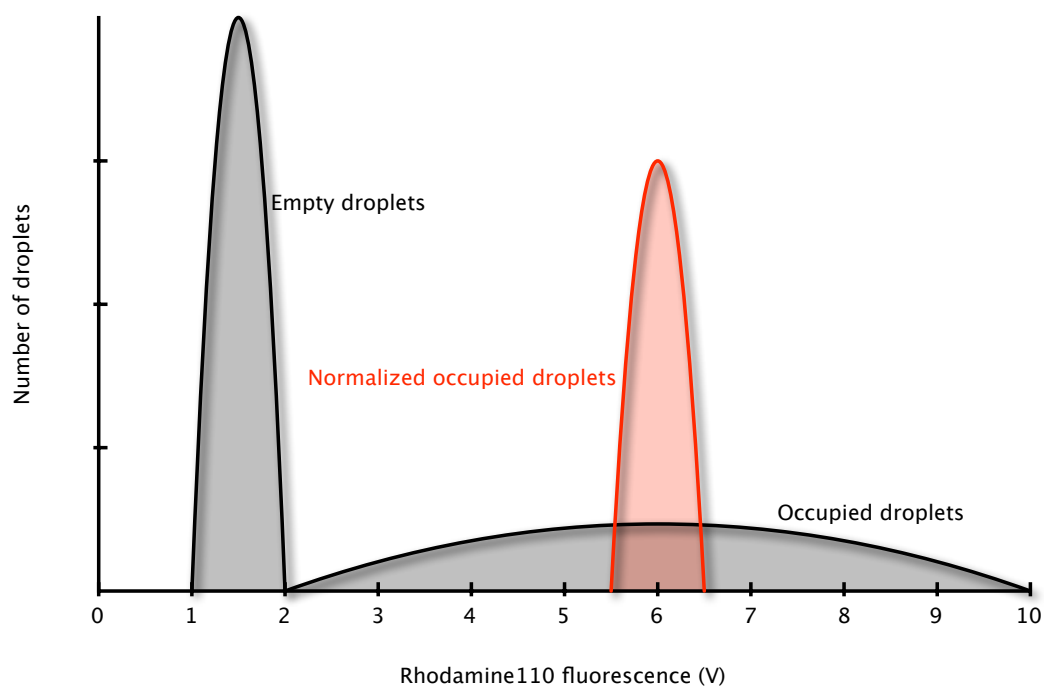


Fig. 9.11: Hypothetical graph indicating what would happen when fluorescence signals in microfluidics can be normalized based on expression level. A black line indicates what is generally the form of an emulsion with a λ of 0.1 with bacteria. A big peak is present at low fluorescence, representing the empty droplets. Then the droplets that contain bacteria show fluorescence, but over a very wide distribution (in this case from 2 to 10 V). However, if the signal could be normalized on the basis of expression level of the protein of interest, the second population containing bacteria might be contracted (red) with respect to the population in which there is no normalization.

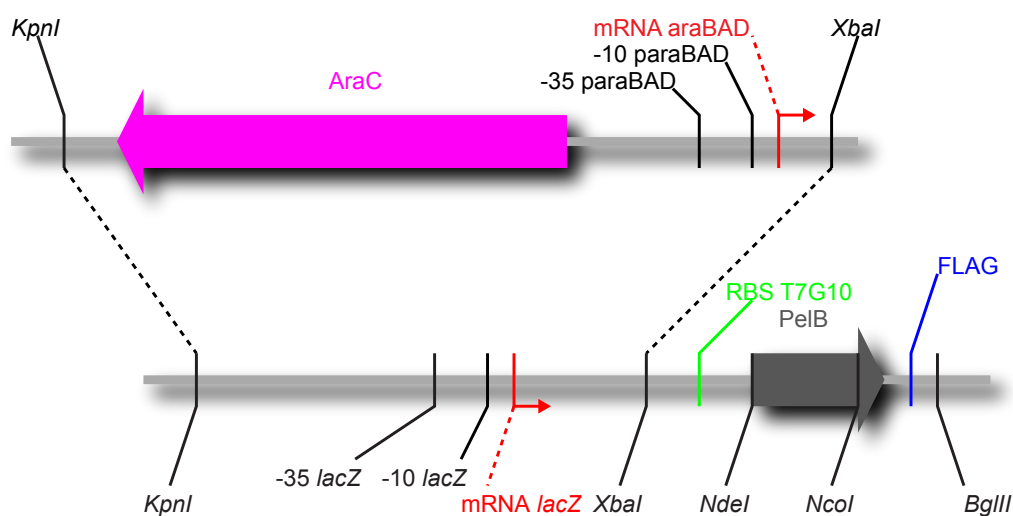


Fig. 9.12: The cloning procedure to introduce the arabinose induction cassette into pKB3-CalB-his. This cloning replaces the *lac* promoter in the plasmid. The arabinose cassette (including the *araC* repressor and the *araBAD* promoter) comes from the pBAD plasmid (Invitrogen) and is amplified by PCR, restricted by BglII and EcoRI and introduced in pKB3-CalB-his, which has been restricted with the same enzymes, in lieu of the *lac* promoter.

BIBLIOGRAPHY

- [1] L. M. Mayr and P. Fuerst, "The future of high-throughput screening," *Journal of Biomolecular Screening*, vol. 13, pp. 443–448, Jul 2008.
- [2] M. Eisenstein, "Cell sorting: divide and conquer," *Nature*, vol. 441, pp. 1179–1185, Jun 2006.
- [3] H. M. Shapiro, *Practical flow cytometry*. Wiley-Liss, 2003.
- [4] I. Schmid, C. Lambert, D. Ambrozak, G. E. Marti, D. M. Moss, S. P. Perfetto, and I. S. of Analytical Cytology, "International society for analytical cytology biosafety standard for sorting of unfixed cells," *Cytometry A*, vol. 71, pp. 414–437, Jun 2007.
- [5] V. Kiermer, "FACS-on-a-chip," *Nature Methods*, vol. 2, pp. 91–91, Feb. 2005.
- [6] T. D. Perroud, J. N. Kaiser, J. C. Sy, T. W. Lane, C. S. Branda, A. K. Singh, and K. D. Patel, "Microfluidic-based cell sorting of *Francisella tularensis* infected macrophages using optical forces," *Analytical Chemistry*, vol. 80, pp. 6365–6372, Aug 2008.
- [7] D. S. Tawfik and A. D. Griffiths, "Man-made cell-like compartments for molecular evolution," *Nature Biotechnology*, vol. 16, pp. 652–656, Jul 1998.
- [8] A. Aharoni, G. Amitai, K. Bernath, S. Magdassi, and D. S. Tawfik, "High-throughput screening of enzyme libraries: thiolactonases evolved by fluorescence-activated sorting of single cells in emulsion compartments," *Chemistry and Biology*, vol. 12, pp. 1281–1289, Dec 2005.
- [9] E. Mastrobattista, V. Taly, E. Chanudet, P. Treacy, B. T. Kelly, and A. D. Griffiths, "High-throughput screening of enzyme libraries: *in vitro* evolution of a beta-galactosidase by fluorescence-activated sorting of double emulsions," *Chemistry and Biology*, vol. 12, pp. 1291–1300, Dec 2005.
- [10] A. D. Griffiths and D. S. Tawfik, "Miniaturising the laboratory in emulsion droplets," *Trends in Biotechnology*, vol. 24, pp. 395–402, Sep 2006.
- [11] S. L. Anna, N. Bontoux, and H. A. Stone, "Formation of dispersions using "flow focusing" in microchannels," *Applied Physics Letters*, vol. 82, no. 3, pp. 364–366, 2003.
- [12] H. Song, J. D. Tice, and R. F. Ismagilov, "A microfluidic system for controlling reaction networks in time," *Angewandte Chemie International Edition*, vol. 42, pp. 768–772, Feb 2003.
- [13] K. Ahn, J. Agresti, H. Chong, M. Marquez, and D. A. Weitz, "Electrocoalescence of drops synchronized by size-dependent flow in microfluidic channels," *Applied Physics Letters*, vol. 88, no. 26, p. 264105, 2006.
- [14] C. Priest, S. Herminghaus, and R. Seemann, "Controlled electrocoalescence in microfluidics: Targeting a single lamella," *Applied Physics Letters*, vol. 89, no. 13, p. 134101, 2006.
- [15] D. R. Link, S. L. Anna, D. A. Weitz, and H. A. Stone, "Geometrically mediated breakup of drops in microfluidic devices," *Physical Review Letters*, vol. 92, p. 054503, Feb 2004.
- [16] L. Ménétrier-Deremble and P. Tabeling, "Droplet breakup in microfluidic junctions of arbitrary angles," *Physical Review E (Statistical, Nonlinear, and Soft Matter Physics)*, vol. 74, no. 3, p. 035303, 2006.
- [17] D. R. Link, E. Grasland-Mongrain, A. Duri, F. Sarrazin, Z. Cheng, G. Cristobal, M. Marquez, and D. A. Weitz, "Electric control of droplets in microfluidic devices," *Angewandte Chemie International Edition*, vol. 45, pp. 2556–2560, Apr 2006.

- [18] K. Ahn, C. Kerbage, T. P. Hunt, R. M. Westervelt, D. R. Link, and D. A. Weitz, "Dielectrophoretic manipulation of drops for high-speed microfluidic sorting devices," *Applied Physics Letters*, vol. 88, no. 2, p. 024104, 2006.
- [19] L. M. Fidalgo, G. Whyte, D. Bratton, C. F. Kaminski, C. Abell, and W. T. S. Huck, "From microdroplets to microfluidics: selective emulsion separation in microfluidic devices," *Angewandte Chemie International Edition*, vol. 47, no. 11, pp. 2042–2045, 2008.
- [20] C. N. Baroud, J.-P. Delville, F. Gallaire, and R. Wunenburger, "Thermocapillary valve for droplet production and sorting," *Physical Review E (Statistical, Nonlinear, and Soft Matter Physics)*, vol. 75, no. 4, p. 046302, 2007.
- [21] M. Chabert and J.-L. Viovy, "Microfluidic high-throughput encapsulation and hydrodynamic self-sorting of single cells," *Proceedings of the National Academy of Sciences of the USA*, vol. 105, pp. 3191–3196, Mar 2008.
- [22] J.-C. Baret, O. J. Miller, V. Taly, M. Ryckelynck, A. El-Harrak, L. Frenz, C. Rick, M. J. Samuels, J. B. Hutchison, J. J. Agresti, D. R. Link, D. A. Weitz, and A. D. Griffiths, "Fluorescence-activated droplet sorting (FADS): efficient microfluidic cell sorting based on enzymatic activity," *Lab on a Chip*, vol. 9, pp. 1850–1858, 2009.
- [23] S.-Y. Teh, R. Lin, L.-H. Hung, and A. P. Lee, "Droplet microfluidics," *Lab on a Chip*, vol. 8, pp. 198–220, Feb 2008.
- [24] L. Mazutis, A. F. Araghi, O. J. Miller, J.-C. Baret, L. Frenz, A. Janoshazi, V. Taly, B. J. Miller, J. B. Hutchison, D. Link, A. D. Griffiths, and M. Ryckelynck, "Droplet-based microfluidic systems for high-throughput single DNA molecule isothermal amplification and analysis," *Analytical Chemistry*, vol. 81, pp. 4813–21, Jun 2009.
- [25] L. Frenz, K. Blank, E. Brouzes, and A. D. Griffiths, "Reliable microfluidic on-chip incubation of droplets in delay-lines," *Lab on a Chip*, vol. 9, pp. 1344–8, May 2009.
- [26] K. D. Vosbeck, K. F. Chow, and W. M. Awad, "The proteolytic enzymes of the K-1 strain of *Streptomyces griseus* obtained from a commercial preparation (Pronase). Purification and characterization of the aminopeptidases," *Journal of Biological Chemistry*, vol. 248, pp. 6029–6034, Sep 1973.
- [27] K. D. Vosbeck, B. D. Greenberg, and W. M. Awad, "The proteolytic enzymes of the K-1 strain of *Streptomyces griseus* obtained from a commercial preparation (Pronase). Specificity and immobilization of aminopeptidase," *Journal of Biological Chemistry*, vol. 250, pp. 3981–3987, May 1975.
- [28] K. D. Vosbeck, B. D. Greenberg, M. S. Ochoa, P. L. Whitney, and W. M. Awad, "Proteolytic enzymes of the K-1 strain of *Streptomyces griseus* obtained from a commercial preparation (Pronase). Effect of pH, metal ions, and amino acids on aminopeptidase activity," *Journal of Biological Chemistry*, vol. 253, pp. 257–260, Jan 1978.
- [29] Y. Narahashi and M. Yanagita, "Studies on proteolytic enzymes (pronase) of *Streptomyces griseus* K-1. I. Nature and properties of the proteolytic enzyme system," *Journal of Biochemistry*, vol. 62, pp. 633–641, Dec 1967.
- [30] T. Gonzales and J. Robert-Baudouy, "Bacterial aminopeptidases: properties and functions," *FEMS Microbiology Reviews*, vol. 18, pp. 319–344, Jul 1996.
- [31] A. Spungin and S. Blumberg, "*Streptomyces griseus* aminopeptidase is a calcium-activated zinc metalloprotein. Purification and properties of the enzyme," *European Journal of Biochemistry*, vol. 183, no. 2, pp. 471–477, 1989.
- [32] D. Ben-Meir, A. Spungin, R. Ashkenazi, and S. Blumberg, "Specificity of *Streptomyces griseus* aminopeptidase and modulation of activity by divalent metal ion binding and substitution," *European Journal of Biochemistry*, vol. 212, no. 1, pp. 107–112, 1993.
- [33] B. Maras, H. M. Greenblatt, G. Shoham, A. Spungin-Bialik, S. Blumberg, and D. Barra, "Aminopeptidase from *Streptomyces griseus*: primary structure and comparison with other zinc-containing aminopeptidases," *European Journal of Biochemistry*, vol. 236, pp. 843–846, Mar 1996.
- [34] G. Papir, A. Spungin-Bialik, D. Ben-Meir, E. Fudim, R. Gilboa, H. M. Greenblatt, G. Shoham, U. Lessel, D. Schomburg, R. Ashkenazi, and S. Blumberg, "Inhibition of *Streptomyces griseus* aminopeptidase and

- effects of calcium ions on catalysis and binding—comparisons with the homologous enzyme *Aeromonas proteolytica* aminopeptidase,” *European Journal of Biochemistry*, vol. 258, pp. 313–319, Dec 1998.
- [35] N. D. Rawlings and A. J. Barrett, “Evolutionary families of metallopeptidases,” *Methods in Enzymology*, vol. 248, pp. 183–228, 1995.
- [36] V. Nagy, K. M. Nampoothiri, A. Pandey, R. Rahulan, and G. Szakacs, “Production of L-leucine aminopeptidase by selected *Streptomyces* isolates,” *Journal of Applied Microbiology*, vol. 104, pp. 380–387, Feb 2008.
- [37] S. W. Melbye and F. H. Carpenter, “Leucine aminopeptidase (bovine lens). Stability and size of subunits,” *Journal of Biological Chemistry*, vol. 246, pp. 2459–2463, Apr 1971.
- [38] M. P. Allen, A. H. Yamada, and F. H. Carpenter, “Kinetic parameters of metal-substituted leucine aminopeptidase from bovine lens,” *Biochemistry*, vol. 22, no. 16, pp. 3778–3783, 1983.
- [39] S. Himmelhoch, “Leucine aminopeptidase: a zinc metalloenzyme,” *Archives of Biochemistry and Biophysics*, vol. 134, pp. 597–602, Nov 1969.
- [40] H. E. van Wart and S. H. Lin, “Metal binding stoichiometry and mechanism of metal ion modulation of the activity of porcine kidney leucine aminopeptidase,” *Biochemistry*, vol. 20, pp. 5682–5689, Sep 1981.
- [41] J. M. Prescott, S. H. Wilkes, F. W. Wagner, and K. J. Wilson, “*Aeromonas* aminopeptidase. Improved isolation and some physical properties,” *Journal of Biological Chemistry*, vol. 246, pp. 1756–1764, Mar 1971.
- [42] W. Lipscomb and N. Sträter, “Recent advances in zinc enzymology,” *Chemical Reviews*, vol. 96, pp. 2375–2434, Nov 1996.
- [43] J. M. Prescott, F. W. Wagner, B. Holmquist, and B. L. Vallee, “Spectral and kinetic studies of metal-substituted *Aeromonas* aminopeptidase: nonidentical, interacting metal-binding sites,” *Biochemistry*, vol. 24, pp. 5350–5356, Sep 1985.
- [44] F. H. Carpenter and J. M. Vahl, “Leucine aminopeptidase (bovine lens). Mechanism of activation by Mg^{2+} and Mn^{2+} of the zinc metalloenzyme, amino acid composition, and sulfhydryl content,” *Journal of Biological Chemistry*, vol. 248, pp. 294–304, Jan 1973.
- [45] E. L. Smith and D. H. Spackman, “Leucine aminopeptidase. V. Activation, specificity, and mechanism of action,” *Journal of Biological Chemistry*, vol. 212, pp. 271–299, Jan 1955.
- [46] C. Hasselgren, H. I. Park, and L. J. Ming, “Metal ion binding and activation of *Streptomyces griseus* dinuclear aminopeptidase: cadmium(II) binding as a model,” *Journal of Biological Inorganic Chemistry*, vol. 6, pp. 120–127, Feb 2001.
- [47] A. Taylor, “Aminopeptidases: structure and function,” *FASEB Journal*, vol. 7, pp. 290–298, Feb 1993.
- [48] H. Umezawa, “Low-molecular-weight enzyme inhibitors of microbial origin,” *Annu Rev Microbiol*, vol. 36, pp. 75–99, 1982.
- [49] H. M. Greenblatt, O. Almog, B. Maras, A. Spungin-Bialik, D. Barra, S. Blumberg, and G. Shoham, “*Streptomyces griseus* aminopeptidase: X-ray crystallographic structure at 1.75 Å resolution,” *Journal of Molecular Biology*, vol. 265, pp. 620–636, Jan. 1997.
- [50] R. Gilboa, H. M. Greenblatt, M. Perach, A. Spungin-Bialik, U. Lessel, G. Wohlfahrt, D. Schomburg, S. Blumberg, and G. Shoham, “Interactions of *Streptomyces griseus* aminopeptidase with a methionine product analogue: a structural study at 1.53 Å resolution,” *Acta Crystallographica Section D Biological Crystallography*, vol. 56, pp. 551–558, May 2000.
- [51] R. Gilboa, A. Spungin-Bialik, G. Wohlfahrt, D. Schomburg, S. Blumberg, and G. Shoham, “Interactions of *Streptomyces griseus* aminopeptidase with amino acid reaction products and their implications toward a catalytic mechanism,” *Proteins: Structure, Function, and Genetics*, vol. 44, no. 4, pp. 490–504, 2001.
- [52] J. Arima, Y. Uesugi, M. Uraji, S. Yatsushiro, S. Tsuboi, M. Iwabuchi, and T. Hatanaka, “Modulation of *Streptomyces* leucine aminopeptidase by calcium: Identification and functional analysis of key residues in activation and stabilization by calcium,” *Journal of Biological Chemistry*, vol. 281, no. 9, pp. 5885–5894, 2006.

- [53] W. T. Lowther and B. W. Matthews, "Metalloaminopeptidases: common functional themes in disparate structural surroundings," *Chemical Reviews*, vol. 102, pp. 4581–4608, Dec 2002.
- [54] W. Desmarais, D. L. Bienvenue, K. P. Bzymek, G. A. Petsko, D. Ringe, and R. C. Holz, "The high-resolution structures of the neutral and the low pH crystals of aminopeptidase from *Aeromonas proteolytica*," *Journal of Biological Inorganic Chemistry*, vol. 11, pp. 398–408, Jun 2006.
- [55] E. F. Pettersen, T. D. Goddard, C. C. Huang, G. S. Couch, D. M. Greenblatt, E. C. Meng, and T. E. Ferrin, "UCSF Chimera—a visualization system for exploratory research and analysis," *Journal of Computational Chemistry*, vol. 25, pp. 1605–1612, Oct 2004.
- [56] J. Arima, Y. Uesugi, M. Iwabuchi, and T. Hatanaka, "Study on peptide hydrolysis by aminopeptidases from *Streptomyces griseus*," *Applied Microbiology and Biotechnology*, vol. 70, pp. 541–547, May 2006.
- [57] H. I. Park and L.-J. Ming, "A 10^{10} rate enhancement of phosphodiester hydrolysis by a dinuclear aminopeptidase - transition-state analogues as substrates?," *Angewandte Chemie International Edition*, vol. 38, no. 19, pp. 2914–2916, 1999.
- [58] A. Ercan, H. I. Park, and L.-J. Ming, "Remarkable enhancement of the hydrolyses of phosphoesters by dinuclear centers: *Streptomyces* aminopeptidase as a 'natural model system'," *Chemical Communications*, no. 24, pp. 2501–2502, 2000.
- [59] G. da Silva and L.-J. Ming, "Catechol oxidase activity of di-Cu²⁺-substituted aminopeptidase from *Streptomyces griseus*," *Journal of the American Chemical Society*, vol. 127, no. 47, pp. 16380–16381, 2005.
- [60] A. Ercan, H. Park, and L.-J. Ming, "A "moonlighting" dizinc aminopeptidase from *Streptomyces griseus*: Mechanisms for peptide hydrolysis and the 4×10^{10} -fold acceleration of the alternative phosphodiester hydrolysis," *Biochemistry*, vol. 45, no. 46, pp. 13779–13793, 2006.
- [61] A. Ercan, W. M. Tay, S. H. Grossman, and L.-J. Ming, "Mechanistic role of each metal ion in *streptomyces* dinuclear aminopeptidase: Peptide hydrolysis and 7×10^{10} -fold rate enhancement of phosphodiester hydrolysis," *Journal of Inorganic Biochemistry*, vol. 104, pp. 19–29, Jan 2010.
- [62] E. Fischer, "Einfluss der Configuration auf die Wirkung der Enzyme," *Berichte der deutschen chemischen Gesellschaft*, vol. 27, no. 3, pp. 2985–93, 1894.
- [63] K. D.E., "Application of a theory of enzyme specificity to protein synthesis," *Proceedings of the National Academy of Sciences of the USA*, vol. 44, no. 2, pp. 98–104, 1958.
- [64] K. A. Dill and H. S. Chan, "From Levinthal to pathways to funnels," *Nature Structural Biology*, vol. 4, pp. 10–19, Jan 1997.
- [65] P. Tompa, "Intrinsically unstructured proteins," *Trends in Biochemical Sciences*, vol. 27, pp. 527–533, Oct 2002.
- [66] V. N. Uversky, "Natively unfolded proteins: a point where biology waits for physics," *Protein Science*, vol. 11, pp. 739–756, Apr 2002.
- [67] P. E. Wright and H. J. Dyson, "Intrinsically unstructured proteins: re-assessing the protein structure-function paradigm," *Journal of Molecular Biology*, vol. 293, pp. 321–331, Oct 1999.
- [68] P. J. O'Brien and D. Herschlag, "Catalytic promiscuity and the evolution of new enzymatic activities," *Chemistry and Biology*, vol. 6, pp. R91–R105, Apr 1999.
- [69] S. D. Copley, "Enzymes with extra talents: moonlighting functions and catalytic promiscuity," *Current Opinion Chemical Biology*, vol. 7, pp. 265–272, Apr 2003.
- [70] E. B. Lewis, "Pseudoallelism and gene evolution," *Cold Spring Harbor Symposia on Quantitative Biology*, vol. 16, pp. 159–174, 1951.
- [71] S. Ohno, *Evolution by gene duplication*. Springer-Verlag, 1970.
- [72] R. A. Jensen, "Enzyme recruitment in evolution of new function," *Annual Review of Microbiology*, vol. 30, pp. 409–425, 1976.
- [73] M. Rossmann, A. Liljas, C.-I. Branden, and L. Banaszak, *The enzymes*. Academic Press, 1975.

- [74] M. Wilmanns, C. C. Hyde, D. R. Davies, K. Kirschner, and J. N. Jansonius, "Structural conservation in parallel beta/alpha-barrel enzymes that catalyze three sequential reactions in the pathway of tryptophan biosynthesis," *Biochemistry*, vol. 30, pp. 9161–9169, Sep 1991.
- [75] D. L. Ollis, E. Cheah, M. Cygler, B. Dijkstra, F. Frolow, S. M. Franken, M. Harel, S. J. Remington, I. Silman, and J. Schrag, "The alpha/beta hydrolase fold," *Protein Engineering*, vol. 5, pp. 197–211, Apr 1992.
- [76] P. C. Babbitt, G. T. Mrachko, M. S. Hasson, G. W. Huisman, R. Kolter, D. Ringe, G. A. Petsko, G. L. Kenyon, and J. A. Gerlt, "A functionally diverse enzyme superfamily that abstracts the alpha protons of carboxylic acids," *Science*, vol. 267, pp. 1159–1161, Feb 1995.
- [77] P. C. Babbitt, M. S. Hasson, J. E. Wedekind, D. R. Palmer, W. C. Barrett, G. H. Reed, I. Rayment, D. Ringe, G. L. Kenyon, and J. A. Gerlt, "The enolase superfamily: a general strategy for enzyme-catalyzed abstraction of the alpha-protons of carboxylic acids," *Biochemistry*, vol. 35, pp. 16489–16501, Dec 1996.
- [78] P. C. Babbitt and J. A. Gerlt, "Understanding enzyme superfamilies. Chemistry as the fundamental determinant in the evolution of new catalytic activities," *Journal of Biological Chemistry*, vol. 272, pp. 30591–30594, Dec 1997.
- [79] B. A. Bernat, L. T. Laughlin, and R. N. Armstrong, "Fosfomycin resistance protein (FosA) is a manganese metalloglutathione transferase related to glyoxalase I and the extradiol dioxygenases," *Biochemistry*, vol. 36, pp. 3050–3055, Mar 1997.
- [80] L. Holm and C. Sander, "An evolutionary treasure: unification of a broad set of amidohydrolases related to urease," *Proteins*, vol. 28, pp. 72–82, May 1997.
- [81] R. N. Armstrong, "Mechanistic imperatives for the evolution of glutathione transferases," *Current Opinion in Chemical Biology*, vol. 2, pp. 618–623, Oct 1998.
- [82] J. A. Gerlt and P. C. Babbitt, "Mechanistically diverse enzyme superfamilies: the importance of chemistry in the evolution of catalysis," *Current Opinion Chemical Biology*, vol. 2, pp. 607–612, Oct 1998.
- [83] P. C. Babbitt and J. A. Gerlt, "New functions from old scaffolds: how nature reengineers enzymes for new functions," *Advances in Protein Chemistry*, vol. 55, pp. 1–28, 2000.
- [84] L. C. James and D. S. Tawfik, "Conformational diversity and protein evolution—a 60-year-old hypothesis revisited," *Trends in Biochemical Sciences*, vol. 28, pp. 361–368, Jul 2003.
- [85] W.-H. Li and D. Grauer, *Fundamentals of molecular evolution*. Sinauer Associates, Incorporated, 1991.
- [86] O. Khersonsky, C. Roodveldt, and D. S. Tawfik, "Enzyme promiscuity: evolutionary and mechanistic aspects," *Current Opinion Chemical Biology*, vol. 10, pp. 498–508, Oct 2006.
- [87] A. Aharoni, L. Gaidukov, O. Khersonsky, S. M. Gould, C. Roodveldt, and D. S. Tawfik, "The 'evolvability' of promiscuous protein functions," *Nature Genetics*, vol. 37, pp. 73–76, Jan. 2005.
- [88] Y. Fundoiano-Hershcovitz, L. Rabinovitch, Y. Langut, V. Reiland, G. Shoham, and Y. Shoham, "Identification of the catalytic residues in the double-zinc aminopeptidase from *Streptomyces griseus*," *FEBS Letters*, vol. 571, pp. 192–196, Jul 2004.
- [89] Y. F. Hershcovitz, R. Gilboa, V. Reiland, G. Shoham, and Y. Shoham, "Catalytic mechanism of SGAP, a double-zinc aminopeptidase from *Streptomyces griseus*," *FEBS Journal*, vol. 274, no. 15, pp. 3864–3876, 2007.
- [90] J. Arima, Y. Uesugi, M. Uraji, M. Iwabuchi, and T. Hatanaka, "The role of Glu196 in the environment around the substrate binding site of leucine aminopeptidase from *Streptomyces griseus*," *FEBS Letters*, vol. 580, pp. 912–917, Feb. 2006.
- [91] W. W. Cleland and A. C. Hengge, "Enzymatic mechanisms of phosphate and sulfate transfer," *Chemical Reviews*, vol. 106, pp. 3252–3278, Aug 2006.
- [92] P. J. O'Brien and D. Herschlag, "Functional interrelationships in the alkaline phosphatase superfamily: phosphodiesterase activity of *Escherichia coli* alkaline phosphatase," *Biochemistry*, vol. 40, pp. 5691–9, May 2001.

- [93] P. J. O'Brien and D. Herschlag, "Alkaline phosphatase revisited: hydrolysis of alkyl phosphates," *Biochemistry*, vol. 41, pp. 3207–25, Mar 2002.
- [94] J. Weston, "Mode of action of bi- and trinuclear zinc hydrolases and their synthetic analogues," *Chemical Reviews*, vol. 105, pp. 2151–2174, Jun 2005.
- [95] S. J. Kelly, D. E. Dardinger, and L. G. Butler, "Hydrolysis of phosphonate esters catalyzed by 5'-nucleotide phosphodiesterase," *Biochemistry*, vol. 14, pp. 4983–4988, Nov 1975.
- [96] S. J. Kelly and L. G. Butler, "Enzymic hydrolysis of phosphonate esters," *Biochemical and Biophysical Research Communications*, vol. 66, pp. 316–321, Sep 1975.
- [97] A. C. Hengge and W. W. Cleland, "Phosphoryl-transfer reactions of phosphodiester: characterization of transition states by heavy-atom isotope effects," *Journal of the American Chemical Society*, vol. 113, no. 15, pp. 5835–5841, 1991.
- [98] W. W. Cleland and A. C. Hengge, "Mechanisms of phosphoryl and acyl transfer," *FASEB Journal*, vol. 9, pp. 1585–1594, Dec 1995.
- [99] A. Rompel, H. Fischer, D. Meiwes, K. Büldt-Karentzopoulos, A. Magrini, C. Eicken, C. Gerdemann, and B. Krebs, "Substrate specificity of catechol oxidase from *Lycopus europaeus* and characterization of the bioproducts of enzymic caffeic acid oxidation," *FEBS Letters*, vol. 445, pp. 103–110, Feb 1999.
- [100] C. Gerdemann, C. Eicken, and B. Krebs, "The crystal structure of catechol oxidase: new insight into the function of type-3 copper proteins," *Accounts of Chemical Research*, vol. 35, pp. 183–191, Mar 2002.
- [101] C. A. Tracewell and F. H. Arnold, "Directed enzyme evolution: climbing fitness peaks one amino acid at a time," *Current Opinion in Chemical Biology*, vol. 13, pp. 3–9, Feb 2009.
- [102] M. Kirschner and J. Gerhart, "Evolvability," *Proceedings of the National Academy of Sciences of the USA*, vol. 95, pp. 8420–7, Jul 1998.
- [103] M. Radman, I. Matic, and F. Taddei, "Evolution of evolvability," *Annals of the New York Academy of Sciences*, vol. 870, pp. 146–55, May 1999.
- [104] D. J. Earl and M. W. Deem, "Evolvability is a selectable trait," *Proceedings of the National Academy of Sciences of the USA*, vol. 101, pp. 11531–6, Aug 2004.
- [105] N. Tokuriki and D. S. Tawfik, "Protein dynamism and evolvability," *Science*, vol. 324, pp. 203–7, Apr 2009.
- [106] H. Hufnagel, A. Huebner, C. Gülch, K. Güse, C. Abell, and F. Hollfelder, "An integrated cell culture lab on a chip: modular microdevices for cultivation of mammalian cells and delivery into microfluidic microdroplets," *Lab Chip*, vol. 9, pp. 1576–82, Jun 2009.
- [107] N. C. Shaner, R. E. Campbell, P. A. Steinbach, B. N. G. Giepmans, A. E. Palmer, and R. Y. Tsien, "Improved monomeric red, orange and yellow fluorescent proteins derived from *Discosoma sp.* red fluorescent protein," *Nature Biotechnology*, vol. 22, pp. 1567–72, Dec 2004.
- [108] M. P. Iacoviello and S. A. Rubin, "Sterile preparation of antibiotic-selective LB agar plates using a microwave oven," *BioTechniques*, vol. 30, pp. 963–5, May 2001.
- [109] C. Holtze, A. C. Rowat, J. J. Agresti, J. B. Hutchison, F. E. Angilè, C. H. J. Schmitz, S. Köster, H. Duan, K. J. Humphry, R. A. Scanga, J. S. Johnson, D. Pisignano, and D. A. Weitz, "Biocompatible surfactants for water-in-fluorocarbon emulsions," *Lab on a Chip*, vol. 8, pp. 1632–9, Oct 2008.
- [110] D. G. Taylor, V. M. Williams, and N. Crawford, "Bis-(4-methylumbelliferyl) phosphate as a substrate for the surface membrane-associated phosphodiesterase activity of pig platelets," *Biochimica et Biophysica Acta*, vol. 465, pp. 667–71, Mar 1977.
- [111] A. Krebber, S. Bornhauser, J. Burmester, A. Honegger, J. Willuda, H. R. Bosshard, and A. Plückthun, "Reliable cloning of functional antibody variable domains from hybridomas and spleen cell repertoires employing a reengineered phage display system," *Journal of Immunological Methods*, vol. 201, pp. 35–55, Feb 1997.
- [112] K. Blank, J. Morfill, H. Gump, and H. E. Gaub, "Functional expression of *Candida antarctica* lipase B in *Escherichia coli*," *Journal of Biotechnology*, vol. 125, pp. 474–83, Oct 2006.

- [113] M. Vaara, "Agents that increase the permeability of the outer membrane," *Microbiological Reviews*, vol. 56, pp. 395–411, Sep 1992.
- [114] R. R. Feiner, K. Meyer, and A. Steinberg, "Bacterial lysis by lysozyme," *Journal of Bacteriology*, vol. 52, pp. 375–84, Sep 1946.
- [115] R. Nir, Y. Yisraeli, R. Lamed, and E. Sahar, "Flow cytometry sorting of viable bacteria and yeasts according to beta-galactosidase activity," *Applied and Environmental Microbiology*, vol. 56, pp. 3861–6, Dec 1990.
- [116] L. Cai, N. Friedman, and X. S. Xie, "Stochastic protein expression in individual cells at the single molecule level," *Nature*, vol. 440, pp. 358–62, Mar 2006.
- [117] R. A. Dixon and I. Chopra, "Leakage of periplasmic proteins from *Escherichia coli* mediated by polymyxin B nonapeptide," *Antimicrobial Agents and Chemotherapy*, vol. 29, pp. 781–8, May 1986.
- [118] H. Nikaïdo, "Molecular basis of bacterial outer membrane permeability revisited," *Microbiology and Molecular Biology Reviews: MMBR*, vol. 67, pp. 593–656, Dec 2003.
- [119] J. A. Orwa, C. Govaerts, K. Gevers, E. Roets, A. Van Schepdael, and J. Hoogmartens, "Study of the stability of polymyxins B₁, E₁ and E₂ in aqueous solution using liquid chromatography and mass spectrometry," *Journal of Pharmaceutical and Biomedical Analysis*, vol. 29, pp. 203–12, Jun 2002.
- [120] A. Z. Sahalan and R. A. Dixon, "Role of the cell envelope in the antibacterial activities of polymyxin B and polymyxin B nonapeptide against *Escherichia coli*," *International Journal of Antimicrobial Agents*, vol. 31, pp. 224–7, Mar 2008.
- [121] D. R. Storm, K. S. Rosenthal, and P. E. Swanson, "Polymyxin and related peptide antibiotics," *Annual Review of Biochemistry*, vol. 46, pp. 723–63, 1977.
- [122] A. P. Zavascki, L. Z. Goldani, J. Li, and R. L. Nation, "Polymyxin B for the treatment of multidrug-resistant pathogens: a critical review," *The Journal of Antimicrobial Chemotherapy*, vol. 60, pp. 1206–15, Dec 2007.
- [123] J.-C. Baret, F. Kleinschmidt, A. El Harrak, and A. D. Griffiths, "Kinetic aspects of emulsion stabilization by surfactants: a microfluidic analysis," *Langmuir*, vol. 25, pp. 6088–93, Jun 2009.
- [124] Y. Sela, S. Magdassi, and N. Garti, "Release of markers from the inner water phase of w / o / w emulsions stabilized by silicone based polymeric surfactants," *Journal of Controlled Release*, vol. 33, no. 1, pp. 1–12, 1995.
- [125] J. Bibette, F. L. Calderon, and P. Poulin, "Emulsions: basic principles," *Reports on Progress in Physics*, vol. 62, no. 6, pp. 969–1033, 1999.
- [126] L. Wen and K. D. Papadopoulos, "Visualization of water transport in w₁/o/w₂ emulsions," *Colloids and Surfaces A: Physicochemical and Engineering Aspects*, vol. 174, no. 1-2, pp. 159–167, 2000.
- [127] M. Hai and S. Magdassi, "Investigation on the release of fluorescent markers from w/o/w emulsions by fluorescence-activated cell sorter," *Journal of Controlled Release : official journal of the Controlled Release Society*, vol. 96, pp. 393–402, May 2004.
- [128] M. Y. Koroleva and E. V. Yurtov, "Water mass transfer in w/o emulsions," *Journal of Colloid and Interface Science*, vol. 297, pp. 778–84, May 2006.
- [129] J. Cheng, J.-F. Chen, M. Zhao, Q. Luo, L.-X. Wen, and K. D. Papadopoulos, "Transport of ions through the oil phase of w₁/o/w₂ double emulsions," *Journal of Colloid and Interface Science*, vol. 305, no. 1, pp. 175–182, 2007.
- [130] F. Courtois, L. F. Olguin, G. Whyte, A. B. Theberge, W. T. S. Huck, F. Hollfelder, and C. Abell, "Controlling the retention of small molecules in emulsion microdroplets for use in cell-based assays," *Analytical Chemistry*, vol. 81, pp. 3008–16, Apr 2009.
- [131] R. G. Ashcroft and P. A. Lopez, "Commercial high speed machines open new opportunities in high throughput flow cytometry (HTFC)," *Journal of Immunological Methods*, vol. 243, pp. 13–24, Sep 2000.
- [132] J. Clausell-Tormos, D. Lieber, J.-C. Baret, A. El-Harrak, O. J. Miller, L. Frenz, J. Blouwolf, K. J. Humphry, S. Köster, H. Duan, C. Holtze, D. A. Weitz, A. D. Griffiths, and C. A. Merten, "Droplet-based microfluidic platforms for the encapsulation and screening of mammalian cells and multicellular organisms," *Chemistry and Biology*, vol. 15, pp. 427–37, May 2008.

- [133] S. Köster, F. E. Angilè, H. Duan, J. J. Agresti, A. Wintner, C. Schmitz, A. C. Rowat, C. A. Merten, D. Pisignano, A. D. Griffiths, and D. A. Weitz, "Drop-based microfluidic devices for encapsulation of single cells," *Lab on a Chip*, vol. 8, pp. 1110–5, Jul 2008.
- [134] W. J. Blake, G. Balazsi, M. A. Kohanski, F. J. Isaacs, K. F. Murphy, Y. Kuang, C. R. Cantor, D. R. Walt, and J. J. Collins, "Phenotypic consequences of promoter-mediated transcriptional noise," *Molecular Cell*, vol. 24, pp. 853–865, Dec. 2006.
- [135] M. B. Elowitz, A. J. Levine, E. D. Siggia, and P. S. Swain, "Stochastic gene expression in a single cell," *Science*, vol. 297, pp. 1183–1186, Aug 2002.
- [136] H. H. McAdams and A. Arkin, "Stochastic mechanisms in gene expression," *Proceedings of the National Academy of Sciences of the USA*, vol. 94, pp. 814–9, Feb 1997.
- [137] H. H. McAdams and A. Arkin, "It's a noisy business! Genetic regulation at the nanomolar scale," *Trends in Genetics*, vol. 15, pp. 65–69, Feb 1999.
- [138] E. M. Ozbudak, M. Thattai, I. Kurtser, A. D. Grossman, and A. van Oudenaarden, "Regulation of noise in the expression of a single gene," *Nature Genetics*, vol. 31, pp. 69–73, May 2002.
- [139] X. Shu, N. C. Shaner, C. A. Yarbrough, R. Y. Tsien, and S. J. Remington, "Novel chromophores and buried charges control color in mFruits," *Biochemistry*, vol. 45, pp. 9639–47, Aug 2006.
- [140] M. Ormö, A. B. Cubitt, K. Kallio, L. A. Gross, R. Y. Tsien, and S. J. Remington, "Crystal structure of the *Aequorea victoria* green fluorescent protein," *Science*, vol. 273, pp. 1392–5, Sep 1996.
- [141] N. C. Shaner, P. A. Steinbach, and R. Y. Tsien, "A guide to choosing fluorescent proteins," *Nature Methods*, vol. 2, pp. 905–9, Dec 2005.
- [142] X. Dong, P. Stothard, I. J. Forsythe, and D. S. Wishart, "PlasMapper: a web server for drawing and auto-annotating plasmid maps," *Nucleic Acids Research*, vol. 32, pp. W660–4, Jul 2004.
- [143] B. J. Bevis and B. S. Glick, "Rapidly maturing variants of the *Discosoma* red fluorescent protein (DsRed)," *Nature Biotechnology*, vol. 20, pp. 83–7, Jan 2002.
- [144] R. E. Campbell, O. Tour, A. E. Palmer, P. A. Steinbach, G. S. Baird, D. A. Zacharias, and R. Y. Tsien, "A monomeric red fluorescent protein," *Proceedings of the National Academy of Sciences of the USA*, vol. 99, pp. 7877–82, Jun 2002.
- [145] N. C. Shaner, G. H. Patterson, and M. W. Davidson, "Advances in fluorescent protein technology," *Journal of Cell Science*, vol. 120, pp. 4247–60, Dec 2007.
- [146] L. Granieri, *Droplet-based microfluidics and engineering of tissue plasminogen activator for biomedical applications*. PhD thesis, Université de Strasbourg, 2009.
- [147] E. Sato, A. Matsuhisa, M. Sakashita, and Y. Kanaoka, "New water-soluble fluorogenic amine. 7-Aminocoumarin-4-methanesulfonic acid (ACMS) and related substrates for proteinases," *Chemical & Pharmaceutical Bulletin (Tokyo)*, vol. 36, pp. 3496–502, Sep 1988.
- [148] R. L. Atkins and D. E. Bliss, "Substituted coumarins and azacoumarins. Synthesis and fluorescent properties," *The Journal of Organic Chemistry*, vol. 43, pp. 1975–1980, 05 2002.
- [149] Z. L. Pianowski and N. Winssinger, "Fluorescence-based detection of single nucleotide permutation in DNA via catalytically templated reaction," *Chemical Communications*, pp. 3820–2, Oct 2007.
- [150] H. E. Gottlieb, V. Kotlyar, and A. Nudelman, "NMR chemical shifts of common laboratory solvents as trace impurities," *The Journal of Organic Chemistry*, vol. 62, pp. 7512–7515, Oct 1997.
- [151] B. Heltweg, F. Dequiedt, B. L. Marshall, C. Brauch, M. Yoshida, N. Nishino, E. Verdin, and M. Jung, "Subtype selective substrates for histone deacetylases," *Journal of Medicinal Chemistry*, vol. 47, pp. 5235–43, Oct 2004.
- [152] J. Sylvestre, *Émulsions inverses cristallisables pour l'évolution dirigée*. PhD thesis, Université Paris VI, Nov 2007.

-
- [153] J. Handelsman, M. R. Rondon, S. F. Brady, J. Clardy, and R. M. Goodman, "Molecular biological access to the chemistry of unknown soil microbes: a new frontier for natural products," *Chemistry and Biology*, vol. 5, pp. R245–9, Oct 1998.
- [154] R. I. Amann, W. Ludwig, and K. H. Schleifer, "Phylogenetic identification and *in situ* detection of individual microbial cells without cultivation," *Microbiological Reviews*, vol. 59, pp. 143–69, Mar 1995.
- [155] D. B. Steele and M. D. Stowers, "Techniques for selection of industrially important microorganisms," *Annual Review of Microbiology*, vol. 45, pp. 89–106, 1991.
- [156] L. Øvreås and V. Torsvik, "Microbial diversity and community structure in two different agricultural soil communities," *Microbial Ecology*, vol. 36, pp. 303–315, Nov 1998.
- [157] V. Torsvik, F. L. Daae, R. A. Sandaa, and L. Øvreås, "Novel techniques for analysing microbial diversity in natural and perturbed environments," *Journal of Biotechnology*, vol. 64, pp. 53–62, Sep 1998.
- [158] K. Liolios, K. Mavromatis, N. Tavernarakis, and N. C. Kyrpides, "The Genomes On Line Database (GOLD) in 2007: status of genomic and metagenomic projects and their associated metadata," *Nucleic Acids Research*, vol. 36, pp. D475–9, Jan 2008.
- [159] M. Monici, "Cell and tissue autofluorescence research and diagnostic applications," *Biotechnology Annual Review*, vol. 11, pp. 227–56, 2005.